Fall 12-2012

Fluorescence and Size Characterization of Dissolved Organic Matter in Riverine and Sea Waters in the Northern Gulf of Mexico

Zhengzhen Zhou
University of Southern Mississippi

The University of Southern Mississippi

FLUORESCENCE AND SIZE CHARACTERIZATION OF DISSOLVED ORGANIC MATTER IN RIVERINE AND SEA WATERS IN THE NORTHERN GULF OF MEXICO

by

Zhengzhen Zhou

Abstract of a Dissertation
Submitted to the Graduate School
of The University of Southern Mississippi
in Partial Fulfillment of the Requirements
for the Degree of Doctor of Philosophy

December 2012

ABSTRACT

FLUORESCENCE AND SIZE CHARACTERIZATION OF DISSOLVED ORGANIC MATTER IN RIVERINE AND SEA WATERS IN THE NORTHERN GULF OF MEXICO

by Zhengzhen Zhou

December 2012

Riverine export of dissolved organic matter (DOM) is an important component in marine carbon budget but the composition and phase partitioning are poorly quantified. Monthly water samples were collected from the lower Mississippi and Pearl rivers between January 2009 to August 2011 for DOM characterization using the fluorescence excitation emission matrix (FluoEEM) technique, coupled with parallel factor analysis (PARAFAC), and flow field-flow fractionation technique. DOM in the Pearl River showed higher dissolved organic carbon (DOC) concentration, temporal fluctuation, and aromaticity, reflecting instantaneous inputs of DOM from local soil and plant litter. In contrast, DOM in the Mississippi River exhibited lower abundance, seasonal variability and aromaticity, but higher proportion of protein-type fluorophores, corresponding to integrated signals and enhanced photochemical degradation largely resulting from of prolonged water residence time, as well as *in situ* phytoplankton production. Distinct DOM characteristics in these two river contribute to explain the effect of source, hydrology and human impacts on composition and colloidal size distribution of riverine DOM.

In addition to terrestrial inputs of organic matter, oil is another source of organic matter in the Gulf of Mexico. The unprecedented Deepwater Horizon oil spill in April 2010 introduced large amount of crude oil into the Gulf of Mexico. The FluoEEM technique and PARAFAC modeling were also used to examine the fate, transport and transformation of oil in the water column during this oil spill. Oil greatly altered the optical properties of DOM in the entire water column during the oil spill. Persistent influence of oil on deep waters was observed even 15 months after the spill. Three major oil components were characterized by FluoEEM and PARAFAC modeling. The oil component ratios varied consistently and quantitatively with degradation states of oil and can be used as an index to track oil in the water column. The chemical evolution of oil and its degradation pathways observed in the field were further tested and confirmed with results from controlled laboratory experiments using Macondo crude oil. Degradation half lives of PAH, *n*-Alkanes and oil components were identified and can help understand the degradation pathways of different oil components.

The University of Southern Mississippi

FLUORESCENCE AND SIZE CHARACTERIZATION OF DISSOLVED ORGANIC MATTER IN RIVERINE AND SEA WATERS IN THE NORTHERN GULF OF MEXICO

by

Zhengzhen Zhou

A Dissertation
Submitted to the Graduate School
of The University of Southern Mississippi
in Partial Fulfillment of the Requirements
for the Degree of Doctor of Philosophy

Approved:

_Laodong Guo_____
Director

_Alan M. Shiller_____

_Steven E. Lohrenz_____

_Kjell Gundersen_____

_Yoko Furukawa_____

_Susan A. Siltanen_____
Dean of the Graduate School

December 2012

ACKNOWLEDGMENTS

I would like to thank the dissertation director, Dr. Laodong Guo, and the other committee members, Dr. Alan Shiller, Kjell Gundersen, Steve Lohrenz and Yoko Furukawa, for their advice and support throughout the duration of this project. I would especially like to thank Dr. Laodong Guo for his patient guidance and enormous support in many aspects and Dr. Alan Shiller for his precious pieces of advice as I encounter a variety of difficulties.

Special thanks go to Dr. Björn Stolpe of the Facility for Environmental Nanoscience Analysis and Characterisation (FENAC) at The University of Birmingham for his great teaching, guidance and help during my sample analysis with the FlFFF system. Appreciation must be expressed to Hailong Huang, Dongjoo Joung, Xuri Wang, Dr. Yihua Cai, Peng Lin, Yao Li, Dr. Huijun He and Dr. Weifeng Yang for their assistance during sample collection. Many thanks also go to Dr. Xiaobiao Xu, Chudong Pan, and Dr. Steve Howden for their help with Matlab programming. I am very thankful for all the help and support that were received from the DMS students, faculty and staff members during the process.

Last but not least, I would like to express my deepest gratitude to my family. Their love greatly supported me during this journal of my life.

TABLE OF CONTENTS

LIST OF TABLES

Table

LIST OF ILLUSTRATIONS

Figure

CHAPTER I

GENERAL INTRODUCTION

As one of the largest dynamic pools of reduced carbon, dissolved organic matter (DOM) plays a major role in the carbon cycle (Hedges, 2002), regulates the fate and transport of trace elements in marine and freshwater ecosystems (Pham and Garnier, 1998; Shiller et al., 2006; Taillefert et al., 2000), and controls the bioavailability and distribution of hydrophobic contaminants (Backhus et al., 2003; Urrestarazu Ramos et al., 1998). The composition and relative abundance of DOM affect its interaction with trace metals and contaminants (Chin et al., 1998; Perminova et al., 1999).

Colloidal DOM, operationally defined as the >1 kDa fraction of DOM (Guo and Macdonald, 2006; Guo and Santschi, 2007; Lyvén et al., 1997), has been found to contain a variety of compounds and acts as a dynamic intermediary between dissolved and particulate species and regulates the transfer of particle reactive metal ions to particles (Amon and Benner, 1996; Baskaran and Santschi, 1993; Guo and Santschi, 1997), and plays a critical role in regulating the concentration and speciation, hence fate, transport and bioavailability of trace metals and pollutants in aquatic systems (Benedetti et al., 2003; Buffle et al., 1998; Lead and Wilkinson, 2006; Wilkinson et al., 1997). The size of colloidal DOM determines its utilization efficiency by microbes (Benner, 2002; Benner, 2003; Findlay, 2003) and degradation status (Amon and Benner, 1996). Therefore, knowledge of the colloidal DOM size spectrum and composition

should provide new insights into biogeochemical cycling pathways and the role DOM plays in regulating the fate and transport of trace elements.

Rivers export a substantial amounts of DOM into the sea each year (~17×10^{12} moles) (Trefry et al., 1994). Riverine DOM has been found to influence water quality and productivity in estuarine and coastal areas (Bianchi et al., 2010; Bianchi et al., 1997; Raymond et al., 2000), and the fate and transport of riverine DOM into the world ocean is an important part of marine carbon cycle (Hedges et al., 1997). The abundance and composition of riverine DOM and its temporal variations are largely controlled by its source material, extent of in situ riverine processes, and other hydrological and biogeochemical processes in rivers and their drainage basins (Bianchi et al., 2004; Dagg et al., 2005; Hedges et al., 2000; Warnken and Santschi, 2004)

As important as it is, the composition and size distribution of DOM in rivers and oceans are still largely uncharacterized, partly due to the diverse complexity of specific compounds in DOM, yet uncharacterized (Coble, 2007; Leenheer and Croué, 2003). The biogeochemical processes associated with the production, transformation and transportation of DOM are still not well understood (Coble, 2007).

Excitation-emission matrix (EEM) fluorescence spectroscopy has been widely used to examine characteristics, distribution and seasonal variations of fluorescent DOM, and to identify DOM sources in various water systems (Coble, 1996; McKnight et al., 2001; Miller and McKnight, 2010; Moran et al., 2000; Parlanti et al., 2000). Application of a multivariate analysis technique, parallel

factor analysis (PARAFAC), on fluorescence EEMs allows one to further characterize DOM components based on their optical properties (Andersen and Bro, 2003), and has been widely used to characterize DOM from diverse sources in aquatic systems (Andersen and Bro, 2003; Stedmon and Markager, 2003; Stedmon and Markager, 2005). Thus, the combination of fluorescence EEMs and PARAFAC can be used to better understand DOM dynamics in natural waters (Jaffé et al., 2008).

Flow field-flow fractionation (FFF) is a chromatography-like analytical technique in which retention force is provided by a cross-flow perpendicular to the channel-flow, and colloids are separated based on their diffusion coefficients and hydrodynamic diameters (Giddings, 1993). A variety of ancillary detectors, for example UV-absorbance and fluorescence detectors, can be coupled on-line to an FFF system to examine continuous size spectra of colloidal DOM and to determine distinct types of colloids characterized with specific size and compositions (Stolpe et al., 2010; Stolpe et al., 2005; Wells, 2004; Zanardi-Lamardo et al., 2002).

No study has applied fluorescence EEMs spectroscopy combined with PARAFAC analysis, and few studies has employed the FFF technique (Stolpe et al., 2010) to compare DOM in the lower Mississippi and Pearl Rivers, two rivers with contrasting size and extent of anthropogenic impact. It provides an approach to identify sources and cycling pathways of DOM and their relation with hydrology and other processes in the rivers.

The first part of this dissertation, including Chapter II and Chapter III, is to examine the abundance, composition and size spectra of colloidal DOM in river systems in the lower Mississippi River and lower Pearl River, to compare the characteristics of DOM in the lower reaches of the Mississippi River, a large turbid river with a massive drainage basin area and under extensive anthropogenic influence (Beckett and Pennington, 1986; Wiener et al., 1996) with the Pearl River, a small and less-human-impacted river (Duan et al., 2007a; Duan et al., 2007b) and to examine the effect of source, hydrological conditions, drainage plain size, land use, and human activities on the abundance, composition and size distribution of colloidal DOM in these two rivers that both export to the central north Gulf of Mexico. Chapter II and Chapter III will address these research problems concerning optical properties and colloidal size spectra of DOM, respectively.

In addition to terrestrial inputs of organic matter, oil is another source of organic matter in the Gulf of Mexico (Anderson et al., 1983; Brooks et al., 1986). The unprecedented Deepwater Horizon oil spill in the northern Gulf of Mexico during April 20 – July 15, 2010 resulted in the release of over 800 million liters of crude oil from the Macondo well into the water column (Mascarelli, 2010; Schrope, 2011). For the remediation of oil, over 7 million liters of dispersant were used during the oil spill (Kujawinski et al., 2011). The vast quantity of oil and its long transit from the deep ocean to the sea surface made this oil spill different from other spill disasters. This Gulf of Mexico oil spill also provided a natural laboratory and an opportunity to examine the fate, transport and transformation

of crude oil components and their interactions with the environment (Camilli et al., 2010; Diercks et al., 2010; Hazen et al., 2010; Wade et al., 2011). How oil interacts with natural organic matter and the subsequent dynamic changes in chemical and optical properties in the water column after the DWH oil spill in the Gulf of Mexico are also research questions of this dissertation.

Many weathering processes, including dissolution, dispersion, evaporation, and photochemical and biological degradation, can affect the distribution and transport of crude oil in the Gulf of Mexico. Although oil in surface waters seemed to be weathered rapidly right after the oil spill, recent studies have shown the persistence of oil signatures in the deeper water column in the northern Gulf of Mexico, even 15 months after the oil spill (Ryerson et al., 2012; Zhou and Guo, 2012). The fate, transport, and transformation of oil components and their degradation pathways and mechanisms in the water column remain poorly understood. The relative importance between photochemical and biological degradation, and the chemical evolution and molecular fractionation of Macondo crude oil during degradation are largely unknown. Therefore, in addition to field studies, controlled laboratory experiments are needed to better understand the degradation pathways and mechanisms of crude oil in marine environments.

Previous studies have shown the usefulness of fluorescence EEM techniques and PARAFAC analysis in the characterization, fingerprinting, and monitoring of oil (Alostaz et al., 2008; Bugden et al., 2008; Christensen et al., 2005; Patra and Mishra, 2002). However, applications of fluorescence EEMs and

PARAFAC analysis are still few for the Deepwater Horizon oil spill in the northern Gulf of Mexico.

Objectives of the second part of this dissertation were to examine the distribution and variation of DOM and UV-vis absorbance in the water column around the Macondo well in the Gulf of Mexico during and after the oil spill, to characterize the fluorescence and other optical properties of oil and seawater samples for identification and fingerprinting of oil components, to determine the relationship between fluorescence component ratios and chemical evolution of oil in the water column, and to conduct laboratory experiments to examine the chemical evolution, the degradation and transformation pathways and mechanisms of oil components during photochemical and biological degradation of the Macondo crude oil. Chapter IV focuses on the characterization of oil components in the Gulf of Mexico during the oil spill. Chapter V looks at the evolution of optical properties of DOM in the water column from the height of the oil spill to 15 months after Macondo well was capped. Using controlled laboratory experiments, Chapter VI reports the degradation pathways and fate and transformation of oil components during the degradation of crude oil.

REFERENCES

Alostaz, M., Biggar, K., Donahue, R. and Hall, G., 2008. Petroleum contamination characterization and quantification using fluorescence emission-excitation matrices (EEMs) and parallel factor analysis (PARAFAC). Journal of Environmental Engineering & Science, 7(3): 183-197, doi: 10.1139/s07-049.

Amon, R.M.W. and Benner, R., 1996. Photochemical and microbial consumption of dissolved organic carbon and dissolved oxygen in the Amazon River system. Geochimica et Cosmochimica Acta, 60(10): 1783-1792.

Andersen, C.M. and Bro, R., 2003. Practical aspects of PARAFAC modeling of fluorescence excitation-emission data. Journal of Chemometrics, 17(4): 200-215, doi: 10.1002/cem.790.

Anderson, R.K., Scalan, R.S., Parker, P.L. and Behrens, E.W., 1983. Seep oil and gas in gulf of Mexico slope sediment. Science (New York, N.Y.), 222(4624): 619-621.

Backhus, D.A., Golini, C. and Castellanos, E., 2003. Evaluation of fluorescence quenching for assessing the importance of interactions between nonpolar organic pollutants and dissolved organic matter. Environmental Science & Technology, 37(20): 4717-4723.

Baskaran, M. and Santschi, P.H., 1993. The role of particles and colloids in the transport of radionuclides in coastal environments of Texas. Marine Chemistry, 43(1-4): 95-114, doi:10.1016/0304-4203(93)90218-d.

Beckett, D.C. and Pennington, C.H., 1986. Water quality, macroinvertebrates, larval fishes, and fishes of the lower mississippi river - a synthesis U.S. Army Corps of Engineers, Technical Report. Waterways Experiment Station, Vicksburg, MS.

Benedetti, M.F., Mounier, S., Filizola, N., Benaim, J. and Seyler, P., 2003. Carbon and metal concentrations, size distributions and fluxes in major rivers of the Amazon basin. Hydrological Processes, 17(7): 1363-1377.

Benner, R., 2002. Chemical composition and reactivity. In: H. D.A. and C.A. Carlson (Editors), Biogeochemistry of marine dissolved organic matter. Academic Press, London, UK, pp. 59-85.

Benner, R., 2003. Molecular indicators of the bioavailability of dissolved organic matter. In: S. Findlay and R.L. Sinsabaugh (Editors), Aquatic Ecosystems: Interactivity of Dissolved Organic Matter. Academic Press, London, UK, pp. 121-135.

Bianchi, T.S. et al., 2010. The science of hypoxia in the Northern Gulf of Mexico: A review. Science of The Total Environment, 408(7): 1471-1484.

Bianchi, T.S., Filley, T., Dria, K. and Hatcher, P.G., 2004. Temporal variability in sources of dissolved organic carbon in the lower Mississippi river. Geochimica et Cosmochimica Acta, 68(5): 959-967.

Bianchi, T.S., Lambert, C.D., Santschi, P.H. and Guo, L., 1997. Sources and transport of land-derived particulate and dissolved organic matter in the Gulf of Mexico (Texas shelf/slope): The use of ligninphenols and loliolides

as biomarkers. Organic Geochemistry, 27(1-2): 65-78, doi: 10.1016/s0146-6380(97)00040-5.

Brooks, J.M. et al., 1986. Association of gas hydrates and oil seepage in the Gulf of Mexico. Organic Geochemistry, 10(1-3): 221-234.

Buffle, J., Wilkinson, K.J., Stoll, S., Filella, M. and Zhang, J., 1998. A generalized description of aquatic colloidal interactions: the three-colloidal component approach. Environmental Science & Technology, 32(19): 2887-2899.

Bugden, J.B.C., Yeung, C.W., Kepkay, P.E. and Lee, K., 2008. Application of ultraviolet fluorometry and excitation-emission matrix spectroscopy (EEMS) to fingerprint oil and chemically dispersed oil in seawater. Marine Pollution Bulletin, 56(4): 677-685, doi: 10.1016/j.marpolbul.2007.12.022.

Camilli, R. et al., 2010. Tracking hydrocarbon plume transport and biodegradation at deepwater horizon. Science, 330(6001): 201-204.

Chin, Y.P., Traina, S.J., Swank, C.R. and Backhus, D., 1998. Abundance and properties of dissolved organic matter in pore waters of a freshwater wetland. Limnology and Oceanography, 43(6): 1287-1296.

Christensen, J.H., Hansen, A.B., Mortensen, J. and Andersen, O., 2005. Characterization and matching of oil samples using fluorescence spectroscopy and parallel factor analysis. Analytical Chemistry, 77(7): 2210-2217, doi: 10.1021/ac048213k.

Coble, P.G., 1996. Characterization of marine and terrestrial DOM in seawater using excitation-emission matrix spectroscopy. Marine Chemistry, 51(4): 325-346, doi: 10.1016/0304-4203(95)00062-3.

Coble, P.G., 2007. Marine Optical Biogeochemistry: The Chemistry of Ocean Color. Chemical Reviews, 107(2): 402-418.

Dagg, M.J. et al., 2005. Biogeochemical Characteristics of the Lower Mississippi River, USA, during June 2003. Estuaries, 28(5): 664-674.

Diercks, A.R. et al., 2010. Characterization of subsurface polycyclic aromatic hydrocarbons at the Deepwater Horizon site. Geophysical Research Letters, 37(20): L20602, doi: 10.1029/2010gl045046.

Duan, S., Bianchi, T.S. and Sampere, T.P., 2007a. Temporal variability in the composition and abundance of terrestrially-derived dissolved organic matter in the lower Mississippi and Pearl Rivers. Marine Chemistry, 103(1-2): 172-184, doi: 10.1016/j.marchem.2006.07.003.

Duan, S. et al., 2007b. Variability in the bulk composition and abundance of dissolved organic matter in the lower Mississippi and Pearl rivers. Journal of Geophysical Research, 112(G2): G02024, doi: 10.1029/2006JG000206.

Findlay, S., 2003. Bacterial response to variation in dissolved organic matter. In: S. Findlay and R.L. Sinsabaugh (Editors), Aquatic Ecosystems: Interactivity of Dissolved Organic Matter. Academic Press, London, UK, pp. 363-377.

Giddings, J.C., 1993. Field-flow fractionation: analysis of macromolecular, colloidal, and particulate materials. Science, 260(5113): 1456-1465.

Guo, L. and Macdonald, R.W., 2006. Source and transport of terrigenous organic matter in the upper Yukon River: Evidence from isotope (δ13C,Δ14C, andδ15N) composition of dissolved, colloidal, and particulate phases. Global Biogeochem. Cycles, 20(2): GB2011, doi: 10.1029/2005gb002593.

Guo, L. and Santschi, P.H., 1997. Composition and cycling of colloids in marine environments. Rev. Geophys., 35(1): 17-40.

Guo, L. and Santschi, P.H., 2007. Ultrafiltration and its applications to sampling and characterisation of aquatic colloids. In: K.J. Wilkinson and J.R. Lead (Editors), Environmental colloids and particles. John Wiley & Sons, Ltd, pp. 159–221, doi: 10.1002/9780470024539.ch4.

Hazen, T.C. et al., 2010. Deep-sea oil plume enriches indigenous oil-degrading bacteria. Science, 330(6001): 204-208, doi: 10.1126/science.1195979.

Hedges, J.I., 2002. Why dissolved organic matter? In: D.A. Hansell and C.A. Carlson (Editors), Biogeochemistry of marine dissolved organic matter. Academic Press: San Diego, London, UK., pp. 1-33.

Hedges, J.I., Keil, R.G. and Benner, R., 1997. What happens to terrestrial organic matter in the ocean? Organic Geochemistry, 27(5-6): 195-212, doi: 10.1016/s0146-6380(97)00066-1.

Hedges, J.I. et al., 2000. Organic matter in Bolivian tributaries of the Amazon River: a comparison to the lower mainstream. Limnology and Oceanography, 45(7): 1449-1466.

Jaffé, R. et al., 2008. Spatial and temporal variations in DOM composition in ecosystems: The importance of long-term monitoring of optical properties. J. Geophys. Res., 113(G4): G04032, doi: 10.1029/2008jg000683.

Kujawinski, E.B. et al., 2011. Fate of dispersants associated with the Deepwater Horizon oil spill. Environmental Science and Technology, 45(4): 1298-1306, doi: 10.1021/es103838p.

Lead, J.R. and Wilkinson, K.J., 2006. Aquatic Colloids and Nanoparticles: Current Knowledge and Future Trends. Environmental Chemistry, 3(3): 159-171.

Leenheer, J.A. and Croué, J.P., 2003. Peer reviewed: characterizing aquatic dissolved organic matter. Environmental Science and Technology, 37(1): 18A-26A, doi: 10.1021/es032333c.

Lyvén, B., Hassellöv, M., Haraldsson, C. and Turner, D.R., 1997. Optimisation of on-channel preconcentration in flow field-flow fractionation for the determination of size distributions of low molecular weight colloidal material in natural waters. Analytica Chimica Acta, 357(3): 187-196, doi: 10.1016/s0003-2670(97)00565-5.

Mascarelli, A., 2010. Deepwater Horizon: After the oil. Nature, 467: 22-24, doi: 10.1038/news.2010.378.

McKnight, D.M. et al., 2001. Spectrofluorometric characterization of dissolved organic matter for indication of precursor organic material and aromaticity. Limnology and Oceanography, 46(1): 38-48.

Miller, M.P. and McKnight, D.M., 2010. Comparison of seasonal changes in fluorescent dissolved organic matter among aquatic lake and stream sites in the Green Lakes Valley. J. Geophys. Res., 115: G00F12, doi: 10.1029/2009jg000985.

Moran, M.A., Sheldon, W.M., Jr. and Zepp, R.G., 2000. Carbon loss and optical property changes during long-term photochemical and biological

degradation of estuarine dissolved organic matter. Limnology and Oceanography, 45(6): 1254-1264.

Parlanti, E., Wörz, K., Geoffroy, L. and Lamotte, M., 2000. Dissolved organic matter fluorescence spectroscopy as a tool to estimate biological activity in a coastal zone submitted to anthropogenic inputs. Organic Geochemistry, 31(12): 1765-1781, doi: 10.1016/s0146-6380(00)00124-8.

Patra, D. and Mishra, A.M., 2002. Total synchronous fluorescence scan spectra of petroleum products. Analytical and Bioanalytical Chemistry, 373(4): 304-309, doi: 10.1007/s00216-002-1330-y.

Perminova, I.V., Grechishcheva, N.Y. and Petrosyan, V.S., 1999. Relationships between structure and binding affinity of humic substances for polycyclic aromatic hydrocarbons: relevance of molecular descriptors. Environmental Science and Technology, 33(21): 3781-3787.

Pham, M.K. and Garnier, J.M., 1998. Distribution of trace elements associated with dissolved compounds (<0.45µm-1 nm) in freshwater using coupled (frontal cascade) ultrafiltration and chromatographic separations. Environmental Science and Technology, 32(4): 440-449.

Raymond, P.A., Bauer, J.E. and Cole, J.J., 2000. Atmospheric CO2 evasion, dissolved inorganic carbon production, and net heterotrophy in the York River Estuary. Limnology and Oceanography, 45(8): 1707-1717.

Ryerson, T.B. et al., 2012. Chemical data quantify Deepwater Horizon hydrocarbon flow rate and environmental distribution. Proceedings of the National Academy of Sciences: doi: 10.1073/pnas.1110564109.

Schrope, M., 2011. Oil cruise finds deep-sea plume. Nature, 465: 274-275, doi: 10.1038/465274a.

Shiller, A.M., Duan, S., Erp, P.v. and Bianchi, T.S., 2006. Photo-oxidation of dissolved organic matter in river water and its effect on trace element speciation. Limnology and Oceanography, 51(4): 1716-1728.

Stedmon, C.A. and Markager, S., 2003. Behaviour of the optical properties of coloured dissolved organic matter under conservative mixing. Estuarine, Coastal and Shelf Science, 57(5-6): 973-979.

Stedmon, C.A. and Markager, S., 2005. Resolving the Variability in Dissolved Organic Matter Fluorescence in a Temperate Estuary and Its Catchment Using PARAFAC Analysis. Limnology and Oceanography, 50(2): 686-697.

Stolpe, B., Guo, L., Shiller, A.M. and Hassellöv, M., 2010. Size and composition of colloidal organic matter and trace elements in the Mississippi River, Pearl River and the northern Gulf of Mexico, as characterized by flow field-flow fractionation. Marine Chemistry, 118(3-4): 119-128.

Stolpe, B., Hassellöv, M., Andersson, K. and Turner, D.R., 2005. High resolution ICPMS as an on-line detector for flow field-flow fractionation; multi-element determination of colloidal size distributions in a natural water sample. Analytica Chimica Acta, 535(1-2): 109-121, doi: 10.1016/j.aca.2004.11.067.

Taillefert, M., Lienemann, C.P., Gaillard, J.F.O. and Perret, D., 2000. Speciation, reactivity, and cycling of Fe and Pb in a meromictic lake. Geochimica et Cosmochimica Acta, 64(2): 169-183.

Trefry, J.H., Metz, S., Nelsen, T.A., Trocine, R.P. and Eadie, B.J., 1994. Transport of particulate organic carbon by the mississippi river and its fate in the gulf of mexico. Estuaries, 17(4): 839-849.

Urrestarazu Ramos, E., Meijer, S.N., Vaes, W.H.J., Verhaar, H.J.M. and Hermens, J.L.M., 1998. Using solid-phase microextraction to determine partition coefficients to humic acids and bioavailable concentrations of hydrophobic chemicals. Environmental Science and Technology, 32(21): 3430-3435.

Wade, T.L. et al., 2011. Analyses of water samples from the Deepwater Horizon oil spill: documentation of the subsurface plume, Monitoring and Modeling the Deepwater Horizon Oil Spill: A Record-Breaking Enterprise. Geophys. Monogr. Ser. AGU, Washington, DC, pp. 77-82, doi: 10.1029/2011gm001103.

Warnken, K.W. and Santschi, P.H., 2004. Biogeochemical behavior of organic carbon in the Trinity River downstream of a large reservoir lake in Texas, USA. Science of The Total Environment, 329(1-3): 131-144.

Wells, M.L., 2004. The colloidal size spectrum of CDOM in the coastal region of the Mississippi Plume using flow field-flow fractionation. Marine Chemistry, 89(1-4): 89-102, doi: 10.1016/j.marchem.2004.02.009.

Wiener, J.G. et al., 1996. Mississippi River, Status and Trends of Nation's Biological Resources. National Weahter Resouces Center, U.S. Geological Survey, Washington, D.C., pp. 351-384.

Wilkinson, K.J., Joz-Roland, A. and Buffle, J., 1997. Different Roles of Pedogenic Fulvic Acids and Aquagenic Biopolymers on Colloid Aggregation and Stability in Freshwaters. Limnology and Oceanography, 42(8): 1714-1724.

Zanardi-Lamardo, E., Clark, C.D., Moore, C.A. and Zika, R.G., 2002. Comparison of the molecular mass and optical properties of colored dissolved organic material in two rivers and coastal waters by Flow Field-Flow Fractionation. Environmental Science and Technology, 36(13): 2806-2814.

Zhou, Z. and Guo, L., 2012. Evolution of the optical properties of seawater influenced by the Deepwater Horizon oil spill in the Gulf of Mexico. Environmental Research Letters, 7(2): 025301, doi: 10.1088/1748-9326/7/2/025301.

CHAPTER II

A COMPARATIVE STUDY OF COLORED- AND FLUORESCENT DISSOLVED ORGANIC MATTER IN THE LOWER MISSISSIPPI RIVER AND PEARL RIVER

Introduction

The global dissolved organic carbon (DOC) export from rivers to ocean is approximately 0.25 Gt annually (Aitkenhead and McDowell, 2000). Riverine dissolved organic matter (DOM) has been found to influence estuarine and coastal marine productivity (Bianchi et al., 1997; Findlay et al., 1998; Hopkinson and Vallino, 1995; Raymond et al., 2000). The fate and transport of riverine DOM to the ocean is an indispensable part of the global carbon cycle (Hedges et al., 1997; Hope et al., 1994).

The abundance and composition of riverine DOM, as well as its diagenetic state, overall reactivity and ultimate fate, are largely controlled by its source material, extent of *in situ* riverine processes, and other hydrological and biogeochemical processes in rivers and their drainage basins (Dagg et al., 2005; Duan et al., 2007a; Findlay and Sinsabaugh, 1999; Hedges et al., 2000; Ittekkot et al., 1985; Kaiser et al., 2004a; Thurman, 1985; Volk et al., 1997).

In many small streams, the concentration of DOC has been found to show a positive correlation with river discharge (Boyer et al., 1997; Moore, 1989), and appeared to have a general origin from allochthonous terrestrial plant litter and event sources during flood from soil organic matter (Engelhaupt and Bianchi, 2001). Also, watershed land use, morphology and microbial activity have been found to be the main contributors of DOM quantity and quality in streams

(Williams et al., 2010). In large rivers, however, the source and compositions of DOM are controlled by more complicated processes, due to the broad range of hydrological and chemical conditions in their multiple tributaries (Coynel et al., 2005; Leenheer et al., 1995; Richey et al., 1990). Studies have shown that compared with DOM in smaller rivers, that in large rivers, especially in the lower reaches, is more likely to be degraded and has more origin from *in situ* sources (Hedges et al., 2000; Vannote et al., 1980). However, little research has been done to elucidate the differences of DOM in two water systems that are distinct in watershed size, yet both export to the Gulf of Mexico within close proximity (Duan et al., 2007a; Duan et al., 2007b).

Natural factors such as biome type and soil C:N ratio, as contrasted by anthropogenic influences, have been found to determine the riverine DOC flux globally (Aitkenhead and McDowell, 2000). However, along with the growth of human population in watersheds around the entire globe, human activities such as man-made levees and dam constructions have suppressed terrestrial input from floodplains, increased residence time and promoted extensive *in situ* processing of DOM in the rivers (Beckett and Pennington, 1986; Wiener et al., 1996). Relatively recent studies have demonstrated human impacts on the composition and export of DOM by rivers (Dalzell et al., 2005; Guo and Chorover, 2003; Jacinthe et al., 2001; Lal, 2004). There is now a significant need to separate natural and anthropogenic mechanisms responsible for river biogeochemistry of DOM (Meybeck, 2003).

The diverse sources and high molecular complexity of DOM (Leenheer and Croué, 2003; Spitzy and Leenheer, 1990; Thurman, 1985) make it hard to capture variations of bulk characteristics of riverine DOM, especially in large rivers such as the Mississippi River (Duan et al., 2007a). Excitation-emission matrix (EEM) fluorescence spectroscopy has been widely used to examine characteristics, distribution (Boyd and Osburn, 2004; Coble, 1996; Coble et al., 1998; De Souza Sierra et al., 1994; Mopper and Schultz, 1993; Moran et al., 2000) and seasonal variations (Miller and McKnight, 2010) of fluorescent DOM, and to identify DOM sources (Boyd and Osburn, 2004; Coble, 1996; Hall et al., 2005; McKnight et al., 2001; Parlanti et al., 2000) in various water systems. Application of a multivariate analysis technique, parallel factor analysis (PARAFAC), on fluorescence EEMs allows one to further characterize DOM components based on their optical properties (Andersen and Bro, 2003), and has been widely used to characterize DOM from diverse sources in aquatic systems (Cory and McKnight, 2005; Fulton et al., 2004; Jaffé et al., 2008; Stedmon and Markager, 2005; Stedmon et al., 2003), and to investigate the influence of land use on fluorescent DOM distribution (Stedmon et al., 2003). Thus, the combination of fluorescence EEMs and PARAFAC can be used to better understand DOM dynamics in natural waters (Jaffé et al., 2008). It provides an approach to identify sources and cycling pathways of DOM and their relation with hydrology and other processes in the rivers. No previous study has applied fluorescence EEMs in combination of PARAFAC to identify DOM in the lower Mississippi and Pearl Rivers. The objective of this study is to examine the

abundance and optical properties of dissolved and colloidal organic matter and their temporal variability in the lower Mississippi River and lower Pearl River from January 2009 to August 2011.

In this study, we compared DOM in the lower reach of Mississippi River, a large turbid river with massive drainage area and subjected to extensive human impacts (Beckett and Pennington, 1986; Wiener et al., 1996), with that in the lower Pearl River, a small and relatively less anthropogenically influenced black water river (Cai and Guo, 2009; Duan et al., 2007b). We also examined the effect of drainage basin size, hydrological conditions, and extent of human perturbation on the abundance, composition and optical properties of DOM in these two rivers that both export to the central north Gulf of Mexico.

Our working hypotheses include, 1) DOM in the Pearl River should have higher temporal variability in abundance and composition due to its instantaneous local inputs (forest soils and wetlands) and hydrological effect from the drainage basin, while DOM in the Mississippi River should be less temporally variable as it is controlled largely by major tributaries and *in situ* photochemical and biological processing; 2) prolonged water residence time due to human activates such as dam and levee constructions in the lower Mississippi River, as compared to the Pearl River, should have resulted in DOM with more highly degraded terrestrial and more aquagenic components.

Materials and Methods

Study Sites

The Mississippi River is the largest river in North America, and its drainage basin, with a total area of ~3,220,000 km^2, covers about 40% of the contiguous United States and a small part of Canada (Meade et al., 1990). With its length at 3,770 km and average flow rate at 17,000 m^3/s, the Mississippi River is the fourth longest and tenth largest world river (Kammerer, 1990). Cropland takes about 58% of its drainage basin, making the Mississippi River one of the most productive farming regions in the world (Goolsby and Battaglin, 2001; Goolsby et al., 2000). Dam systems and flood-control levees have restrained the river and reduced sediment discharge to the Gulf of Mexico (Keown et al., 1986; Meade et al., 1990). Decreased suspended sediment and increased nutrients, organic contaminants and trace elements in the recent few decades have caused great concern (Bianchi et al., 2010; Shiller et al., 2006).

The Pearl River on the contrary is a small black-water river that only drains the east-central Mississippi and southeastern Louisiana, with a total drainage area of about 22690 km^2. It is 790 km long and ranks as s 3rd stream order. Natural forests cover about 43% of the drainage basin. Agricultural region only represents ~27% of the land use. Marsh and/or swamp areas cover a small part of the basin (~10%) (Duan et al., 2007a; Duan et al., 2007b). Hydrological and land cover characteristics of the Mississippi and Pearl rivers are listed in Table 1. These two rivers are considerably different not only in their basin size, but also in hydrology, land use, and water residence time.

The Mississippi River receives integrated signals from its wide drainage basin and subjected to massive human impact, while the Pearl River represents waters from a less human-perturbed black water system. These differences allow one to examine the effect of hydrological conditions, land use, and anthropogenic influences on the quantity and quality of DOM in river systems.

Table 1

Hydrological and Land Cover Characteristics of the Mississippi River and Pearl River

	Mississippi River	Pearl River
Area (km^2)	3,220,000	22,690
Length (km)	3,770	790
Discharge (m^3/s)	17,000	260
Land cover - Crop land (%)	58%	27%
Land cover - Forest (%)	NA	43%
Land cover - Marsh & Wetland (%)	NA	10%

Sampling Locations

Water samples from the lower Mississippi River were collected near the U.S. Geological Survey (USGS) hydrological station at Baton Rouge, Louisiana (30˚26'17.01" N, 91˚11'33.14" W). The Pearl River water samples were collected at the East Pearl River at Stennis Space Center (SSC, 30°20'55.52"N, 89°38'28.74"W), at the lower Pearl River near the USGS hydrological station at

Bogalusa, Louisiana (PRB, 30°47'30"N, 89°49'20"W), and at the West Pearl River at the State Wildlife Management Area, Louisiana (PRW, 30°23'10.92"N, 89°44'13.08"W) (Figure 1). The sampling dates, locations and basic parameters are listed in Tables 2 and 3. Discharge data at the two USGS hydrological stations are from USGS websites (http://waterdata.usgs.gov/nwis/rt).

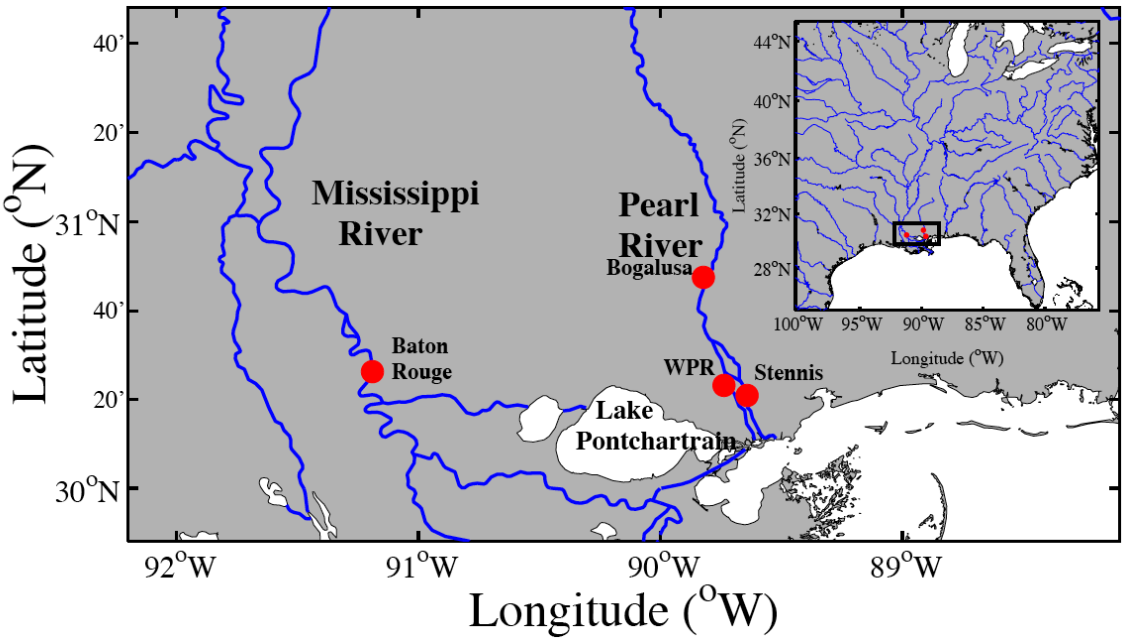

Figure 1. Sampling Locations In The Lower Mississippi River And Pearl River.

Sample Processing

About 40 L water samples from just below the river surface were filtered in the field through a 0.45 µm Memtrex polycarbonate pleated cartridge filters (GE Water & Process Technologies). Aliquots of filtered waters were collected in amber glass vials for the measurements of DOC (with acidification) and CDOM and FDOM (without acidification). Samples were then kept in an iced cooler and transported back to the lab within 3 hours of collection and stored in the dark in a refrigerator at 4˚C until further analysis. Water temperature and salinity were measured with a YSI meter at the time of sample collection.

Ultrafiltration

High-molecular-weight (HMW) DOM was separated and concentrated using the cross-flow ultra-filtration technique (Guo and Santschi, 1996; Guo and Santschi, 2007) with nominal cartridge pore size of 1 kDa (kilo-Dalton). The size-fractionated samples, including the <1 kDa low-molecular-weight (LMW) fraction and the >1 kDa colloidal or HMW fraction, as well as the bulk water sample were further analyzed for optical and chemical characterization. Permeate time-series samples during ultrafiltration were collected at different concentration factors (CF) and determined for DOC concentration to examine the colloidal fraction (percentage) of bulk DOC, and hence the partitioning of organic carbon and other chemical species between LMW and colloidal phases. According to the ultrafiltration permeation model (Logan and Jiang, 1990), by fitting the DOC concentration of the permeate time-series samples as C_p and volume ratio of initial solution to the retentate solution as CF to the following equation:

$$\ln C_p = \ln\left(P_c \times C_f^0\right) + \left(1 - P_c\right) \times \ln\left(CF\right)$$

where P_c is the permeation coefficient, determined by the ratio of C_p to C_f, and the latter is the feed concentration, C_f^0 is the initial feed concentration (i.e. DOC concentration of the bulk dissolved phase) (Guo and Santschi, 2007).

Measurements of DOC, UV-vis Absorption and ancillary chemical analysis

Concentrations of DOC and DIC of the river samples were measured with a Shimadzu TOC-V total organic carbon analyzer using a high temperature combustion method (Guo et al., 1995). Calibration curves were generated before sample analysis. For DOC measurements, samples were acidified with

concentrated HCl to pH < 2 before analysis. Three to five replicate measurements, each using 150 µL sample. Coefficient of variance of triplicate sample measurements were <2%. Concentrations of Nanopure water, working standards and certified DOC standards (from Dr. Hansell's Lab at the University of Miami) were measured every eight samples to check the performance of the instrument and ensure data quality. The concentration of DIC was calculated from the difference between total dissolved carbon (TDC) and DOC concentrations, DIC = TDC-DOC (Guo and Macdonald, 2006).

The UV-vis absorption spectra of samples were measured using a Cary 300 Bio UV-visible spectrophotometer or an Agilent 8453 UV-visible spectrophotometer using a 1-cm path-length quartz cuvette over 200-1100 nm with 1 nm increments. The water blank was subtracted, and the refractive index effect was corrected by subtracting the average absorbance between 650 and 800 nm (Stedmon and Bro, 2008). Values of specific UV absorbance ($SUVA_{254}$) were calculated by dividing the UV absorbance at 254 nm (m^{-1}) by the DOC concentration (mg-C/L). Spectral slope values were calculated using non-linear regression over wavelength interval between 290-400 nm (Zhou and Guo, 2012).

Ancillary chemical analysis of nutrients, such as dissolved inorganic phosphorus (DIP), was done by Dr. Huijun He using standard methods (SEPA, 2002).

Measurements of Fluorescence EEMs and PARAFAC Analysis

Sample was transferred into a 4.5 mL UV-grade quartz cuvette (10 mm light path). Fluorescence excitation–emission matrix (EEMs) spectra were

obtained with a RF-5301PC scanning spectrofluorometer (Shimadzu Corp., Kyoto, Japan) running Panorama fluorescence 1.1 software (LabCognition, Dortmund, Germany). In order to blank correct the spectra, scans of pure water were obtained in the same manner as the samples. These blank spectra were then subtracted from the sample spectra, before EEM contour plots were generated. For each fluorescence EEM, emission spectra were recorded over the range of 240-680 nm with 1nm intervals under excitation from 220 nm to 400nm with 2 nm step. Slit widths of 5 nm excitation and 5 nm emission along with a sampling interval of 1.0 nm, a scan speed set to “fast”, which is approximately 8 nm/s, and the response time set to ‘‘auto” was used to generate fluorescence spectra of samples. The scans of emission wavelengths at fixed excitation wavelengths were then combined to produce EEM spectra. Contour plots of the EEMs were generated by exporting the data into Microsoft Excel spreadsheets to be plotted using Matlab (Mathworks). On the fluorescence EEMs, the first and second order Raman and Raman peaks were removed. Contour plots were generated as normalized blank-corrected data (where spectral intensity was normalized to 1ppb-Quinine sulfate). All PARAFAC analyses were performed in MATLAB 6.5.1 (Mathworks) using the DOMfluor toolbox (Stedmon and Bro, 2008). Before modeling, the EEM area that was influenced by Rayleigh scattering and Raman scattering was eliminated from the dataset by the EEM algorithm. The model was constrained to nonnegative values and the results were validated using split half analysis (Andersen and Bro, 2003; Stedmon et al., 2003).

Results and Discussion

Hydrologic Characteristics

Discharge in the Pearl River at Bogalusa during our sampling period ranged from 37 to 2010 m^3/s (mean=338 m^3/s; n = 45), with the two most prominent peaks in April 2009 and March 2011, respectively (Figure 2, from USGS website: http://waterdata.usgs. gov/nwis/rt). The four water samples collected at Stennis Space Center from the Pearl River in July and August, 2009 and July and August, 2011 had specific conductivity at 25˚C (SPC) higher than 500 µS/cm. This is probably caused by seawater intrusion in the East Pearl River (Cai et al., 2012). These four samples were removed from our DOM analysis, as our objective was to investigate the influence of terrestrial sources and human impact on riverine DOM, instead of that from salt water. With high specific conductivity samples excluded, specific conductivity from the Pearl River samples ranged from 37 to 266 µS/cm (mean=81 µS/cm; n = 41). Positive correlations were found between specific conductivity and discharge ($P<0.005$, $r^2=0.20$, Table 2). Dissolved inorganic phosphorus (DIP) concentration in our Pearl River samples ranged from 0.1-1.7 µM (mean = 0.7µM; n = 41).

Discharge in the lower Mississippi River at Baton Rouge during our sampling period between 2009 and 2011 ranged from 7,538 to 40,012 m^3/s (mean=20,283 m^3/s; n = 33), with two most prominent peaks in May 2009 and May 2011, respectively (Figure 2, Table 3 from USGS website: http://waterdata.usgs.gov/nwis/rt). Specific conductivity for the lower Mississippi River samples ranged from 254 to 494 µS/cm (mean=358 µS/cm; n = 33), and

was closely correlated with discharge ($P<0.00001$ $r^2=0.59$). DIP concentration in our lower Mississippi River samples ranged from 0.8-3.3 µM (mean = 2.0µM; n = 41).

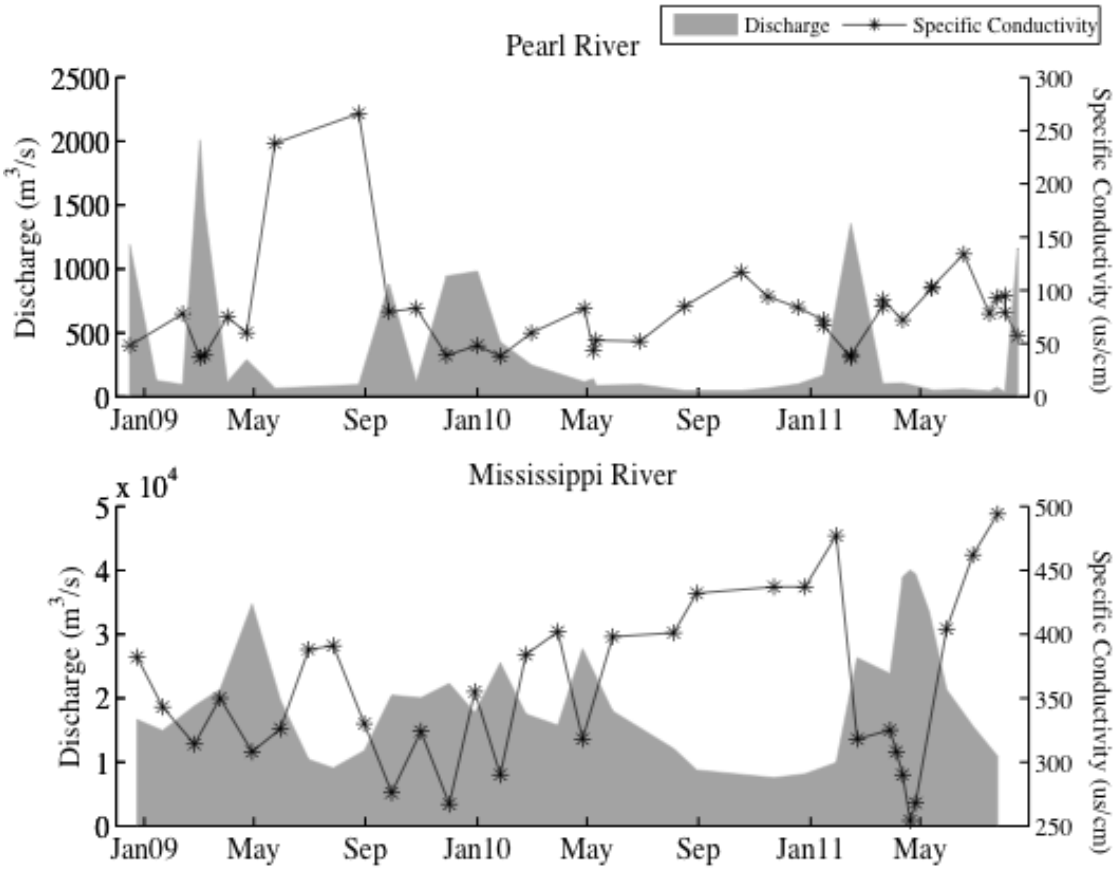

Figure 2. Seasonal Variations Of Discharge (m3/s) And Specific Conductivity At 25˚C (SPC, µS/cm) In The Lower Pearl and Mississippi Rivers.

Temporal Variations in DOC and Optical Properties

Dissolved Organic Carbon Concentrations. Concentrations of DOC varied from 225 to 1,121 µM (mean=543±206 µM, cv=38%) in the lower Pearl River, showing significant temporal changes in bulk abundance of DOM (Figure 3). Highest DOC concentration was observed in samples collected during highest discharge (April 2009). Significant positive correlation was found between DOC and discharge ($P<0.0001$, $r^2=0.55$) in the lower Pearl River. Dissolved organic

matter in the lower Mississippi River, in contrast, showed smaller seasonal change in its bulk abundance as the DOC concentration ranged from 236 to 388 µM (mean=306±40 µM, cv = 13%, Figure 3). Highest DOC concentration was observed in samples collected during highest discharge (May 2011). A good correlation with discharge ($P<0.001$, $r^2=0.38$) was also found for DOC in the lower Mississippi River, although not as good a relation as that in the Pearl River. Similar seasonal variations of these characteristics of DOM were also observed by Duan et al. (2007 a,b). The high seasonal variation of DOC in the Pearl River, especially in the East Pearl River, can also be controlled by the change in the water sources between the main stem and Hobolochitto Creek during high and low flow periods (Shiller et al., 2012).

Table 2

Hydrodrologic Parameters and DOC Concentrations in the East Pearl River at Stennis Space Center (SSC) and Bogalusa Station (PRB).

Date	Discharge (m^3/s)	Specific conductivity(µS/ cm)	Temp (˚C)	DOC (µM)
15-Jan-09$_{SSC}$	1,189	48	10.3	728
13-Feb-09$_{SSC}$	127	NA	16.0	376
14-Mar-09$_{SSC}$	96	78	21.7	326
2-Apr-09$_{SSC}$	2,010	37	18.8	1121

Table 2 (continued).

Date	Discharge (m^3/s)	Specific conductivity(µS/ cm)	Temp (˚C)	DOC (µM)
7-Apr-09$_{SSC}$	1,469	39	17.5	834
2-May-09$_{SSC}$	116	75	27.4	438
22-May-09$_{SSC}$	289	60	24.9	666
23-Jun-09$_{SSC}$	66	238	32.8	398
23-Sep-09$_{SSC}$	94	266	28.3	899
26-Oct-09$_{SSC}$	881	80	17.7	889
25-Nov-09$_{SSC}$	114	83	18.2	569
28-Dec-09$_{SSC}$	943	39	9.8	790
31-Jan-10$_{SSC}$	983	48	10.5	736
25-Feb-10$_{SSC}$	428	38	11.3	579
31-Mar-10$_{SSC}$	248	60	18.0	429
28-May-10$_{SSC}$	116	83	32.4	506
7-Jun-10$_{SSC}$	140	43	26.3	666
10-Jun-10$_{SSC}$	87	53	28.7	N/A
28-Jul-10$_{SSC}$	96	52	30.4	671
15-Sep-10$_{PRB}$	48	85	28.2	225
16-Nov-10$_{PRB}$	47	117	16.6	398
15-Dec-10$_{PRB}$	67	94	8.6	325

Table 2 (continued).

Date	Discharge (m^3/s)	Specific conductivity(µS/ cm)	Temp (˚C)	DOC (µM)
17-Jan-11$_{PRB}$	99	84	9.2	337
14-Feb-11$_{PRB}$	167	72	8.2	482
14-Feb-11$_{SSC}$	167	67	11.7	571
16-Mar-11$_{PRB}$	1,354	37	17.8	747
16-Mar-11$_{SSC}$	1,354	39	18.5	870
20-Apr-11$_{PRB}$	103	85	24.4	430
20-Apr-11$_{SSC}$	103	91	24.4	552
12-May-11$_{PRB}$	107	72	26.2	539
12-May-11$_{SSC}$	107	72	28.9	501
13-Jun-11$_{PRB}$	53	102	30.9	304
13-Jun-11$_{SSC}$	51	103	31.2	358
18-Jul-11$_{PRB}$	61	134	29.2	392
15-Aug-11$_{PRB}$	43	78	32.0	277
23-Aug-11$_{SSC}$	73	NA	NA	545
23-Aug-11$_{PRW}$	73	93	30.9	281
1-Sep-11$_{PRB}$	37	95	30.2	302
1-Sep-11$_{PRW}$	37	79	30.5	297
15-Sep-11$_{PRB}$	1,164	57	24.5	611

Table 3

Hydrologic Parameters and DOC Concentrations in the Lower Mississippi River between January 2009 and August 2011.

Date	Discharge (m^3/s)	Specific conductivity (µS/cm)	Temp (˚C)	DOC (µM)
23-Jan-09	16,622	382	6.3	256
20-Feb-09	14,926	343	8.8	235
27-Mar-09	18,774	314	13.0	324
24-Apr-09	21,345	350	15.9	296
29-May-09	34,688	308	36.7	339
29-Jun-09	19,658	326	29.8	317
30-Jul-09	10,395	388	27.8	270
26-Aug-09	9,047	391	28.8	264
29-Sep-09	11,771	330	25.6	299
29-Oct-09	20,445	276	16.1	343
30-Nov-09	20,048	324	13.0	337
31-Dec-09	22,283	267	7.0	265
28-Jan-10	17,695	355	7.3	275
25-Feb-10	25,482	290	5.7	237
25-Mar-10	17,505	384	11.9	266
29-Apr-10	15,741	402	20.5	299

Table 3 (continued).

Date	Discharge (m^3/s)	Specific conductivity (µS/cm)	Temp (˚C)	DOC (µM)
28-Jun-10	17,950	398	31.7	267
26-May-10	27,694	318	24.1	315
27-Jul-10	16,342	397	31.6	N/A
3-Sep-10	12,074	401	29.5	291
28-Sep-10	8,753	432	26.3	306
29-Oct-10	8,243	454	19.8	N/A
22-Nov-10	7,088	523	4.4	N/A
22-Dec-10	7,538	437	6.6	284
25-Jan-11	8,150	437	4.6	277
28-Feb-11	9,902	477	11.6	270
23-Mar-11	26,292	318	12.9	313
28-Apr-11	23,806	325	19.3	290
5-May-11	31,177	308	19.7	388
12-May-11	38,964	290	30.4	353
20-May-11	40,012	254	19.8	388
26-May-11	39,360	268	21.6	355
10-Jun-11	33,499	NA	NA	352
29-Jun-11	21,303	404	29.7	373

Table 3 (continued).

Date	Discharge (m^3/s)	Specific conductivity (µS/cm)	Temp (˚C)	DOC (µM)
28-Jul-11	15,580	462	31.7	336
24-Aug-11	10,871	494	30.2	320

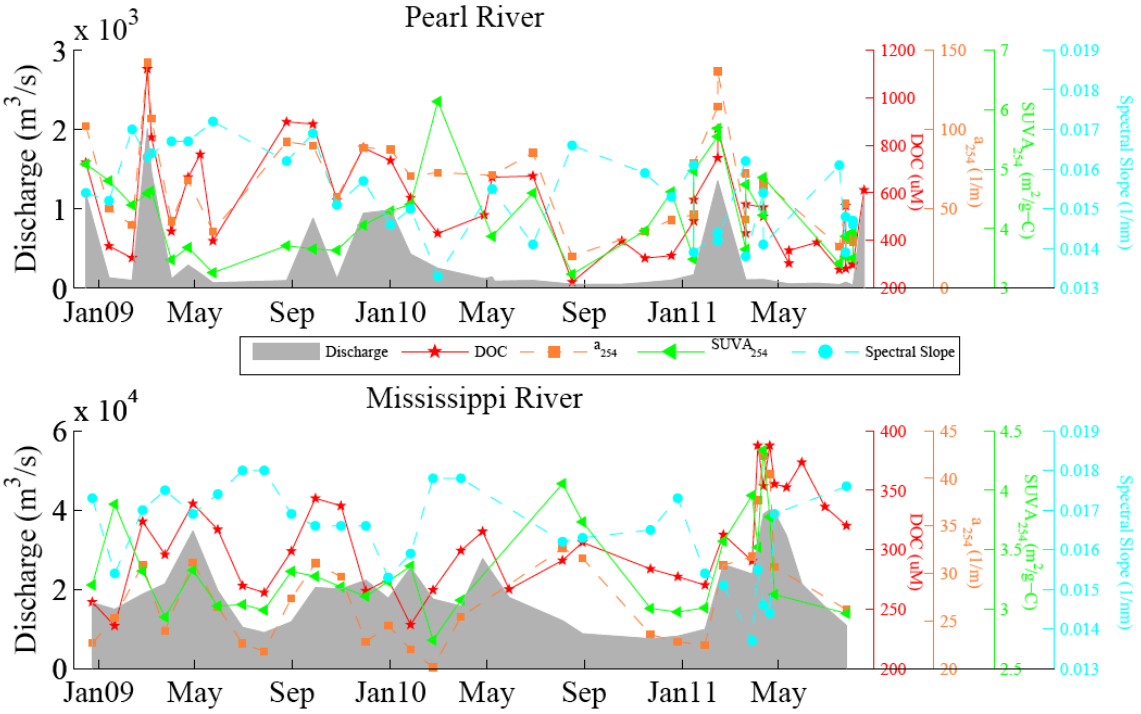

Figure 3. Seasonal Variations Of Discharge (m3/s) And Dissolved Organic Carbon (DOC, mg-C/L), Absorption Coefficient At 254 nm (a254), Specific UV Absorbance At 254 nm (SUVA254) And Spectral Slope Between 290-400 nm (S290-400) In The Lower Pearl And Mississippi Rivers.

Absorption Coefficient at 254 nm and Relationship between Bulk

Properties. A large fraction of riverine DOM is comprised of humic-like

substances that are high in aromatic components and unsaturated in nature. Laboratory experiments have established the link of unsaturated structure with absorption coefficient at 254 nm (a_{254}) (Trulleyová and Rulík, 2004). Measurements of a_{254} has been used for determination of DOC (Martin-Mousset et al., 1997), and good empirical correlation with DOC has been found (Alberts and Takács, 2004).

Samples collected from the lower Pearl River had a_{254} values ranging from 20.1-142.2m^{-1} (mean = 66.4 m^{-1}, cv = 47%, Figure 3). Large coefficient of variance indicates significant temporal changes in bulk composition of DOM. Highest a_{254} in the lower Pearl River during our sampling period was observed during April 2009 with the highest discharge (Figure 4). Positive correlation was found between a_{254} and discharge in the lower Pearl River ($P<0.00001$, $r^2=0.72$). In contrast, a_{254} values of samples from the lower Mississippi River ranged from 20.1 to 42.3 m^{-1} (mean=27.9 m^{-1}, cv=20%, Figure 3), showing smaller seasonal changes in bulk composition of DOM. Highest a_{254} in the Mississippi River was observed during May 2011 which coincided with the highest discharge during the past 28 years. Positive correlation was found between a_{254} and discharge in the lower Mississippi River ($P=0.0001$, $r^2=0.44$).

As shown above, positive correlations with discharge were found for DOC and a_{254} in the lower Pearl and Mississippi Rivers. Strong relationships were also observed between a_{254} and DOC in the Pearl River ($r^2=0.87$, $P<0.0001$, n=41) and the Mississippi River ($r^2=0.69$, $P<0.0001$,n=33) (Figure 4). The relationships between DOC and a_{254} showed positive intercepts of on the *x* axes at 53 µM for

Pearl River and at 66 µM for the Mississippi River (Figure 4). As discussed in previous studies, these intercept values are corresponding to the abundance of nonchromophoric DOC in river waters (Spencer et al., 2008). Thus, the nonchromophoric fractions of DOC in the lower Pearl and Mississippi Rivers are ~53 µM and ~66 µM, representing 10% and 21% of their corresponding bulk DOC, respectively. The higher amount of nonchromophoric fraction of DOC in the Mississippi River likely resulted from intensive photo- and bio- degradation of DOM in this river system due to it longer transit time (Duan et al., 2007a).

Concentration of dissolved inorganic carbon (DIC) in the Pearl River did not seem to have obvious correlation with discharge in the Pearl River (Figure 4), suggesting complex sources of inorganic material in the Pearl River. The varying contributions from the main stem, Hobolochitto Creak, freshwater swamps and seawater intrusions are likely related to the source of DIC in the river water (Shiller et al., 2012). In contrast, discharge showed negative correlation with DIC ($P<0.0001$, $r2 = 0.45$, Figure 4), suggesting dilution of inorganic material during high discharge in the Mississippi River (De Souza Sierra et al., 1994). These contrasting facts further emphasize the different hydrological conditions and sources of materials in the two rivers.

Spectral Slope. Spectral slope has been used as an indicator of CDOM molecular weight, as higher slope values are associated with lower molecular weight or lower aromaticity, and lower slope values suggests higher molecular weight and greater aromatic content (Blough and Del Vecchio, 2002; Moran et al., 2000). Spectral slope values derived from the wavelength interval 290-400 nm

($S_{290-400}$)varied in the lower Pearl River from 13.3-17.2 $\times 10^{-3}$ nm^{-1} (mean=15.4$\times 10^{-3}$ nm^{-1}, Figure 3).

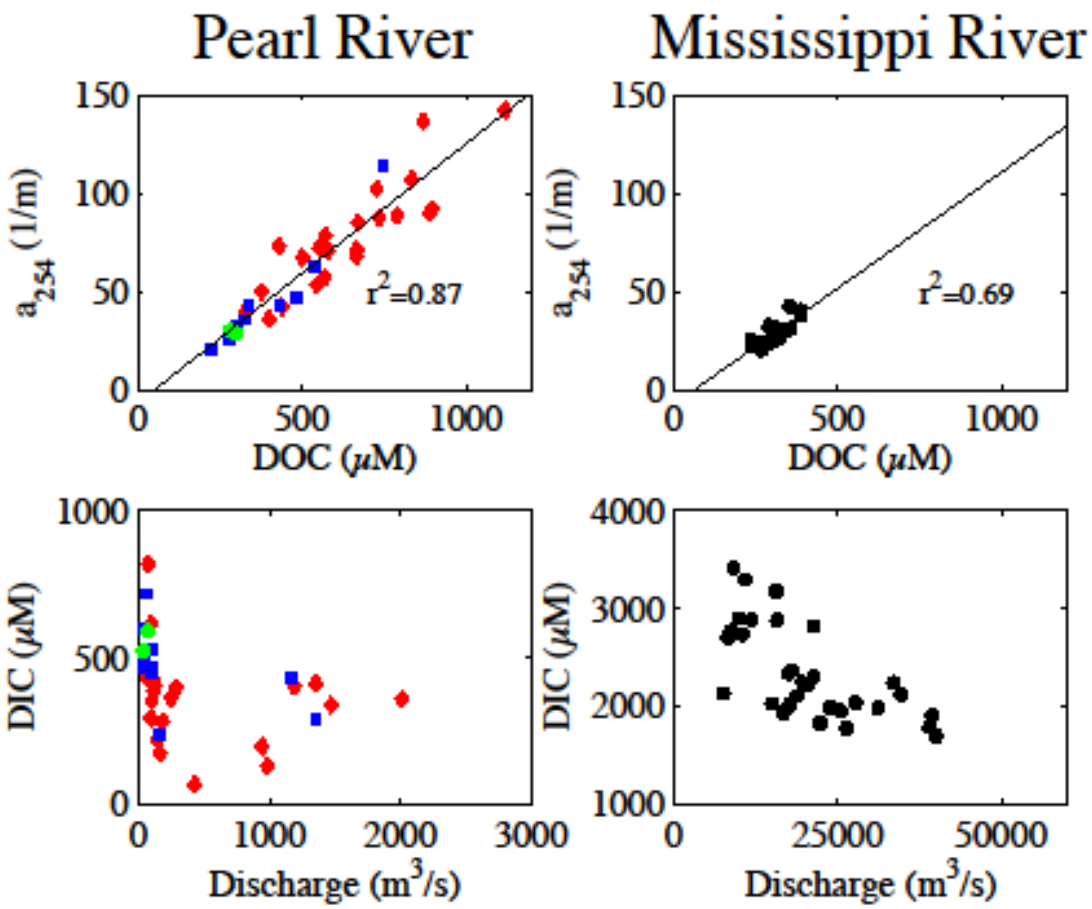

Figure 4. Relations Among DOC, a254, pH, Discharge And Dissolved Inorganic Carbon In The Lower Pearl And Mississippi Rivers. The Red Diamonds Represent Pearl River Samples Taken At The Stennis Space Center. Blue Squares Represent Samples From Bogalusa. Green Circles Are For Samples At The West Pearl River.

No significant relationship was found between $S_{290-400}$ and discharge. The $S_{290-400}$ in the lower Mississippi River ranged from 13.7-18.0 $\times 10^{-3}$ nm^{-1} (mean=16.4$\times 10^{-3}$ nm^{-1}, Figure 3), and showed a inverse seasonal variation to discharge (P=0.015, r^2=0.21).

Specific Ultraviolet Absorbance. Specific UV absorbance at 254 nm ($SUVA_{254}$) has been associated with aromaticity of DOM (Weishaar et al., 2003).

In this study, $SUVA_{254}$ ranged from 3.23 to 6.14 m^2/g-C (mean=4.23 m^2/g-C, Figure 3) in the lower Pearl River. Samples collected from the lower Mississippi River ranged from 2.74-4.34 m^2/g-C (mean=3.32 m^2/g-C, Figure 3). Week or no correlations between $SUVA_{254}$ and discharge were found in the Pearl ($P<0.01$, $r^2=0.20$) and Mississippi rivers, respectively. The $SUVA_{254}$ and $S_{290-400}$ values are intensive properties that are irrelevant to the abundance of DOM but the state and characteristics of it. As compared with the quantitative parameters (i.e. DOC and a_{254}) that are closely correlated with discharge, these intensive parameters showing week or no significant correlation with discharge seemed to have more than one controlling factors besides river flow rate.

HMW-DOC

The colloidal size fraction of DOC (between 1kDa and 0.45 µm) in the Pearl River ranged from 62-77% (mean=69%), while colloidal fraction for samples from the lower Mississippi River ranged from 52-64% (mean=58%). The concentration of high molecular weight (HMW) DOC in the Pearl River ranged from 140- 460 µM (mean=327 µM). Samples collected from the lower Mississippi River had HMW DOC concentration ranging from 151-204 µM (mean=176 µM).

No positive correlation was observed between discharge and colloidal size fraction. However, HMW DOC concentration was found to correlate with discharge in Pearl River ($P<0.05$, $r^2=0.57$) and Mississippi River ($P<0.02$, $r^2=0.44$) (Figure 5). HMW DOC in both rivers seemed to increase with increasing discharge, suggesting flushing of more HMW-DOC from the surface soil during higher discharge. It's noteworthy that during the flood in the Pearl River in April

2009, the concentration of HMW-DOC was not as high as one can expect from the interpolation of the discharge and HMW-DOC data at relatively lower discharge (< 500m^3/s) scenario. HWM-DOC only increased to a very limited extent during the flood, suggesting changes in water sources and possibly limited supply of HMW-DOC from the surface soil horizon and the effect of dilution during flood season.

No positive correlation was found between DOC concentration and colloidal fraction in the two rivers. Interestingly, higher colloidal fraction of DOM seemed to occur during high DOC concentration period in the Pearl River, while lower colloidal DOM fraction seemed to associate more with higher DOC concentration in the Mississippi River (Figure 5). This could be linked to DOM source and composition in these two rivers. DOM in the Pearl River has relatively limited sources; mainly instantaneous inputs from terrestrial origins such as soil, plant litter, fresh water swamps. In the contrast, DOM in the Mississippi River has more diverse origins and exist in more degraded status due to degradation. In addition to terrestrial sources, relatively high amount of DOM is also produced *in situ* by phytoplankton. Thus, increased flow rate in the Pearl River is likely accompanied with increased input of DOM, while in the Mississippi River can cause dilution of the aquagenic DOM. Limited data points and the difference in the abundance of DOM in the two rivers make this comparison difficult. Increased sample collection would provide better elucidation of the source of colloidal DOM.

Fluorescence Characteristics of DOM in the Rivers

Fluorescence EEMs. Fluorescence EEMs can provide additional information regarding CDOM in the river samples. Figure 6 shows some examples of the fluorescence EEMs from the two rivers. The left column of Figure 6 shows the fluorescence EEMs of the dissolved phase (<0.45 µM), low molecular weight (LMW, <1 kD) and high molecular weight (HMW, >1kD and <0.45µM) fractions of the sample collected from the Mississippi River on May 29, 2009.

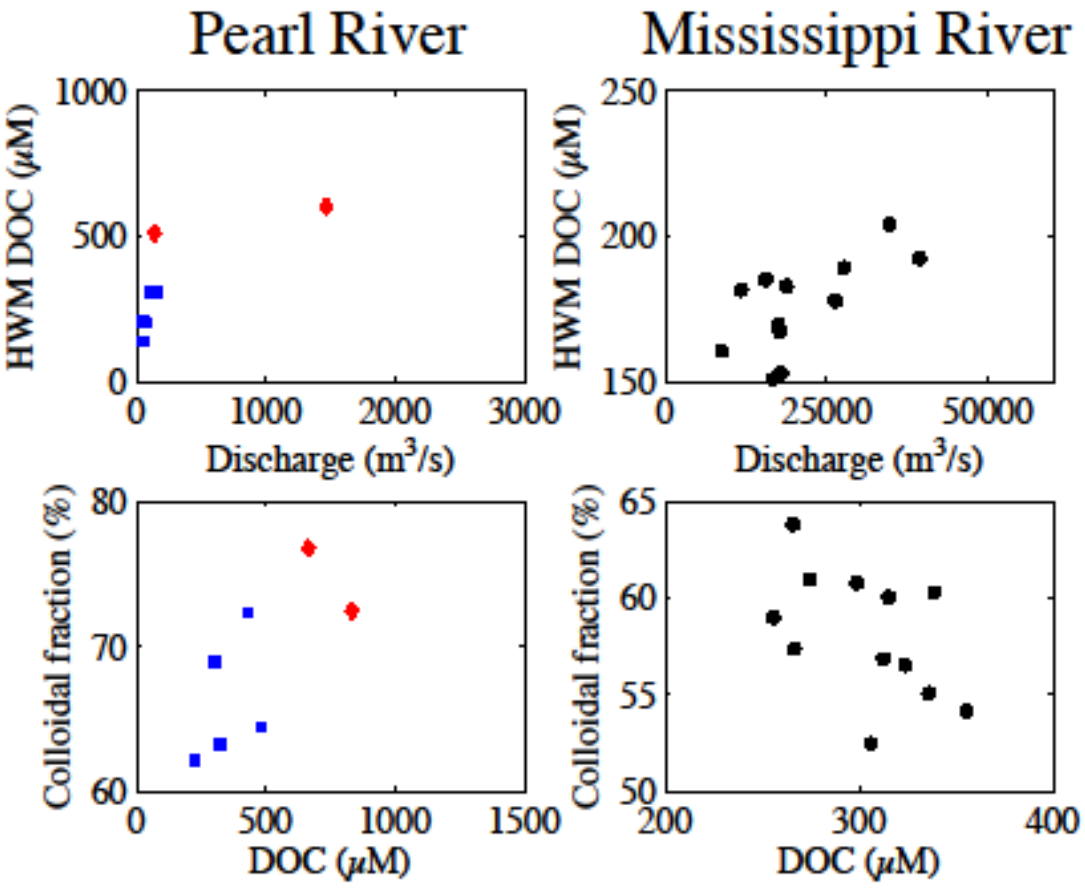

Figure 5. Relations Among Discharge, Concentration Of DOC And High Molecular Weight (HMW) DOC, And The Fraction Colloidal DOM In The Lower Pearl And Mississippi Rivers. The Red Diamonds Represent Pearl River Samples Taken At The Stennis Space Center. Blue Squares Represent Samples From Bogalusa.

LMW DOM seemed to have high relative importance of UV-humic like DOM at ~ Ex/Em 240/460 nm, and also some fractions of tryptophan-like material at Ex/Em ~230/340 nm. In contrast, HMW DOM showed high fluorescence intensity at Ex/Em wavelengths 340/450 nm, but greatly decreased fluorescence signals at lower excitation and emission wavelengths, suggesting partitioning of distinct DOM in specific size fractions.

The right column of Figure 6 shows the variation of fluorescence EEMs before, during the peak, and at the end of a flood in the Pearl River. The flood seemed to have resulted in elevated fluorescence intensity, especially at wavelengths corresponding the terrestrial humic-like materials at Ex/Em ~ 340/450 nm, on April 02, 2009, as compared to that in January 2009. Fluorescence intensity began to fall at the end of flood on April 07, 2009 to lower than that during the flood peak.

PARAFAC Components. To statistically analyze the fluorescent DOM components, a six-component model was successfully validated when applying the PARAFAC analysis on our monthly samples from the Pearl River and Mississippi River. The excitation and emission wavelengths corresponding to the peak of these components are listed in Table 4, and the EEM contours of them are shown in Figure 7. It has been found that DOM present in different environments show similar fluorescence characteristics (Alberts and Takács, 2004), very likely caused by the quinone-like fluorophores existing in natural DOM (Cory and McKnight, 2005), including humic and fulvic acid (Thorn et al., 1992).

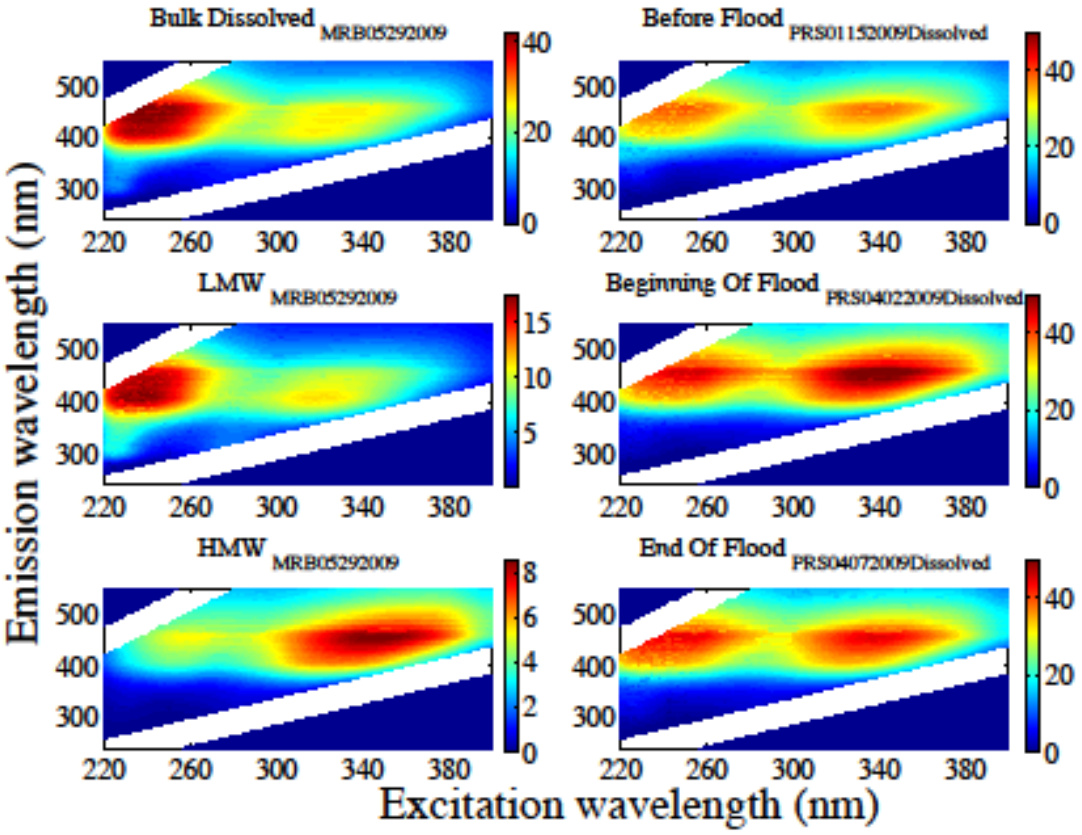

Figure 6. Examples Of fluorescence EEMs Of River Samples, Including Those Of Bulk DOM, LMW-DOM (<1 kDa), And HMW-DOM (>1 kDa) In The Mississippi River (left column, sample collected on May 29, 2009) And Those Of Samples Before, During And At The End Of A Flood Event In The Pearl River During April 2009.

This allows one to associate the PARAFAC components to other fluorophores described in the literature. The first component in the river waters, with Ex/Em maximum at 374/465 nm, has the characteristic of the Peak “C” in literature (Coble, 1996) and also resembles that of the component 3 reported by Stedmon et al. (2003), thus can be identified as a visible humic- like component. The second component has a peak at Ex/Em 244/454 nm, likely associated with the Peak “A” (UV humic-like) reported by Coble (1996). The third component with

Ex/Em at 334/409 nm, seems to be similar to the component 4 in Stedmon et al. (2003), which was suggested to be terrestrially derived organic matter.

Table 4

Characteristics of the Six Fluorescence DOM Components in Mississippi and Pearl Rivers Identified by PARAFAC Modeling.

Component	Excitation Maximum (nm)	Emission Maximum (nm)	Description
Component – 1	374	465	Visible humic-like DOM
Component – 2	244	454	UV humic-like DOM
Component – 3	334	409	Terrestrially derived organic matter
Component – 4	264	511	Intermediates of photo-chemically degraded terrestrial DOM
Component – 5	224	477	Photochemical degradation product of terrestrial organic matter
Component – 6	236	366	Amino acids from biological production

The fourth component, characterized with emission peak at >500 nm under excitation at 264 nm, lies within close proximity of the component 3 in Stedmon et al. (2007), and is likely to be a terrestrially derived material that acts as an intermediate of photochemical degradation of terrestrial DOM. The fifth component, showing an Ex/Em maximum at 224/477 nm, appears to be a

photochemical product of terrestrial organic matter, although the origin is not certain yet (Stedmon et al., 2007).

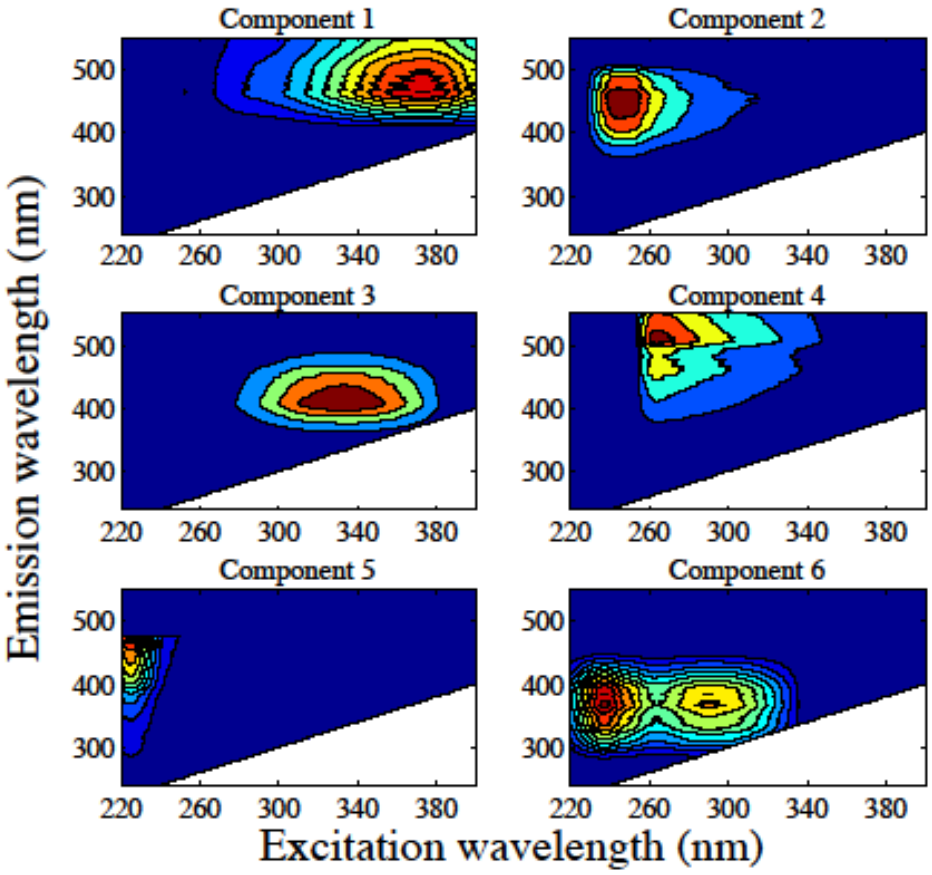

Figure 7. Characteristics Of Six Major DOM Components Identified By Fluorescence PARAFAC Modeling For Samples From The Lower Pearl And Mississippi Rivers.

The sixth component has two peaks at Ex/Em ~230/360 and ~275/360 nm, respectively, and seems to be a combination of the “N” and the “T” peaks in the literature (Coble, 1996; Coble et al., 1998; Stedmon et al., 2003). The “N” peak has been linked to some labile materials derived from biological production (Coble et al., 1998), while the “T” peak is believed due to the indole ring structure of tryptophan and likely to have origin from biological production in surface

waters. The sixth component, thus, is linked to amino acids and biological production. As pointed out by Stedmon et al. (2003), failure to separate the two peaks is probably caused by the limited number of samples. A larger sample set with increased number of samples would possibly allow us to separate the two chemical compounds in this fluorescent component.

The emission wavelength of component 1 (Em >400nm) is likely linked to more conjugated fluorescent molecules (Sharma and Schulman, 1999), and Stedmon et al. (2003) suggested a component with a similar peak position to be terrestrially derived humic-like material with high molecular weight. Our results are in correspondence with these finding through the fluorescence signatures of ultra-filtered river water samples, where showed fluorescence intensity at Ex/Em 340/450 nm is low in the LMW-DOM fraction and high in the HWM-DOM fraction, and the PARAFAC results identifying peak at Ex/Em 340/450 nm as visible terrestrial humic-like material, “C”, (Component 1). Thus Component 1 is identified as visible humic-like DOM with high molecular weight. Component 6, in contrast, is low in emission wavelength and low in the >1 kDa HMW fraction in both rivers. Fluorescence EEM of LMW-DOM also showed a higher fraction of tryptophan-like material, in agreement with the origin of component 6. Thus, component 6 shows signatures of amino acids with low molecular weight. Similar linkage between fluorescence component and molecular weight have also been found using both fluorescence EEM and flow field flow fractionation (Cuss and Guéguen, 2012).

PARAFAC components and fluorescence indices in the rivers. The fluorescence intensities of DOM components derived from PARAFAC analysis varied differently in the two rivers (Figure 8), showing different source, composition and behavior in the rivers.

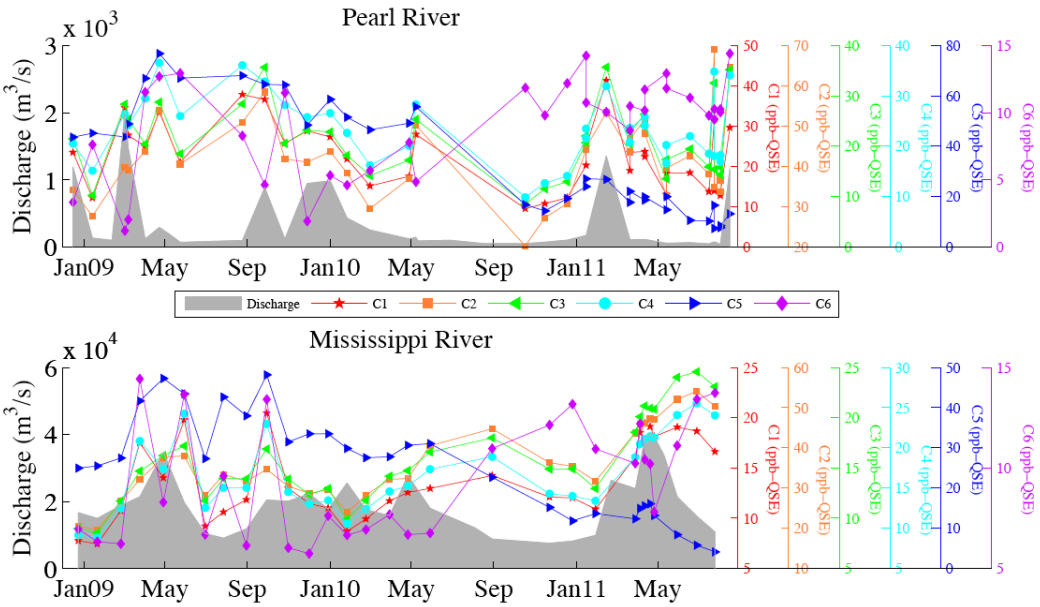

Figure 8. Seasonal Variations In Discharge (m3/s) And Fluorescence Intensities (ppb-QSE) Of DOM Components Derived From PARAFAC Modeling In The Lower Pearl And Mississippi Rivers.

The relative importance of component 1 (as normalized to the total fluorescence intensity of all the six components) increased with increasing discharge in both rivers (Figure 9) while that of component 6 decreased with increasing discharge, reflecting different sources of the two DOM components. Component 1 probably has its origin from flushing of surface soil during high flow, while component 6 is likely aquagenic DOM produced autochthonously. Sources of DOM can be indicated by different indices. The biological index (BIX), defined as the ratio of fluorescence intensity at 380 nm to that at 430 nm under the excitation wavelength of 310 nm, represents the existence of beta

fluorophore, which is indicative of autochthonous biological activity in natural waters (Huguet et al., 2009). Values of BIX between 0.8 and 1.0 have been measured in freshly produced (biological/microbial origin) DOM, and BIX values smaller than 0.6 represent little autochthonous DOM.

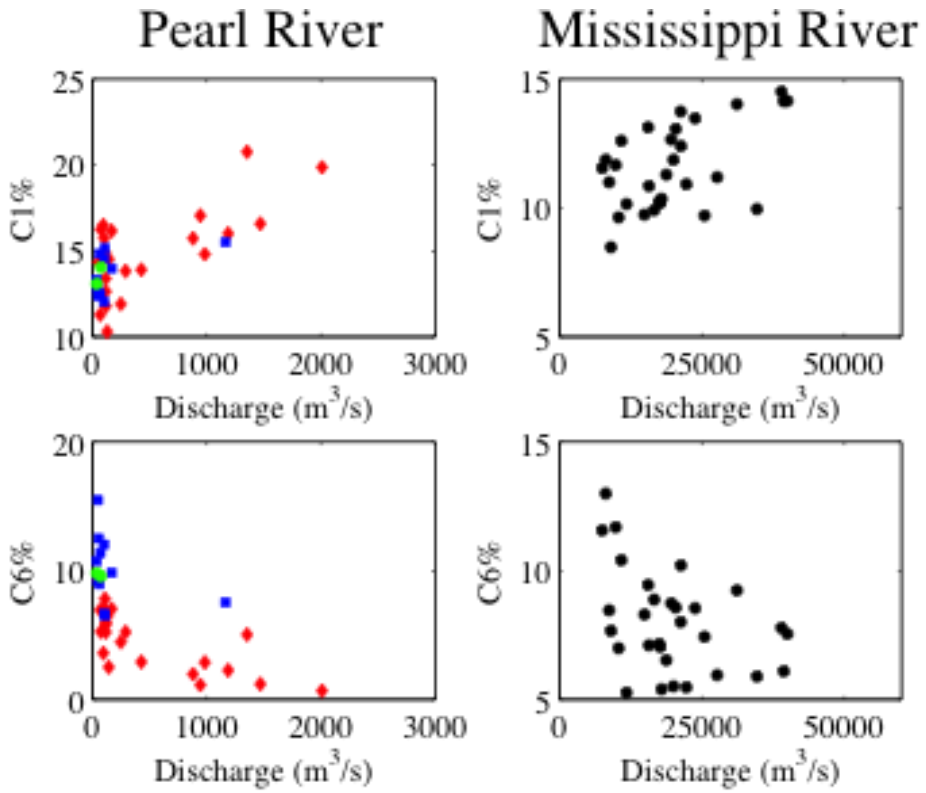

Figure 9. Relations Among Discharge, Percentage Of C1 And C6 In The Lower Pearl And Mississippi Rivers.

Biological index values decreased with increasing discharge in both the Pearl River ($P<0.00001$, $r^2=0.38$) and Mississippi River ($P<0.00001$, $r^2=0.61$) (Figure 10). Very similar correlation with discharge has been found for BIX and C6% values. It is reflecting the close relation of both these two parameters to *in situ* phytoplankton production. The negative correlations of BIX and C6% with discharge are likely caused by the dilution of freshly produced DOM during high flow.

Comparisons between the Mississippi River and Pearl River

In the lower Pearl River, our results show a large seasonal variability in both DOC and a_{254} and a significant correlation of DOC (or absorbance) with discharge, similar to findings in previous studies and highlighting a strong seasonal fluctuation of DOC in small rivers (Malcolm and Durum, 1976).

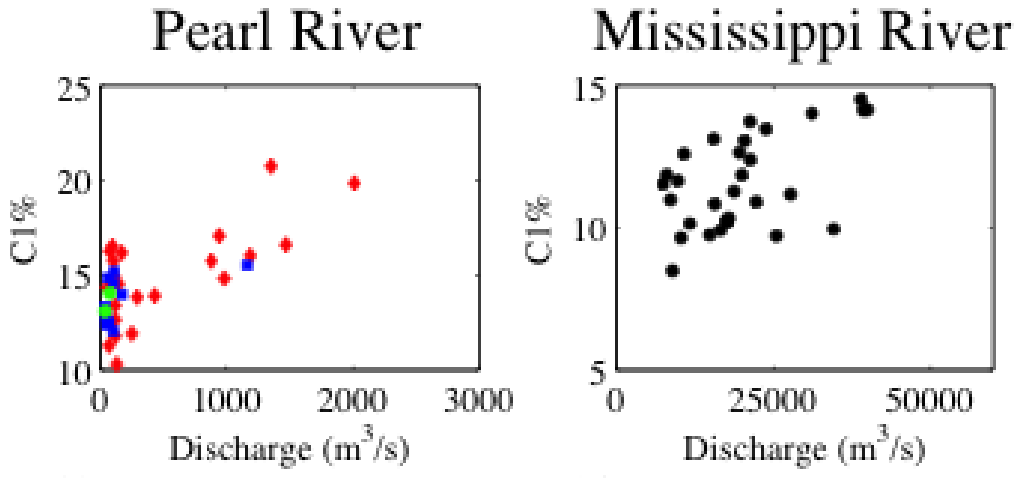

Figure 10. Relations Among Discharge And Biological Index in The Lower Pearl And Mississippi Rivers.

This high seasonality is likely indicative of sources of DOM from local inputs controlled by hydrological processes, such as surface soils and plant litters (Duan et al., 2007a). The substantial seasonal variations of DOM in the Pearl River concurrent with changes in hydrological conditions suggest a strong connection of riverine processes to the type of landscape and land cover in the drainage basin.

DOM in the Mississippi River, in the contrast, showed a small seasonal variation, and was probably controlled by complex upstream inputs from primary tributaries (Duan et al., 2007a), instead of hydrological transport of local inputs. Duan et al. (2007a, b) suggested mixing water from three primary tributaries as

main contributors of seasonal variation in DOC abundance in the lower Mississippi River, and that *in situ* processing of DOM plays an important role in regulating DOC concentrations.

DIP concentration were found significantly higher in the Mississippi River, as compared with that in the Pearl River, reflecting higher extent of human impacts (Cai and Guo, 2009). Construction of dams and levees could have substantially increased the transition time of water and DOM in the Mississippi River, and thus make them subject to extensive photo- and bio- degradation before reaching the lower section of the river. Longer transition time of river waters may also increase the production of aquagenic DOM in the river, altering the composition of riverine DOM. Indeed, *in situ* processing of DOM has been linked with decreased aromatic carbons and increased carboxyl carbon in DOM under exposure to bacterial decomposition and photochemical oxidation (Engelhaupt and Bianchi, 2001; Osburn et al., 2001). A low fraction of CDOM or acidic DOM in the lower Mississippi River implies longer-term *in situ* river processing. The lower percentage of HMW DOC, higher spectral slope or more low molecular weight DOM in the lower Mississippi River further suggests greater extent of photochemical and microbial removal of organic matter, as compared with the Pearl River (Figure 5).

Consistently, higher BIX values in the Mississippi River (Figure 10) suggest more freshly produced DOM and higher microbial activity in the water column. Furthermore, higher non-chromophoric DOC in the Mississippi River further indicates the presence of a fraction of degraded DOM.

In the Pearl River, more local sources from surface soils and plant litters and limited *in situ* river processing of DOM are consistent with previous studies using biomarkers and bulk DOM (Duan et al., 2007a; Duan et al., 2007b).

Effect of flood on river DOM

Higher DOC and absorbance values were found in both the Pearl and Mississippi Rivers during flood seasons. Elevated DOC export (~90 fold) during flooding as compared to that of base flow was found in a Midwestern agricultural watershed, and increase in both discharge and DOC concentration were responsible for the flux change (Dalzell et al., 2005). Duan et al. (2007b) also observed higher DOC concentrations, enriched carboxyl and aromatic carbons in high molecular weight (HWM) DOM in the Pearl River during flooding. Greater proportion of hydrophilic carbon and less acid fractions of DOM in deep layers of soils as compared with surface soils (Cronan and Aiken, 1985; Kaiser et al., 2004b; Williams and Melack, 1997; Yano et al., 2005a; Yano et al., 2005b) was likely responsible for this change in sources and characteristics of DOM during different flood conditions.

Conclusions

Dissolved organic matter was characterized using CDOM measurement and fluorescence EEM analysis coupled with PARAFAC modeling in the lower Mississippi River and Pearl River.

Higher bulk DOM abundance was found in the Pearl River with higher HMW-DOM and colloidal fraction, readily linked to fresh source of DOM. Higher

non-chromophoric DOM was found in the Mississippi River, indicating the presence of more degraded DOM in the river system.

DOM in the Pearl River showed a great seasonal variability and sources from surface soil and plan litters. *In situ* processing is limited in the Pearl River. In contrast, DOM in the Mississippi River is subjected to a completely different set of sources and processing. An integrated signal from large amount of tributaries make the seasonal variability of DOM in the Mississippi River limited. Dam constructions and levees largely increased the retention time of DOM in the Mississippi River, resulting in strong photo- and bio-degradation of DOM and thus a decrease in aromatic and an increase in aquagenic DOM components.

A six-component model was validated from the river samples. Terrestrial humic-like DOM, UV humic-like DOM, degradation products of terrestrial organic matter, as well as protein-like materials are all amount the components.

REFERENCE

Aitkenhead, J.A. and McDowell, W.H., 2000. Soil C:N ratio as a predictor of annual riverine DOC flux at local and global scales. Global Biogeochem. Cycles 14(1), 127-138, doi: 10.1029/1999gb900083.

Alberts, J.J. and Takács, M., 2004. Total luminescence spectra of IHSS standard and reference fulvic acids, humic acids and natural organic matter: comparison of aquatic and terrestrial source terms. Organic Geochemistry 35(3), 243-256, doi: 10.1016/j.orggeochem.2003.11.007.

Andersen, C.M. and Bro, R., 2003. Practical aspects of PARAFAC modeling of fluorescence excitation-emission data. Journal of Chemometrics 17(4), 200-215, doi: 10.1002/cem.790.

Beckett, D.C. and Pennington, C.H., 1986. Water quality, macroinvertebrates, larval fishes, and fishes of the lower mississippi river - a synthesis U.S. Army Corps of Engineers, Technical Report. Waterways Experiment Station, Vicksburg, MS.

Bianchi, T.S. et al., 2010. The science of hypoxia in the Northern Gulf of Mexico: A review. Science of The Total Environment 408(7), 1471-1484.

Bianchi, T.S., Lambert, C.D., Santschi, P.H. and Guo, L., 1997. Sources and transport of land-derived particulate and dissolved organic matter in the Gulf of Mexico (Texas shelf/slope): The use of ligninphenols and loliolides as biomarkers. Organic Geochemistry 27(1-2), 65-78, doi: 10.1016/s0146-6380(97)00040-5.

Blough, N.V. and Del Vecchio, R., 2002. Chromophoric DOM in the coastal environment. In: D.A. Hansell and C.A. Carlson (Editors), Biogeochemistry of marine dissolved organic matter. Academic Press, San Diego, CA, pp. 509-546.

Boyd, T.J. and Osburn, C.L., 2004. Changes in CDOM fluorescence from allochthonous and autochthonous sources during tidal mixing and bacterial degradation in two coastal estuaries. Marine Chemistry 89(1-4), 189-210, doi: 10.1016/j.marchem.2004.02.012.

Boyer, E.W., Hornberger, G.M., Bencala, K.E. and McKnight, D.M., 1997. Response characteristics of DOC flushing in an alpine catchment. Hydrological Processes 11(12), 1635-1647, doi: 10.1002/(sici)1099-1085(19971015)11:12<1635::aid-hyp494>3.0.co;2-h.

Cai, Y. and Guo, L., 2009. Abundance and variation of colloidal organic phosphorus in riverine, estuarine, and coastal waters in the northern Gulf of Mexico. Limnology and Oceanography 54(4), 1393-1402, doi: 10.4319/lo.2009.54.4.1393.

Cai, Y., Guo, L., Wang, X., Lohrenz, S.E. and Mojzis, A.K., 2012. Effects of tropical cyclones on river chemistry: A case study of the Pearl River, Mississippi during Hurricanes Gustav and Ike. Estuaries and Coasts, (in review).

Coble, P.G., 1996. Characterization of marine and terrestrial DOM in seawater using excitation-emission matrix spectroscopy. Marine Chemistry 51(4), 325-346, doi: 10.1016/0304-4203(95)00062-3.

Coble, P.G., Del Castillo, C.E. and Avril, B., 1998. Distribution and optical properties of CDOM in the Arabian Sea during the 1995 Southwest Monsoon. Deep Sea Research Part II: Topical Studies in Oceanography 45(10-11), 2195-2223, doi: 10.1016/s0967-0645(98)00068-x.

Cory, R.M. and McKnight, D.M., 2005. Fluorescence spectroscopy reveals ubiquitous presence of oxidized and reduced quinones in dissolved organic matter. Environmental Science & Technology 39(21), 8142-8149, doi: 10.1021/es0506962.

Coynel, A., Seyler, P., Etcheber, H., Meybeck, M. and Orange, D., 2005. Spatial and seasonal dynamics of total suspended sediment and organic carbon species in the Congo River. Global Biogeochem. Cycles 19(4), GB4019, doi: 10.1029/2004gb002335.

Cronan, C.S. and Aiken, G.R., 1985. Chemistry and transport of soluble humic substances in forested watersheds of the Adirondack Park, New York. Geochimica et Cosmochimica Acta 49(8), 1697-1705, doi: 10.1016/0016-7037(85)90140-1.

Cuss, C.W. and Guéguen, C., 2012. Determination of relative molecular weights of fluorescent components in dissolved organic matter using asymmetrical flow field-flow fractionation and parallel factor analysis. Analytica Chimica Acta 733(0), 98-102, 10.1016/j.aca.2012.05.003.

Dagg, M.J. et al., 2005. Biogeochemical Characteristics of the Lower Mississippi River, USA, during June 2003. Estuaries 28(5), 664-674.

Dalzell, B.J., Filley, T.R. and Harbor, J.M., 2005. Flood pulse influences on terrestrial organic matter export from an agricultural watershed. J. Geophys. Res. 110(G2), G02011, doi: 10.1029/2005jg000043.

De Souza Sierra, M.M., Donard, O.F.X., Lamotte, M., Belin, C. and Ewald, M., 1994. Fluorescence spectroscopy of coastal and marine waters. Marine Chemistry 47(2), 127-144, doi: 10.1016/0304-4203(94)90104-x.

Duan, S., Bianchi, T.S. and Sampere, T.P., 2007a. Temporal variability in the composition and abundance of terrestrially-derived dissolved organic matter in the lower Mississippi and Pearl Rivers. Marine Chemistry 103(1-2), 172-184, doi: 10.1016/j.marchem.2006.07.003.

Duan, S. et al., 2007b. Variability in the bulk composition and abundance of dissolved organic matter in the lower Mississippi and Pearl rivers. Journal of Geophysical Research 112(G2), G02024, doi: 10.1029/2006JG000206.

Engelhaupt, E. and Bianchi, T.S., 2001. Sources and Composition of High-Molecular-Weight Dissolved Organic Carbon in a Southern Louisiana Tidal Stream (Bayou Trepagnier). Limnology and Oceanography 46(4), 917-926.

Findlay, S. and Sinsabaugh, R.L., 1999. Unravelling the sources and bioavailability of dissolved organic matter in lotic aquatic ecosystems. Marine and Freshwater Research 50(8), 781-790, doi: org/10.1071/MF99069.

Findlay, S., Sinsabaugh, R.L., Fischer, D.T. and Franchini, P., 1998. Sources of dissolved organic carbon supporting planktonic bacterial production in the

tidal freshwater hudson river. Ecosystems 1(3), 227-239, doi: 10.1007/s100219900018.

Fulton, J. et al., 2004. Changes in fulvic acid redox state through the oxycline of a permanently ice-covered Antarctic lake. Aquatic Sciences - Research Across Boundaries 66(1), 27-46, doi: 10.1007/s00027-003-0691-4.

Goolsby, D.A. and Battaglin, W.A., 2001. Long-term changes in concentrations and flux of nitrogen in the Mississippi River Basin, USA. Hydrological Processes 15(7), 1209-1226, doi: 10.1002/hyp.210.

Goolsby, D.A., Battaglin, W.A., Aulenbach, B.T. and Hooper, R.P., 2000. Nitrogen flux and sources in the Mississippi River Basin. Science of The Total Environment 248(2-3), 75-86, doi: 10.1016/s0048-9697(99)00532-x.

Guo, L. and Macdonald, R.W., 2006. Source and transport of terrigenous organic matter in the upper Yukon River: Evidence from isotope (δ13C,∆14C, andδ15N) composition of dissolved, colloidal, and particulate phases. Global Biogeochem. Cycles 20(2), GB2011, doi: 10.1029/2005gb002593.

Guo, L. and Santschi, P.H., 1996. A critical evaluation of the cross-flow ultrafiltration technique for sampling colloidal organic carbon in seawater. Marine Chemistry 55(1-2), 113-127.

Guo, L. and Santschi, P.H., 2007. Ultrafiltration and its applications to sampling and characterisation of aquatic colloids. In: K.J. Wilkinson and J.R. Lead (Editors), Environmental colloids and particles. John Wiley & Sons, Ltd, pp. 159–221, doi: 10.1002/9780470024539.ch4.

Guo, L., Santschi, P.H. and Warnken, K.W., 1995. Dynamics of dissolved organic carbon (DOC) in oceanic environments. Limnology and Oceanography 40(8), 1392-1403.

Guo, M. and Chorover, J., 2003. Transport and fractionation of dissolved organic matter in soil columns. Soil Science 168(2), 108-118.

Hall, G.J., Clow, K.E. and Kenny, J.E., 2005. Estuarial fingerprinting through multidimensional fluorescence and multivariate analysis. Environmental Science & Technology 39(19), 7560-7567, doi: 10.1021/es0503074.

Hedges, J.I., Keil, R.G. and Benner, R., 1997. What happens to terrestrial organic matter in the ocean? Organic Geochemistry 27(5-6), 195-212, doi: 10.1016/s0146-6380(97)00066-1.

Hedges, J.I. et al., 2000. Organic matter in Bolivian tributaries of the Amazon River: a comparison to the lower mainstream. Limnology and Oceanography 45(7), 1449-1466.

Hope, D., Billett, M.F. and Cresser, M.S., 1994. A review of the export of carbon in river water: Fluxes and processes. Environmental Pollution 84(3), 301-324, doi: 10.1016/0269-7491(94)90142-2.

Hopkinson, C.S., Jr. and Vallino, J.J., 1995. The relationships among man's activities in watersheds and estuaries: a model of runoff effects on patterns of estuarine community metabolism. Estuaries 18(4), 598-621.

Huguet, A. et al., 2009. Properties of fluorescent dissolved organic matter in the Gironde Estuary. Organic Geochemistry 40(6), 706-719, doi: 10.1016/j.orggeochem.2009.03.002.

Ittekkot, V., Safiullah, S., Mycke, B. and Seifert, R., 1985. Seasonal variability and geochemical significance of organic matter in the River Ganges, Bangladesh. Nature 317(6040), 800-802, doi: 10.1038/317800a0.

Jacinthe, P.-A., Lal, R. and Kimble, J.M., 2001. Organic carbon storage and dynamics in croplands and terrestrial deposits as influenced by subsurface tile drainage. Soil Science 166(5), 322-335.

Jaffé, R. et al., 2008. Spatial and temporal variations in DOM composition in ecosystems: The importance of long-term monitoring of optical properties. J. Geophys. Res. 113(G4), G04032, doi: 10.1029/2008jg000683.

Kaiser, E., Arscott, D., Tockner, K. and Sulzberger, B., 2004a. Sources and distribution of organic carbon and nitrogen in the Tagliamento River, Italy. Aquatic Sciences - Research Across Boundaries 66(1), 103-116, doi: 10.1007/s00027-003-0683-4.

Kaiser, K., Guggenberger, G. and Haumaier, L., 2004b. Changes in dissolved lignin-derived phenols, neutral sugars, uronic acids, and amino sugars with depth in forested Haplic Arenosols and Rendzic Leptosols. Biogeochemistry 70(1), 135-151, doi: 10.1023/b:biog.0000049340.77963.18.

Kammerer, J.C., 1990. Largest Rivers in the United States. U.S. Geological Survey.

Keown, M.P., Dardeau, E.A., Jr. and Causey, E.M., 1986. Historic Trends in the Sediment Flow Regime of the Mississippi River. Water Resour. Res. 22(11), 1555-1564, doi: 10.1029/WR022i011p01555.

Lal, R., 2004. Soil carbon sequestration impacts on global climate change and food security. Science 304(5677), 1623-1627.

Leenheer, J.A. and Croué, J.P., 2003. Peer reviewed: characterizing aquatic dissolved organic matter. Environmental Science and Technology 37(1), 18A-26A, doi: 10.1021/es032333c.

Leenheer, J.A., Noyes, T.I., Brown, P.A. and Geological, S., 1995. Data on natural organic substances in dissolved, colloidal, suspended-silt and -clay, and bed-sediment phases in the Mississippi River and some of its tributaries, 1987-90. U.S. Dept. of the Interior, U.S. Geological Survey ; U.S. Geological Survey, Earth Science Information Center, Open-File Reports Section [distributor], Denver, Colo.; Denver, CO.

Logan, B. and Jiang, Q., 1990. Molecular Size Distributions of Dissolved Organic Matter. Journal of Environmental Engineering 116(6), 1046-1062, doi:10.1061/(ASCE)0733-9372(1990)116:6(1046).

Malcolm, R.L. and Durum, W.H., 1976. Organic carbon and nitrogen concentrations and annual organic carbon load of six selected rivers of the United States. U.S. Geol. Surv. Wateer Supply Pap. U.S. Dept. of the Interior, U.S. Geological Survey : for sale by the Supt. of Docs., U.S. Govt. Print. Off. (Washington), Washington, 1-29 pp.

Martin-Mousset, B., Croue, J.P., Lefebvre, E. and Legube, B., 1997. Distribution and characterization of dissolved organic matter of surface waters. Water Research 31(3), 541-553, 10.1016/s0043-1354(96)00259-x.

McKnight, D.M. et al., 2001. Spectrofluorometric characterization of dissolved organic matter for indication of precursor organic material and aromaticity. Limnology and Oceanography 46(1), 38-48.

Meade, R.H., Yuzyk, T.R. and Day, T.J., 1990. Movement and storage of sediment in rivers of the United States and Canada. In: M.G. Wolman and H.C. Riggs (Editors), Surface Water Hydrology. Geological Society of America, Boulder, Colorado, pp. 255-280.

Meybeck, M., 2003. Global analysis of river systems: from Earth system controls to Anthropocene syndromes. Philosophical Transactions of the Royal Society of London. Series B: Biological Sciences 358(1440), 1935-1955, doi: 10.1098/rstb.2003.1379.

Miller, M.P. and McKnight, D.M., 2010. Comparison of seasonal changes in fluorescent dissolved organic matter among aquatic lake and stream sites in the Green Lakes Valley. J. Geophys. Res. 115, G00F12, doi: 10.1029/2009jg000985.

Moore, T.R., 1989. Dynamics of dissolved organic carbon in forested and disturbed catchments, Westland, New Zealand: 1. Maimai. Water Resour. Res. 25(6), 1321-1330, doi: 10.1029/WR025i006p01321.

Mopper, K. and Schultz, C.A., 1993. Fluorescence as a possible tool for studying the nature and water column distribution of DOC components. Marine Chemistry 41(1-3), 229-238, doi: 10.1016/0304-4203(93)90124-7.

Moran, M.A., Sheldon, W.M., Jr. and Zepp, R.G., 2000. Carbon loss and optical property changes during long-term photochemical and biological

degradation of estuarine dissolved organic matter. Limnology and Oceanography 45(6), 1254-1264.

Osburn, C., Morris, D., Thorn, K. and Moeller, R., 2001. Chemical and optical changes in freshwater dissolved organic matter exposed to solar radiation. Biogeochemistry 54(3), 251-278, doi: 10.1023/a:1010657428418.

Parlanti, E., Wörz, K., Geoffroy, L. and Lamotte, M., 2000. Dissolved organic matter fluorescence spectroscopy as a tool to estimate biological activity in a coastal zone submitted to anthropogenic inputs. Organic Geochemistry 31(12), 1765-1781, doi: 10.1016/s0146-6380(00)00124-8.

Raymond, P.A., Bauer, J.E. and Cole, J.J., 2000. Atmospheric CO2 evasion, dissolved inorganic carbon production, and net heterotrophy in the York River Estuary. Limnology and Oceanography 45(8), 1707-1717.

Richey, J.E. et al., 1990. Biogeochemistry of Carbon in the Amazon River. Limnology and Oceanography 35(2), 352-371.

Sharma, A. and Schulman, S.G., 1999. Introduction to fluorescence spectroscopy. Wiley, New York.

Shiller, A.M., Duan, S., Erp, P.V. and Bianchi, T.S., 2006. Photo-oxidation of dissolved organic matter in river water and its effect on trace element speciation. Limnology and Oceanography 51(4), 1716-1728.

Shiller, A.M. et al., 2012. Hurricane Katrina impact on water quality in the East Pearl River, Mississippi. Journal of Hydrology 414-415(0), 388-392.

Spencer, R.G.M., Aiken, G.R., Wickland, K.P., Striegl, R.G. and Hernes, P.J., 2008. Seasonal and spatial variability in dissolved organic matter quantity

and composition from the Yukon River basin, Alaska. Global Biogeochem. Cycles 22(4), GB4002.

Spitzy, A. and Leenheer, J.A., 1990. Dissolved organic carbon in rivers. In: E.T. Degens, S. Kempe and J.E. Richey (Editors), Biogeochemistry of Major World Rivers. John Wiley and Sons Ltd, Chichester, West Sussex (United Kingdom), pp. 105-125.

State Environmental Protection Administration (SEPA) of China, 2002. Monitor and Analysis Method of Water and Wastewater. Chinese Environmental Science Publishing House, Beijing.

Stedmon, C.A. and Bro, R., 2008. Characterizing dissolved organic matter fluorescence with parallel factor analysis: a tutorial. Limnology and Oceanography - Methods 6, 572-579, doi: 10.4319/lom.2008.6.572.

Stedmon, C.A. and Markager, S., 2005. Resolving the Variability in Dissolved Organic Matter Fluorescence in a Temperate Estuary and Its Catchment Using PARAFAC Analysis. Limnology and Oceanography 50(2), 686-697.

Stedmon, C.A., Markager, S. and Bro, R., 2003. Tracing dissolved organic matter in aquatic environments using a new approach to fluorescence spectroscopy. Marine Chemistry 82(3-4), 239-254, doi: 10.1016/s0304-4203(03)00072-0.

Stedmon, C.A. et al., 2007. Photochemical production of ammonium and transformation of dissolved organic matter in the Baltic Sea. Marine Chemistry 104(3-4), 227-240, doi: 10.1016/j.marchem.2006.11.005.

Thorn, K.A., Arterburn, J.B. and Mikita, M.A., 1992. Nitrogen-15 and carbon-13 NMR investigation of hydroxylamine-derivatized humic substances. Environmental Science and Technology 26(1), 107-116, doi: 10.1021/es00025a011.

Thurman, E.M., 1985. Organic geochemistry of natural waters. Developments in biogeochemistry, 2. Martinus Nijhoff/Dr W. Junk, Hingham, MA, USA.

Trulleyová, Š. and Rulík, M., 2004. Determination of biodegradable dissolved organic carbon in waters: comparison of batch methods. Science of The Total Environment 332(1-3), 253-260, 10.1016/j.scitotenv.2004.04.018.

Vannote, R.L., Minshall, G.W., Cummins, K.W., Sedell, J.R. and Cushing, C.E., 1980. The river continuum concept. Canadian Journal of Fisheries and Aquatic Sciences 37(1), 130-137.

Volk, C.J., Volk, C.B. and Kaplan, L.A., 1997. Chemical composition of biodegradable dissolved organic matter in streamwater. Limnology and Oceanography 42(1), 39-44.

Weishaar, J.L. et al., 2003. Evaluation of specific ultraviolet absorbance as an indicator of the chemical composition and reactivity of dissolved organic carbon. Environmental Science and Technology 37(20), 4702-4708, doi: 10.1021/es030360x.

Wiener, J.G. et al., 1996. Mississippi River, Status and Trends of Nation's Biological Resources. National Weahter Resouces Center, U.S. Geological Survey, Washington, D.C., pp. 351-384.

Williams, C.J., Yamashita, Y., Wilson, H.F., Jaffé, R. and Xenopoulos, M.A., 2010. Unraveling the role of land use and microbial activity in shaping dissolved organic matter characteristics in stream ecosystems. Limnology and Oceanography 55(3), 1159-1171.

Williams, M.R. and Melack, J.M., 1997. Solute export from forested and partially deforested chatchments in the central Amazon. Biogeochemistry 38(1), 67-102, doi: 10.1023/a:1005774431820.

Yano, Y., Lajtha, K., Sollins, P. and Caldwell, B.A., 2005a. Chemical and seasonal controls on the dynamics of dissolved organic matter in a coniferous old-growth stand in the Pacific northwest, USA. Biogeochemistry 71(2), 197-223, doi: 10.1007/s10533-004-8130-8.

Yano, Y., Lajtha, K., Sollins, P. and Caldwell, B.A., 2005b. Chemistry and dynamics of dissolved organic matter in a temperate coniferous forest on andic soils: effects of litter quality. Ecosystems 8(3), 286-300, doi: 10.1007/s10021-005-0022-9.

Zhou, Z. and Guo, L., 2012. Evolution of the optical properties of seawater influenced by the Deepwater Horizon oil spill in the Gulf of Mexico. Environmental Research Letters 7(2), 025301.

CHAPTER III

SIZE DISTRIBUTION OF COLLOIDAL ORGANIC MATTER IN RIVER WATERS AS CHARACTERIZED BY FLOW FIELD FLOW FRACTIONATION

Introduction

Rivers discharge large amounts of dissolved organic carbon (DOC), trace elements and nutrients to the ocean (Aitkenhead and McDowell, 2000; Meybeck, 2003). Dissolved organic matter (DOM) exported from rivers has been found to affect water quality and primary production in estuaries and continental shelves (Bianchi et al., 1997; Findlay et al., 1998; Hopkinson and Vallino, 1995; Raymond et al., 2000).The fate and transport of riverine DOM to the ocean is an indispensable part of the global carbon cycle (Hedges et al., 1997; Hope et al., 1994). The abundance and composition of riverine DOM and its temporal variations are largely controlled by its source material, extent of *in situ* riverine processes, and other hydrological and biogeochemical processes in rivers and their drainage basins (Bianchi et al., 2004; Dagg et al., 2005; Duan et al., 2007b; Hedges et al., 2000; Warnken and Santschi, 2004).

Colloidal organic matter (COM), operationally defined as the DOM fraction between 1 kDa and 0.45 μm, has been found to consist of a variety of compounds and acts as a dynamic intermediary between dissolved and particulate species that regulates the transfer of particle reactive metals to particles (Amon and Benner, 1996b; Baskaran and Santschi, 1993; Guo and Santschi, 1997; Guo and Santschi, 2007; Lyvén et al., 1997). COM is a significant part of DOM (Benner et al., 1992; Guo and Macdonald, 2006; Guo et

al., 1995) and plays a critical role in regulating the concentration and speciation, hence the fate, transport and bioavailability of trace metals and pollutants in aquatic systems (Benedetti et al., 2003; Buffle et al., 1998; Lead and Wilkinson, 2006; Wilkinson et al., 1997). The size of DOM also determines its utilization efficiency by microbes (Benner, 2002; Benner, 2003; Findlay, 2003). The molecular weight of DOM is in return controlled by microbial and photochemical degradation. As Amon and Benner (1996) stated in their size-reactivity continuum model, large colloids are associated with higher reactivity and are more bioavailable, while smaller colloids are normally older in terms of C-14 ages and more refractory (Guo et al., 1996). Therefore, knowledge of the colloidal DOM size spectrum and composition would provide insights into the biogeochemical cycling pathways and the role DOM plays in regulating the fate and transport of trace elements.

Flow field-flow fractionation (FFF) is a chromatography-like elution technique in which retention force is provided by a cross-flow perpendicular to the channel-flow, and colloids are separated based on their diffusion coefficients and hydrodynamic diameters (Giddings, 1993). A variety of ancillary detectors, for example UV-absorbance and fluorescence detectors, can be coupled online to a FFF system to examine continuous size spectra of colloidal DOM and to determine distinct types of colloids characterized with specific size and compositions (Stolpe et al., 2010; Stolpe et al., 2005; Wells, 2004; Zanardi-Lamardo et al., 2002).

So far, applications of FFF techniques to the characterization of DOM in natural waters are few. Limited research has been done to examine the size distribution and chemical composition of colloids in the East Pearl River and the lower Mississippi River. Very recently, Stolpe et al. (2010) showed the size spectra of DOM in a sample collected from each river during near high flow of the two rivers. Nevertheless, the seasonality of size and composition of DOM and their controlling factors are largely unknown. Other applications of FFF to the characterization of DOM in the Mississippi River are restricted to UV-absorbing organic matter (Chen and Gardner, 2004; Wells, 2004).

The objectives of this study include 1) to examine the abundance and size spectra of colloidal DOM in the lower Mississippi River and East Pearl River and their seasonal dynamics between January 2009 to February 2010, 2) to compare the characteristics of DOM in the lower reaches of the Mississippi River, a large turbid river with a massive drainage basin area and under extensive anthropogenic influence (Beckett and Pennington, 1986; Wiener et al., 1996), with the Pearl River, a small and less-human-impacted river (Duan et al., 2007a; Duan et al., 2007b), and 3) to examine the effect of source, hydrological conditions, drainage plain size, land use, and human activities on the abundance and size distribution of colloidal DOM in these two rivers that both export to the central north Gulf of Mexico.

Our working hypothesis is colloidal DOM in the Pearl River should have higher abundance due to high bulk DOM concentration from large local input from forest soils and wetlands, while lower colloidal DOM abundance should be

found in the Mississippi River due to extensive human impacts, more degradation of terrestrial material and more production of aquagenic components.

Materials and Methods

Study Sites

The Pearl River is a small 3rd order black-water river that is 790 km long with a total drainage area of about 22,690 km^2 covering the east-central Mississippi and southeastern Louisiana. The largest land type of the Pearl River basin is natural forests (~43%). Marsh and/or swamp areas cover ~10% of the drainage basin. Agricultural regions represent ~27% of the land cover.

The Mississippi River, in contrast, with its length of 3,770 km and average flow rate of 17,000 m^3/s, ranks at the fourth longest and tenth largest world river (Kammerer, 1990). Its drainage basin covers about 40% of the contiguous United States and a small part of Canada (~3,220,000 km^2) (Meade et al., 1990). Cropland takes about 58% of its drainage basin, making the Mississippi River one of the most productive farming regions in the world (Goolsby and Battaglin, 2001; Goolsby et al., 2000). This river is largely constrained by dam systems and levees (Keown et al., 1986; Meade et al., 1990). Decreased suspended sediment and increased nutrients, organic matter and trace elements in the recent few decades have caused eutrophication, hypoxia and other environmental issues in the northern Gulf of Mexico (Boesch et al., 2009).

These two rivers show distinct river size, hydrological conditions, land use and degree and human impacts. The Mississippi River receives integrated signals from its wide drainage basin and is subjected to massive human impact,

while the Pearl River represents waters from a less human-perturbed black water system. These differences allow one to examine the effect of hydrological conditions, land use, and anthropogenic influences on the quantity and quality of DOM in river systems.

Sampling Locations

Monthly water samples were collected between January 2009 and February 2010 from the lower Mississippi River at Baton Rouge, Louisiana (30˚26'17.01" N, 91˚11'33.14" W) and the East Pearl River at Stennis Space Center, Mississippi (30°20'55.52"N, 89°38'28.74"W) (Figure 1). The sampling dates, locations and basic parameters are listed in Table 1.

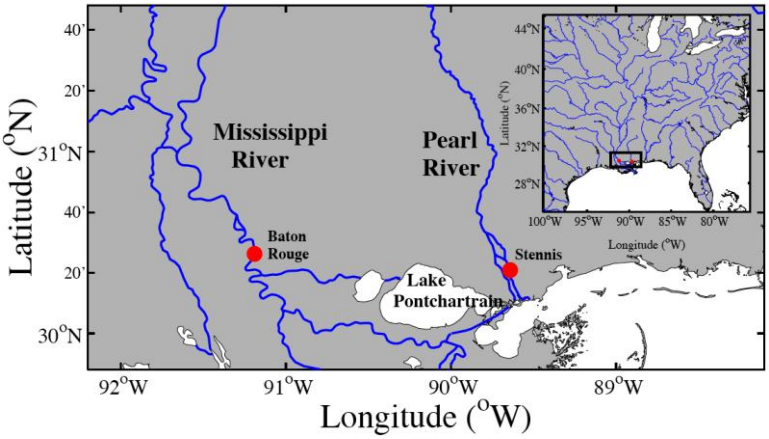

Figure 1. Sampling Locations In The East Pearl River and Lower Mississippi River.

Sample Processing

Water samples of approximately 40 L taken from just below the river surface were filtered in the field through a 0.45 µm Memtrex polycarbonate pleated cartridge filters (GE water & process technologies). Aliquots of filtered waters were collected in amber glass vials for the measurements of DOC (with acidification) and CDOM and FDOM (without acidification), and in plastic HDPE

Table 1

Hydrologic Parameters and DOC Concentrations in the East Pearl River and lower Mississippi River.

Location	Date	Discharge (m^3/s)	Specific Conductivity (µs/ cm)	Temp (˚C)	DOC (ppm)
PR	15-Jan-09	189	48	10.3	8.7
PR	13-Feb-09	127	NA	16.0	4.5
PR	14-Mar-09	96	78	21.7	3.9
PR	2-Apr-09	2011	37	18.8	13.5
PR	7-Apr-09	1470	39	17.5	10.0
PR	2-May-09	116	75	27.4	5.3
PR	22-May-09	289	60	24.9	8.0
PR	23-Jun-09	66	238	32.8	4.8
PR	15-Jul-09	56	2,500	31.0	4.2
PR	17-Aug-09	65	4,470	30.4	7.4
PR	23-Sep-09	94	266	28.3	10.8
PR	26-Oct-09	881	80	17.7	10.7
PR	25-Nov-09	114	83	18.2	6.8
PR	28-Dec-09	943	39	9.8	9.5
PR	31-Jan-10	983	48	10.5	8.8
PR	25-Feb-10	428	38	11.3	7.0

Table 1 (continued).

Location	Date	Discharge (m^3/s)	Specific Conductivity (µs/ cm)	Temp (˚C)	DOC (ppm)
MR	23-Jan-09	16,622	382	6.3	3.1
MR	20-Feb-09	14,926	343	8.8	2.8
MR	27-Mar-09	18,774	314	13.0	3.9
MR	24-Apr-09	21,345	350	15.9	3.6
MR	29-May-09	34,688	308	36.7	4.1
MR	29-Jun-09	19,658	326	29.8	3.8
MR	30-Jul-09	10,395	388	27.8	3.2
MR	26-Aug-09	9,047	391	28.8	3.2
MR	29-Sep-09	11,771	330	25.6	3.6
MR	29-Oct-09	20,445	276	16.1	4.1
MR	30-Nov-09	20,048	324	13.0	4.0
MR	31-Dec-09	22,283	267	7.0	3.2
MR	28-Jan-10	17,695	355	7.3	3.3
MR	25-Feb-10	25,482	290	5.7	2.8

bottles for FFF analysis. Samples were then kept in an iced cooler and transported back to the lab within 2-3 hours of collection and stored in dark in a refrigerator at 4˚C until further analysis. Water temperature, salinity, and pH were measured with a YSI meter at the time of sample collection.

Ultrafiltration

High-molecular-weight (HMW) DOM was separated and concentrated using the cross-flow ultrafiltration technique (Guo and Santschi, 1996; 2007), with an ultrafiltration membrane having nominal pore size of 1 kDa (kilo-Dalton). The size-fractionated samples, including the <1 kDa low-molecular-weight (LMW) fraction and the >1 kDa colloidal or HMW fraction, as well as the bulk water sample (<0.45 μm) were further analyzed for optical and chemical characterization. Time-series permeate samples (< 1kDa) during ultrafiltration were collected at different concentration factors (CF) and determined for DOC concentration to quantify the colloidal fraction (percentage) of the bulk DOC, and hence the partitioning of organic carbon and other chemical species between LMW and colloidal phases. This was done according to the ultrafiltration permeation model (Logan and Jiang, 1990), by fitting the DOC concentration of the permeate time-series samples as C_p and volume ratio of initial solution to the retentate solution as CF to the following equation:

$$\ln C_p = \ln\left(P_c \times C_f^0\right) + \left(1 - P_c\right) \times \ln(CF)$$

where P_c is the permeation coefficient, determined by the ratio of C_p to C_f, and the latter is the feed concentration, C_f^0 is the initial feed concentration (i.e., initial DOC concentration in the <0.45 μm phase) (Guo and Santschi, 2007).

Measurements of DOC Concentration

Concentrations of DOC of the river samples were measured with a Shimadzu TOC-V total organic carbon analyzer using a high temperature combustion method (Guo et al., 1995). Calibration curves were generated before

sample analysis. For DOC measurements, samples were acidified with concentrated HCl to pH < 2 before analysis. Three to five replicate measurements, each using a 150 µL sample. Coefficient of variance was <2% for all samples. Concentrations of nanopure water, working standards and certified DOC standards (from Dr. Hansell's Lab at the University of Miami) were measured every eight samples to check the performance of the instrument and ensure data quality.

Flow Field-flow Fractionation Analysis

The FFF system (F-1000, Postnova) was coupled on-line to optical detectors, including a UV-absorbance detector (Model 228, ISCO), two fluorescence detectors (Model 474, Waters and Acufluor LC-305, LabAlliance) and a refractive index detector (Model 214, Waters). Details of the on-line coupling of the FFF system and optical detectors followed that described in Stolpe et al. (2005, 2010). Dissolved river water samples (0.45µm filtrate) was preconcentrated on-channel(Lyvén et al., 1997). The FFF settings used in this study are shown in Table 2. These conditions allow determination of high-resolution 0.5-20 nm colloidal spectra. Most UV-absorbing and fluorescent colloidal matter reside within this size range (Stolpe et al., 2010), even though it only is a limited fraction of the overall operationally defined colloids. At the end of the run time (60 min), the cross flow was turned off for fast elution of materials larger than 20 nm in size. Thus, the bulk concentrations of colloids in the >20 nm size range were also examined. The optical parameters measured by the on-line optical detectors include UV-absorbance at 254 nm (UV_{254}), for indication of

CDOM, as well as fluorescence at excitation/emission wavelengths 350/450 nm ($Fluo_{350/450}$) and 275/340 nm ($Fluo_{275/340}$), representing humic-type and protein-type fluorescence, respectively.

Table 2

Instrument Parameters for FFF Analysis.

Parameter	Value
Accumulation wall membrane	1 kDa polyether sulfone (Omega, Pall Filtron)
Carrier solution	10 mM NaOH, 5 mM boric acid, pH = 8
Sample volume (ml)	10
Cross flow rate (ml/min)	3.0
Channel flow rate (ml/min)	0.5
Focus flow rate (ml/min)	4.5
Focus (Injection) time (min)	10
Equilibration time (min)	1
Run time (min)	60

The conversion of FFF retention time (t_R) to diffusion coefficient (D) was determined through calibration with proteins with known diffusion coefficients, including ovalbumin, bovine serum albumin, ferritin and thyroglobulin (Stolpe et al., 2010) under the same FFF settings for analyzing water samples. The void time (the retention time of non-retained solutes, t_0) was determined by breakthrough measurements (Giddings et al., 1992). Due to the linear

relationship between the reciprocal of hydrodynamic diameter (D^{-1}) and retention time (t_R) at long retention times (t_R>6t_0), the slope, k, determined from the linear relationship between D^{-1} and t_R can be further used to calculate D from t_R using the following equation (Giddings, 1993):

$$t_R = \frac{k}{D} \times \frac{1}{\coth\left(\frac{3k}{t_0 D}\right) - \frac{t_0 D}{3K}}$$

Diffusion coefficient was further converted to hydrodynamic diameter using calibration with polystyrene sulfonate (PSS) standards (Beckett et al., 1987).

A series of a quinine sulfate standards were injected on-line to calibrate concentrations of UV_{254}, $Fluo_{350/450}$ and $Fluo_{275/340}$ in samples. Integration of these optical parameters along the total colloidal size spectra was used to describe the FFF recoverable fraction of colloids and are denoted as $[UV_{254}]_{FFF}$, $[Fluo_{350/450}]_{FFF}$ and $[Fluo_{275/340}]_{FFF}$. Colloidal size spectra were also integrated over smaller size ranges, including 0.5-2.3 nm, 2.3-20 nm and >20 nm to examine the percentages of the FFF-recoverable fraction in each colloidal size fractions.

Results and Discussion

Hydrographic Characteristics

Discharge data of Pearl River at Bogalusa from the hydrological station of USGS during our sampling period ranged from 56 to 2010 m^3/s (mean=536 m^3/s; n = 17), with the highest value during a flood in April, 2009 (Figure 2). The two East Pearl River water samples collected in July and August, 2009 had specific conductivity at 25˚C (SPC) higher than 500 µS/cm, probably resulting from seawater intrusion in the East Pearl River (Cai et al., 2012). SPC ranged from 37

to 266 µS/cm (mean=87 µS/cm; n = 15) in the samples not influenced by seawater intrusion. No positive correlations was found between discharge and specific conductivity.

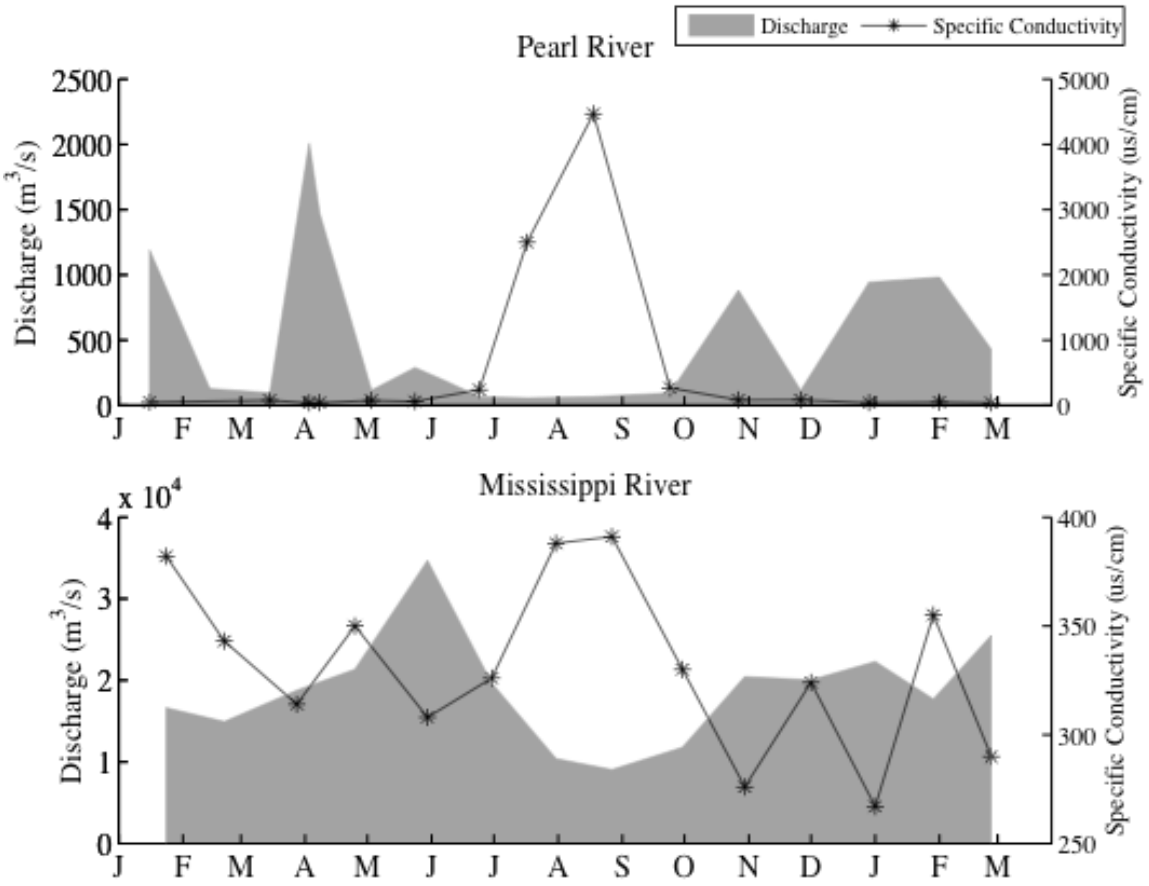

Figure 2. Seasonal Variations Of Discharge (m3/s) And Specific Conductivity At 25˚C (SPC, µS/cm) In The Lower Pearl And Mississippi Rivers.

Discharge in the lower Mississippi River ranged from 9047 to 34688 m3/s (mean=18798 m3/s; n = 14), with the highest flow rate observed during May 2009 (Figure 2). Specific conductivity in Mississippi River ranged from 267 to 391 µS/cm (mean=331 µS/cm; n = 14), and was positively correlated with discharge (P=0.01, r2 =0.41). Concentrations of DOC (3.91-13.45 ppm, mean= 7.82 ppm), colloidal organic matter (COC) (7.25 ppm for samples taken on April 07, 2009)

and colloidal fraction (72% on April 07, 2009) in the East Pearl River during our sampling period were higher than those in the Mississippi River, where DOC concentration ranged from 2.83-4.12 ppm (mean =3.5 ppm, n=5), COC ranged from 1.81-2.54 ppm (mean = 2.13 ppm, n=5), and colloidal fraction was averaged 60% ±2%.

Characteristics of Colloidal Size Spectra

Figure 3 shows the colloidal size spectra of UV_{254}, $Fluo_{350/450}$, and $Fluo_{275/340}$, corresponding to chromophores, humic-type fluorophores, and protein-type fluorophores, respectively, to represent the typical size distribution of distinct types of DOM in the rivers. Fractograms of the sample collected in the East Pearl River on December 28, 2009 are on the left and while those for the sample collected from the lower Mississippi River on November 30, 2009 are on the right.

Fractograms of both UV_{254}, $Fluo_{350/450}$ of all the river samples showed one single narrow peak at 1-4 nm. The hydrodynamic diameter (d_H) corresponding to the UV_{254} peaks were centered at d_H = 1.5 ± 0.5 nm, and the $Fluo_{350/450}$ peaks were centered at d_H = 1.2 ± 0.5 nm. Interestingly, the colloidal size spectra of $Fluo_{275/340}$ not only showed one peak at 0.5-4 nm, matching the UV_{254} and $Fluo_{350/450}$ spectra, but also showed an additional peak at 3-8 nm. The maximum of the $Fluo_{350/450}$ peak at 3-8 nm was centered at d_H = 4.8 ±0 .4 nm. The different colloidal size spectra of UV_{254}, $Fluo_{350/450}$, and $Fluo_{275/340}$ suggests distinct populations of colloids with different compositions. To better quantify the distinct colloidal size distribution of chromophores and fluorophores, the percentages of

$[UV_{254}]_{FFF}$, $[Fluo_{350/450}]_{FFF,}$ and $[Fluo_{275/340}]_{FFF}$ in the size intervals 1-5 nm, 5-20 nm and >20 nm were calculated.

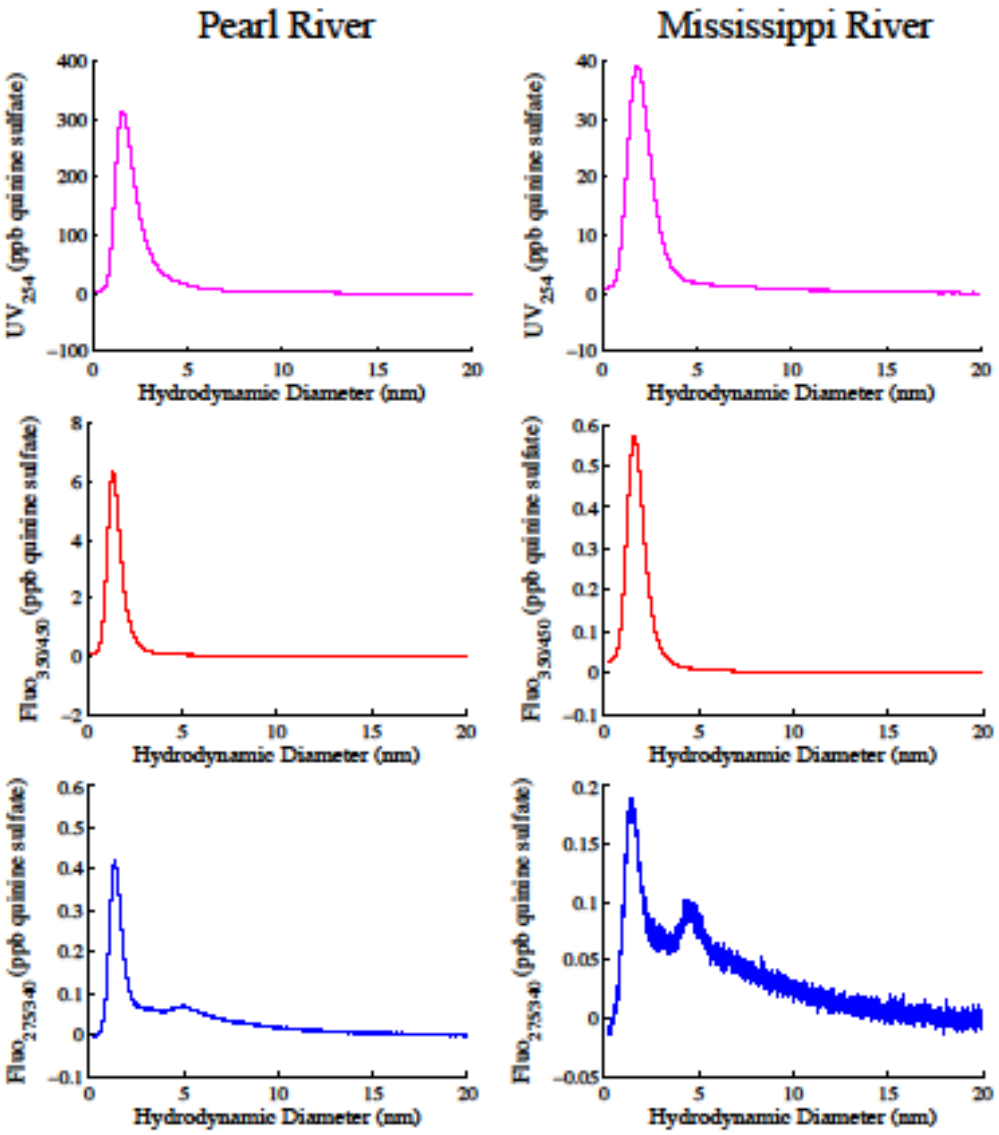

Figure 3. Fractograms Showing The Colloidal Size Spectra of UV254 (chromophores), Fluo350/450 (humic-type fluorophores), And Fluo275/340 (protein-type fluorophores) In The Samples Collected From The Lower Pearl River on December 28, 2009 (left column) And The Lower Mississippi River On November 30, 2009 (right column).

More than 78% of $[UV_{254}]_{FFF}$ and more than 86% of $[Fluo_{350/450}]_{FFF}$ were found in the 1-5 nm size fraction in the East Pearl River and lower Mississippi River, corresponding to the peak between 0.5-4 nm in the colloidal UV_{254} and

$Fluo_{350/450}$ spectra. In contrast, a considerably larger fraction of the $Fluo_{275/340}$ spectra was found in the >20 nm size fraction (41% for the Pearl River and 66% for the Mississippi River, Figure 4).

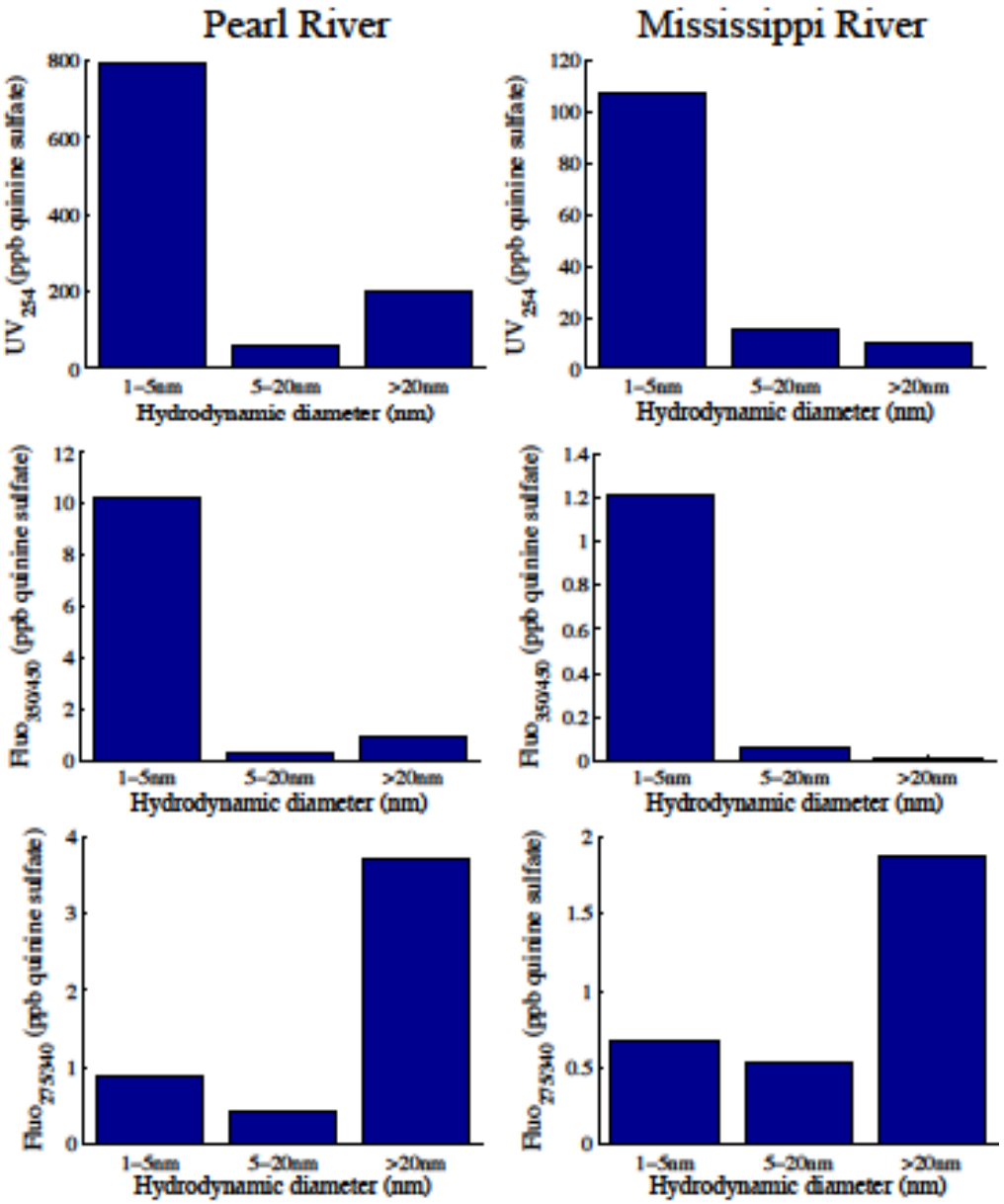

Figure 4. Integrated Size Spectra Of [UV254]FFF, [Fluo350/450]FFF, And [Fluo275/340]FFF Over Size Intervals 1-5nm, 5-20nm And >20nm , In The Samples Collected From The Lower Pearl River On December 28, 2009 (left column) And The Lower Mississippi River On November 30, 2009 (right column).

The colloidal size distributions of protein-type fluorophores are thus characterized by larger sizes compared to chromophores and humic-type fluorophores. The ubiquitous peak ranging from d_H= 1- 4 nm and centering on 1.5 nm is discernible in all the UV_{254}, $Fluo_{350/450}$, and $Fluo_{275/340}$ size spectra. Previous studies demonstrated terrestrial sources of colloidal amino acids in the Mississippi and Pearl River (Duan and Bianchi, 2007). This fluorescent-nature and CDOM-rich colloid is likely to be natural fulvic acid (Beckett et al., 1987; Lead et al., 2000; Stolpe et al., 2010; Zanardi-Lamardo et al., 2002).

The addition peak at 3-8 nm and the major proportion in the >20 nm fraction of $Fluo_{275/340}$ spectra (Figure 3 and 4) suggest different sources of these groups of protein-type fluorophores. Previous studies have found larger size of fresh microbially derived amino acid (Amon and Benner, 1996a), thus, the protein-like colloids in the 3-8 nm and >20 nm size ranges are likely to have autochthonous origin.

Seasonal Variation of DOM with Specific Composition and Size Distribution

By integrating the full spectra of UV_{254} fractograms, including the 0.5-20nm fraction and the >20 nm fraction, the concentration of colloidal CDOM ($[UV_{254}]_{FFF}$) was calculated. Samples collected from the East Pearl River had $[UV_{254}]_{FFF}$ values ranging from 123 ppb during low discharge to 4267 ppb during flood season (mean = 1197 ppb, n = 16). In contrast, $[UV_{254}]_{FFF}$ of water samples from the lower Mississippi River were considerably lower and ranged from 36 ppb during low flow to 261 ppb during high flow (mean = 137 ppb, n = 13). Specific UV absorbance at 254 ($SUVA_{254}$) nm has been found to show strong correlation

with aromaticity (Weishaar et al., 2003). The ratio between $[UV_{254}]_{FFF}$ and COC is the counterpart of SUVA 254 in the colloidal fraction and representative of the aromaticity of colloidal organic matter in the sample (Stolpe et al, 2010). This $[UV_{254}]_{FFF}$/COC index is unit-less if the concentration of $[UV_{254}]_{FFF}$ and COC are both selected as ppb, although the unit is essentially g-quinine sulfate/g-C. The $[UV_{254}]_{FFF}$/COC ratio in the sample from the East Pearl River collected on April 07, 2009 was 0.39, while $[UV_{254}]_{FFF}$/COC ratio in the lower Mississippi River was considerably lower, ranging from 0.03 to 0.09 (mean = 0.05, n=13).

The relative content of protein-type fluorophores in the colloidal CDOM can be represented by the $[Fluo_{275/340}]_{FFF}$ to $[UV_{254}]_{FFF}$ ratio. Samples from the lower Pearl River had $[Fluo_{275/340}]_{FFF}/[UV_{254}]_{FFF}$ ratio ranging from 0.002 to 0.05 (mean =0.01, n=16), while samples from the lower Mississippi River had $[Fluo_{275/340}]_{FFF}$ /$[UV_{254}]_{FFF}$ ratios ranging from 0.01-0.08 (mean = 0.03, n=13), showing higher protein-type fluorophores in the lower Mississippi River.

Figure 5 shows the seasonal variation of chromophores, as represented by $[UV_{254}]_{FFF}$ in the Pearl and Mississippi Rivers. Significantly positive correlation was found between $[UV_{254}]_{FFF}$ and discharge in the Pearl River ($P<0.0001$, $r^2=0.7$, Figure 5), with highest $[UV_{254}]_{FFF}$ found during the flood in April 2009. In contrast, no significant correlation was found between $[UV_{254}]_{FFF}$ and discharge in the Mississippi River. Similarly, $[UV_{254}]_{FFF}$ showed positive correlation with DOC concentration in the Pearl River ($P<0.005$, $r^2=0.45$, Figure 6), but did not show correlation with DOC in the Mississippi River. This is possibly reflecting sources of chromophoric organic matter from surface soils and plant litters during high

flow in the Pearl River, and the integration of signals of large drainage basin in the Mississippi River (Duan et al., 2007a).

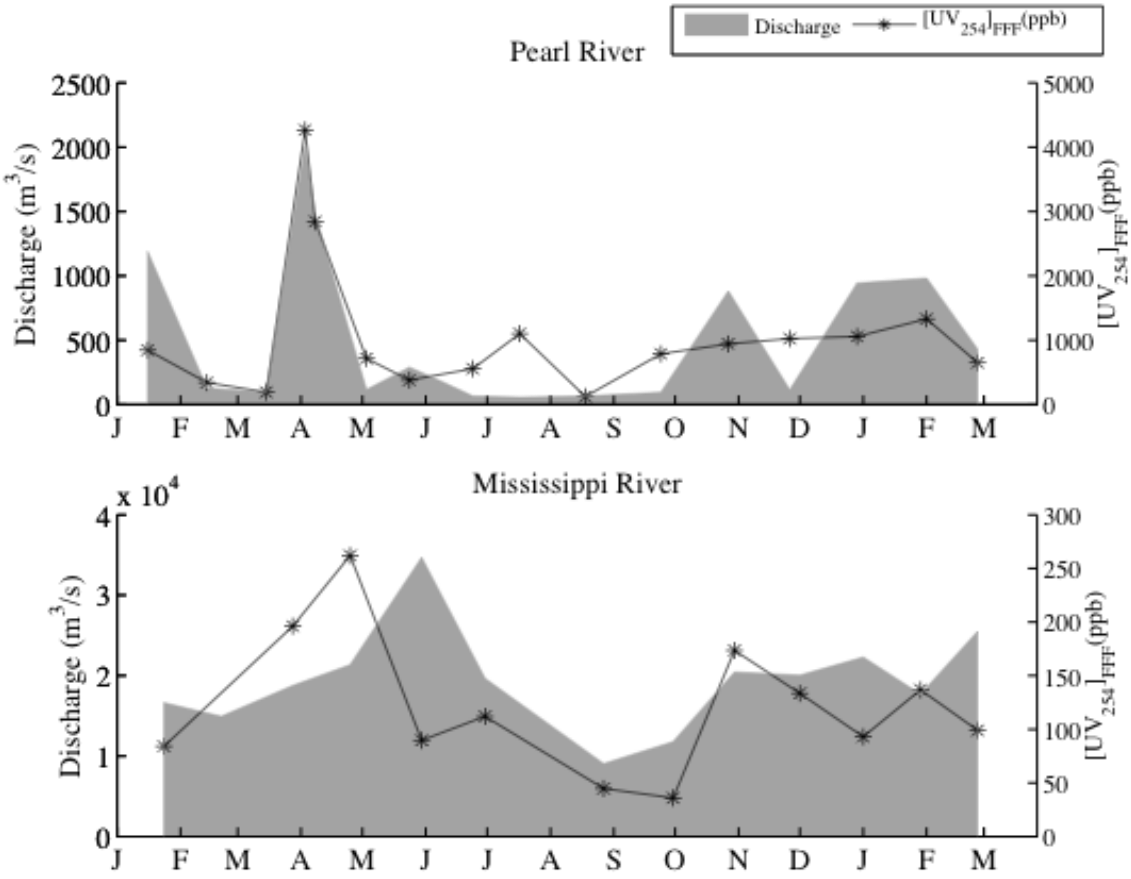

Figure 5. Seasonal Sariations In Discharge (m^3/s) And $[UV_{254}]$FFF (ppb) of Colloidal DOM In The Lower Pearl And Mississippi Rivers.

The proportion of humic-type fluorophores in the bulk dissolved phase is indicated by the ratio of $[Fluo_{350/450}]_{FFF}$ to DOC. In the Pearl River, $[Fluo_{350/450}]_{FFF}$/DOC is positively correlated with discharge ($P<0.01$, $r^2=0.43$, Figure 6), reflecting increased importance of humic substances in the bulk dissolved organic carbon pool with increasing discharge, possibly from allochthnous sources. It is worth noticing that the relationship between $[Fluo_{350/450}]_{FFF}$/DOC and discharge in the East Pearl River seemed to show two

separate relations, one for samples taken during relatively lower (<500m^3/s) discharge, and another during higher (>500m^3/s) flow rate. This is possibly caused by differences in sources of the East Pearl River during different flow rates. Because of the existence of an upstream weir, water from the main channel of Pearl River is largely limited during low flow, and the source water of the East Pearl River would shift to the Hobolochitto Creek. This change of water sources is likely to be reflected in the characteristics of DOM.

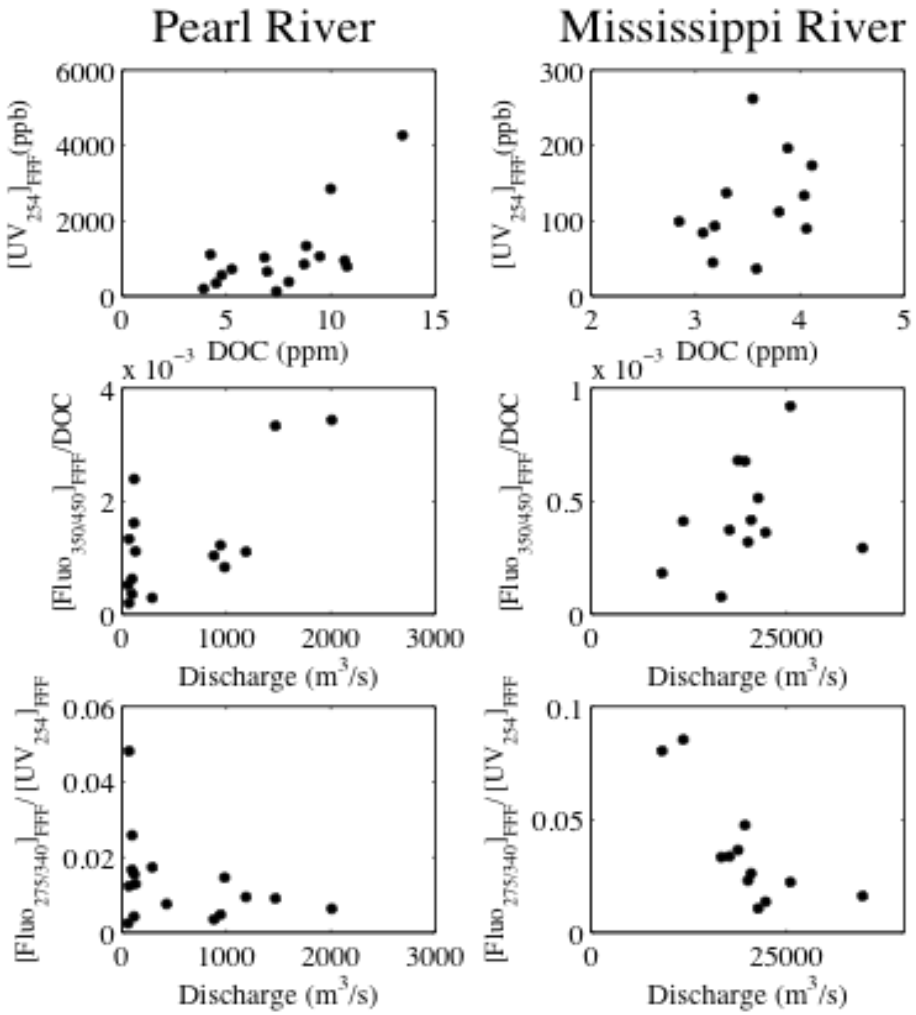

Figure 6. Relations Among DOC (ppm), [UV254]FFF (ppb), Discharge (m3/s), [Fluo350/450]FFF/DOC ratio, and [Fluo275/340]FFF/[UV254]FFF Ratio In The Lower Pearl And Mississippi Rivers.

In contrast, $[Fluo_{350/450}]_{FFF}$/DOC in the Mississippi River failed to show correlation with discharge, possibly due to sources of integrated signal from large river basin and more extensive processing in the river. The relative importance of protein-type fluorophores in the chromophores were determined by the ratio between $[Fluo_{275/340}]_{FFF}/[UV_{254}]_{FFF}$, and was found to show no correlation with discharge in the Pearl River but negative correlation with discharge in the Mississippi River ($P=0.003$, $r^2=0.59$).

The decreasing $[Fluo_{275/340}]_{FFF}/[UV_{254}]_{FFF}$ values with increasing discharge reflect different sources of protein-type fluorophores as compared to other DOM components, and possibly from autochthonous microbial origins subjected to dilution during high flow.

Comparison between the Pearl River and Mississippi River

The great similarity in the colloidal size spectra of UV_{254FFF} and $Fluo_{350/450}$ between the Pearl River and Mississippi River suggests that chromophores and humic-type fluorophores are associated with the same type of organic macromolecules in these two rivers.

Higher DOC concentration, larger colloidal fraction and considerably higher $[UV_{254}]_{FFF}$ and $[UV_{254}]_{FFF}$/COC in the Pearl River suggest higher aromaticity and larger fraction of lignin-phenols in colloidal organic matter, in accordance with previous findings (Duan et al., 2007a; Duan et al., 2007b; Stolpe et al., 2010). Positive correlation between $[UV_{254}]_{FFF}$ and discharge in the Pearl River suggests source of high aromatic from surface soil layer and plant litter.

Higher $[Fluo_{275/340}]_{FFF}/[UV_{254}]_{FFF}$ ratios, its decreasing trend with increasing discharge, and higher relative fraction of the >20 nm protein-type fluorophores in the Mississippi River agrees with previous findings of higher *in situ* phytoplankton production in the Mississippi River (Duan et al., 2007a), likely caused by increased water residence time from dam and levee constructions.

Conclusions

Two types of colloids are likely to present in the river waters. One type with a narrow peak ranging at 1-4 nm in size shows chromophoric and fluorescent properties and is likely natural fulvic acids. The other types of colloids are characterized by two peaks at 3-8 nm and >20 nm with protein-type fluorescence, and are suggested to be from *in situ* phytoplankton production. These two types of colloids are both present in the lower Mississippi and Pearl Rivers.

Sources of colloidal DOM in the Pearl River are more likely to be from forest soils and wetlands, owing to its high aromaticity, higher DOC concentration, larger colloidal fraction and considerably higher $[UV_{254}]_{FFF}$ and $[UV_{254}]_{FFF}$/COC found in the Pearl River. Colloids in the Mississippi River, in contrast, have more aquagenic sources based on the higher $[Fluo_{275/340}]_{FFF}/[UV_{254}]_{FFF}$ ratios and higher proportions of $Fluo_{275/340}$ in the >20nm size range. The difference in the sources of colloidal DOM is coherent with the drainage size, land use and human impact on the two rivers.

Week correlations between the various types of colloidal DOM and discharge in the Mississippi River indicates complex processes governing the

biogeochemistry of riverine DOM in this water system, in accordance with the fact that the DOM signal in the lower Mississippi River is integrated from a large upper river basin with various land types and modified *in situ* by degradation and autochthonous production.

The source and compositions of the DOM in the East Pearl River and the lower Mississippi River as characterized by the colloidal size distribution of specific types of DOM are similar as those determined by optical analysis, such as UV-vis absorbance and fluorescence excitation emission matrix coupled with parallel factor analysis. More size specific characteristics of DOM are revealed by Flow field flow fractionation coupled with on-line detectors.

REFERENCES

Aitkenhead, J.A. and McDowell, W.H., 2000. Soil C:N ratio as a predictor of annual riverine DOC flux at local and global scales. Global Biogeochem. Cycles 14(1), 127-138, doi: 10.1029/1999gb900083.

Amon, R.M.W. and Benner, R., 1996a. Bacterial utilization of different size classes of dissolved organic matter. Limnology and Oceanography 41(1), 41-51.

Amon, R.M.W. and Benner, R., 1996b. Photochemical and microbial consumption of dissolved organic carbon and dissolved oxygen in the Amazon River system. Geochimica et Cosmochimica Acta 60(10), 1783-1792.

Baskaran, M. and Santschi, P.H., 1993. The role of particles and colloids in the transport of radionuclides in coastal environments of Texas. Marine Chemistry 43(1-4), 95-114, doi:10.1016/0304-4203(93)90218-d.

Beckett, D.C. and Pennington, C.H., 1986. Water quality, macroinvertebrates, larval fishes, and fishes of the lower mississippi river - a synthesis U.S. Army Corps of Engineers, Technical Report. Waterways Experiment Station, Vicksburg, MS.

Beckett, R., Jue, Z. and Giddings, J.C., 1987. Determination of molecular weight distributions of fulvic and humic acids using flow field-flow fractionation. Environmental Science & Technology 21(3), 289-295.

Benedetti, M.F., Mounier, S., Filizola, N., Benaim, J. and Seyler, P., 2003. Carbon and metal concentrations, size distributions and fluxes in major rivers of the Amazon basin. Hydrological Processes 17(7), 1363-1377.

Benner, R., 2002. Chemical composition and reactivity. In: H. D.A. and C.A. Carlson (Editors), Biogeochemistry of marine dissolved organic matter. Academic Press, London, UK, pp. 59-85.

Benner, R., 2003. Molecular indicators of the bioavailability of dissolved organic matter. In: S. Findlay and R.L. Sinsabaugh (Editors), Aquatic Ecosystems: Interactivity of Dissolved Organic Matter. Academic Press, London, UK, pp. 121-135.

Benner, R., Pakulski, J.D., McCarthy, M., Hedges, J.I. and Hatcher, P.G., 1992. Bulk Chemical Characteristics of Dissolved Organic Matter in the Ocean. Science 255(5051), 1561-1564.

Bianchi, T.S., Filley, T., Dria, K. and Hatcher, P.G., 2004. Temporal variability in sources of dissolved organic carbon in the lower Mississippi river. Geochimica et Cosmochimica Acta 68(5), 959-967.

Bianchi, T.S., Lambert, C.D., Santschi, P.H. and Guo, L., 1997. Sources and transport of land-derived particulate and dissolved organic matter in the Gulf of Mexico (Texas shelf/slope): The use of ligninphenols and loliolides as biomarkers. Organic Geochemistry 27(1-2), 65-78, doi: 10.1016/s0146-6380(97)00040-5.

Boesch, D.F. et al., 2009. Nutrient Enrichment Drives Gulf of Mexico Hypoxia. Eos Trans. AGU 90(14).

Buffle, J., Wilkinson, K.J., Stoll, S., Filella, M. and Zhang, J., 1998. A generalized description of aquatic colloidal interactions: the three-colloidal component approach. Environmental Science & Technology 32(19), 2887-2899.

Cai, Y., Guo, L., Wang, X., Lohrenz, S.E. and Mojzis, A.K., 2012. Effects of tropical cyclones on river chemistry: A case study of the Pearl River, Mississippi during Hurricanes Gustav and Ike. Estuaries and Coasts, (in review).

Chen, R.F. and Gardner, G.B., 2004. High-resolution measurements of chromophoric dissolved organic matter in the Mississippi and Atchafalaya River plume regions. Marine Chemistry 89(1-4), 103-125.

Dagg, M.J. et al., 2005. Biogeochemical Characteristics of the Lower Mississippi River, USA, during June 2003. Estuaries 28(5), 664-674.

Duan, S. and Bianchi, T.S., 2007. Particulate and dissolved amino acids in the lower Mississippi and Pearl Rivers (USA). Marine Chemistry 107(2), 214-229.

Duan, S., Bianchi, T.S. and Sampere, T.P., 2007a. Temporal variability in the composition and abundance of terrestrially-derived dissolved organic matter in the lower Mississippi and Pearl Rivers. Marine Chemistry 103(1-2), 172-184, doi: 10.1016/j.marchem.2006.07.003.

Duan, S. et al., 2007b. Variability in the bulk composition and abundance of dissolved organic matter in the lower Mississippi and Pearl rivers. Journal of Geophysical Research 112(G2), G02024, doi: 10.1029/2006JG000206.

Findlay, S., 2003. Bacterial response to variation in dissolved organic matter. In: S. Findlay and R.L. Sinsabaugh (Editors), Aquatic Ecosystems: Interactivity of Dissolved Organic Matter. Academic Press, London, UK, pp. 363-377.

Findlay, S., Sinsabaugh, R.L., Fischer, D.T. and Franchini, P., 1998. Sources of dissolved organic carbon supporting planktonic bacterial production in the tidal freshwater hudson river. Ecosystems 1(3), 227-239, doi: 10.1007/s100219900018.

Giddings, C.J., Williams, S.P. and Benincasa, A.M., 1992. Rapid breakthrough measurement of void volume for field-flow fractionation channels. Journal of Chromatography A 627(1-2), 23-35, doi: 10.1016/0021-9673(92)87183-9.

Giddings, J.C., 1993. Field-flow fractionation: analysis of macromolecular, colloidal, and particulate materials. Science 260(5113), 1456-1465.

Goolsby, D.A. and Battaglin, W.A., 2001. Long-term changes in concentrations and flux of nitrogen in the Mississippi River Basin, USA. Hydrological Processes 15(7), 1209-1226, doi: 10.1002/hyp.210.

Goolsby, D.A., Battaglin, W.A., Aulenbach, B.T. and Hooper, R.P., 2000. Nitrogen flux and sources in the Mississippi River Basin. Science of The Total Environment 248(2-3), 75-86, doi: 10.1016/s0048-9697(99)00532-x.

Guo, L. and Macdonald, R.W., 2006. Source and transport of terrigenous organic matter in the upper Yukon River: Evidence from isotope (δ13C,Δ14C, andδ15N) composition of dissolved, colloidal, and particulate phases. Global Biogeochem. Cycles 20(2), GB2011, doi: 10.1029/2005gb002593.

Guo, L. and Santschi, P.H., 1997. Composition and cycling of colloids in marine environments. Rev. Geophys. 35(1), 17-40.

Guo, L. and Santschi, P.H., 2007. Ultrafiltration and its applications to sampling and characterisation of aquatic colloids. In: K.J. Wilkinson and J.R. Lead (Editors), Environmental colloids and particles. John Wiley & Sons, Ltd, pp. 159–221, doi: 10.1002/9780470024539.ch4.

Guo, L., Santschi, P.H. and Warnken, K.W., 1995. Dynamics of dissolved organic carbon (DOC) in oceanic environments. Limnology and Oceanography 40(8), 1392-1403.

Hedges, J.I., Keil, R.G. and Benner, R., 1997. What happens to terrestrial organic matter in the ocean? Organic Geochemistry 27(5-6), 195-212, doi: 10.1016/s0146-6380(97)00066-1.

Hedges, J.I. et al., 2000. Organic matter in Bolivian tributaries of the Amazon River: a comparison to the lower mainstream. Limnology and Oceanography 45(7), 1449-1466.

Hope, D., Billett, M.F. and Cresser, M.S., 1994. A review of the export of carbon in river water: Fluxes and processes. Environmental Pollution 84(3), 301-324, doi: 10.1016/0269-7491(94)90142-2.

Hopkinson, C.S., Jr. and Vallino, J.J., 1995. The relationships among man's activities in watersheds and estuaries: a model of runoff effects on patterns of estuarine community metabolism. Estuaries 18(4), 598-621.

Kammerer, J.C., 1990. Largest Rivers in the United States. U.S. Geological Survey.

Keown, M.P., Dardeau, E.A., Jr. and Causey, E.M., 1986. Historic Trends in the Sediment Flow Regime of the Mississippi River. Water Resour. Res. 22(11), 1555-1564, doi: 10.1029/WR022i011p01555.

Lead, J.R. and Wilkinson, K.J., 2006. Aquatic Colloids and Nanoparticles: Current Knowledge and Future Trends. Environmental Chemistry 3(3), 159-171.

Lead, J.R. et al., 2000. Diffusion Coefficients and Polydispersities of the Suwannee River Fulvic Acid: Comparison of Fluorescence Correlation Spectroscopy, Pulsed-Field Gradient Nuclear Magnetic Resonance, and Flow Field-Flow Fractionation. Environmental Science & Technology 34(16), 3508-3513.

Lyvén, B., Hassellöv, M., Haraldsson, C. and Turner, D.R., 1997. Optimisation of on-channel preconcentration in flow field-flow fractionation for the determination of size distributions of low molecular weight colloidal material in natural waters. Analytica Chimica Acta 357(3), 187-196, doi: 10.1016/s0003-2670(97)00565-5.

Meade, R.H., Yuzyk, T.R. and Day, T.J., 1990. Movement and storage of sediment in rivers of the United States and Canada. In: M.G. Wolman and H.C. Riggs (Editors), Surface Water Hydrology. Geological Society of America, Boulder, Colorado, pp. 255-280.

Meybeck, M., 2003. Global analysis of river systems: from Earth system controls to Anthropocene syndromes. Philosophical Transactions of the Royal

Society of London. Series B: Biological Sciences 358(1440), 1935-1955, doi: 10.1098/rstb.2003.1379.

Raymond, P.A., Bauer, J.E. and Cole, J.J., 2000. Atmospheric CO2 evasion, dissolved inorganic carbon production, and net heterotrophy in the York River Estuary. Limnology and Oceanography 45(8), 1707-1717.

Stolpe, B., Guo, L., Shiller, A.M. and Hassellöv, M., 2010. Size and composition of colloidal organic matter and trace elements in the Mississippi River, Pearl River and the northern Gulf of Mexico, as characterized by flow field-flow fractionation. Marine Chemistry 118(3-4), 119-128.

Stolpe, B., Hassellöv, M., Andersson, K. and Turner, D.R., 2005. High resolution ICPMS as an on-line detector for flow field-flow fractionation; multi-element determination of colloidal size distributions in a natural water sample. Analytica Chimica Acta 535(1-2), 109-121, doi: 10.1016/j.aca.2004.11.067.

Warnken, K.W. and Santschi, P.H., 2004. Biogeochemical behavior of organic carbon in the Trinity River downstream of a large reservoir lake in Texas, USA. Science of The Total Environment 329(1-3), 131-144.

Weishaar, J.L. et al., 2003. Evaluation of specific ultraviolet absorbance as an indicator of the chemical composition and reactivity of dissolved organic carbon. Environmental Science and Technology 37(20), 4702-4708, doi: 10.1021/es030360x.

Wells, M.L., 2004. The colloidal size spectrum of CDOM in the coastal region of the Mississippi Plume using flow field-flow fractionation. Marine Chemistry 89(1-4), 89-102, doi: 10.1016/j.marchem.2004.02.009.

Wiener, J.G. et al., 1996. Mississippi River, Status and Trends of Nation's Biological Resources. National Weahter Resouces Center, U.S. Geological Survey, Washington, D.C., pp. 351-384.

Wilkinson, K.J., Joz-Roland, A. and Buffle, J., 1997. Different Roles of Pedogenic Fulvic Acids and Aquagenic Biopolymers on Colloid Aggregation and Stability in Freshwaters. Limnology and Oceanography 42(8), 1714-1724.

Zanardi-Lamardo, E., Clark, C.D., Moore, C.A. and Zika, R.G., 2002. Comparison of the molecular mass and optical properties of colored dissolved organic material in two rivers and coastal waters by Flow Field-Flow Fractionation. Environmental Science and Technology 36(13), 2806-2814.

CHAPTER IV

CHARACTERIZATION OF OIL COMPONENTS FROM THE DEEPWATER HORIZON OIL SPILL IN THE GULF OF MEXICO USING FLUORESCENCE EEM TECHNIQUES*

Introduction

The unprecedented Deepwater Horizon oil spill in the northern Gulf of Mexico during April 20 –July 15, 2010 resulted in the release of over 800 million liters of crude oil from the Macondo well into the water column (Mascarelli, 2010; Schrope, 2011). For the remediation of oil, over 7 million liters of dispersant were used during the oil spill (Kujawinski et al., 2011). The vast quantity of oil and its long transit from the deep ocean to the sea surface made this oil spill different from other spill disasters. This Gulf of Mexico oil spill also provided a natural laboratory and an opportunity to examine the fate, transport and transformation of crude oil components and their interactions with the environment (Camilli et al., 2010; Diercks et al., 2010; Dietrich et al., 2012; Hazen et al., 2010; Hu et al., 2011; Kujawinski et al., 2011; Leifer et al., 2012; Liu et al., 2011; Wade et al., 2011).

Dissolved organic matter (DOM) in aquatic systems is a complex mixture of organic matter with various sources and composition, and plays an important role in controlling the environmental behavior of many chemical species and

---

* This chapter of the dissertation has been accepted for publication in the Journal of Marine Chemistry
Zhou, Z. et al., 2012. Characterization of oil components from the Deepwater Horizon oil spill in the Gulf of Mexico using fluorescence EEM techniques. Marine Chemistry, (Accepted).

pollutants and their biogeochemical cycles in aquatic environments (Hedges, 2002; Stolpe et al., 2010; Turner and Mawji, 2004). Chromophoric dissolved organic matter (CDOM) is the fraction of DOM that absorbs light mainly in the visible and ultraviolet range, and fluorescent dissolved organic matter (FDOM) is the part of DOM that emits fluorescence after absorption of light. Optical properties, including UV-vis absorbance, fluorescence excitation-emission matrices (EEMs) and their derivative parameters, have been widely used to quantify the abundance, reactivity and molecular weight of DOM and to characterize its composition and sources in aquatic environments (Chen and Gardner, 2004; Coble et al., 1990; Del Vecchio and Blough, 2004; Guéguen et al., 2007; Helms et al., 2008; Sierra et al., 2006; Vodacek et al., 1997; Weishaar et al., 2003), especially when combined with the use of PARAFAC modeling (Kowalczuk et al., 2009; Murphy et al., 2008; Stedmon and Bro, 2008; Stedmon et al., 2003; Walker et al., 2009; Yamashita et al., 2008).

Previous studies have shown the usefulness of fluorescence EEM techniques and PARAFAC analysis in the characterization, fingerprinting, and monitoring of oil (Alostaz et al., 2008; Booksh et al., 1996; Bugden et al., 2008; Christensen et al., 2005; Ferreira et al., 2003; González et al., 2006; Kim et al., 2010; Patra and Mishra, 2002). However, applications of fluorescence EEMs and PARAFAC analysis are still few for the Deepwater Horizon oil spill in the northern Gulf of Mexico. Several recent studies related to the Deepwater Horizon oil spill focused mostly on the extent and transport of oil, methane, and dispersants (Diercks et al., 2010; Hazen et al., 2010; Joye et al., 2011; Kessler et al., 2011;

Kujawinski et al., 2011; Valentine et al., 2010), as well as end member composition of gas and oil (Reddy et al., 2011). Here, we report the distributions of DOM and fluorescence characterization of crude oil, weathered oil, and seawater samples collected from two cruises to the northern Gulf of Mexico during the Deepwater Horizon (DWH) oil spill, using fluorescence EEMs techniques coupled with PARAFAC modeling.

The major objectives of this study were to examine the distribution and variation of DOM and UV-vis absorbance in the water column around the Macondo well in the Gulf of Mexico, to characterize the fluorescence and other optical properties of oil and seawater samples for identification and fingerprinting of oil components, and to determine the relationship between fluorescence component ratios and chemical evolution of oil in the water column.

Materials and Methods

Study Site and Sampling

The study area and sampling stations were located around the Deepwater Horizon oil rig in the northern Gulf of Mexico, covering an area of ~5600 km^2 during two cruises in May/June 2010 during the oil spill (Figure 1). The first cruise was accomplished onboard the R/V Pelican during May 10-14, 2010 and covered 25 stations. The second sampling cruise was accomplished between May 26th and June 1st 2010 onboard the R/V Walton Smith and covered 29 stations (Table 1 and Figure 1). Water samples were collected with Niskin or Go-flo bottles mounted on a CTD rosette system, and were filtered immediately after sample collection through 0.2 µm Whatman polycarbonate membrane filters. Filtered

samples for DOC were stored frozen in 30 ml HDPE bottles, while samples for optical measurements, including UV-vis absorbance and fluorescence EEMs, were collected with pre-combusted (550°C) 125 ml amber bottles and stored in the dark at 4˚C before measurements.

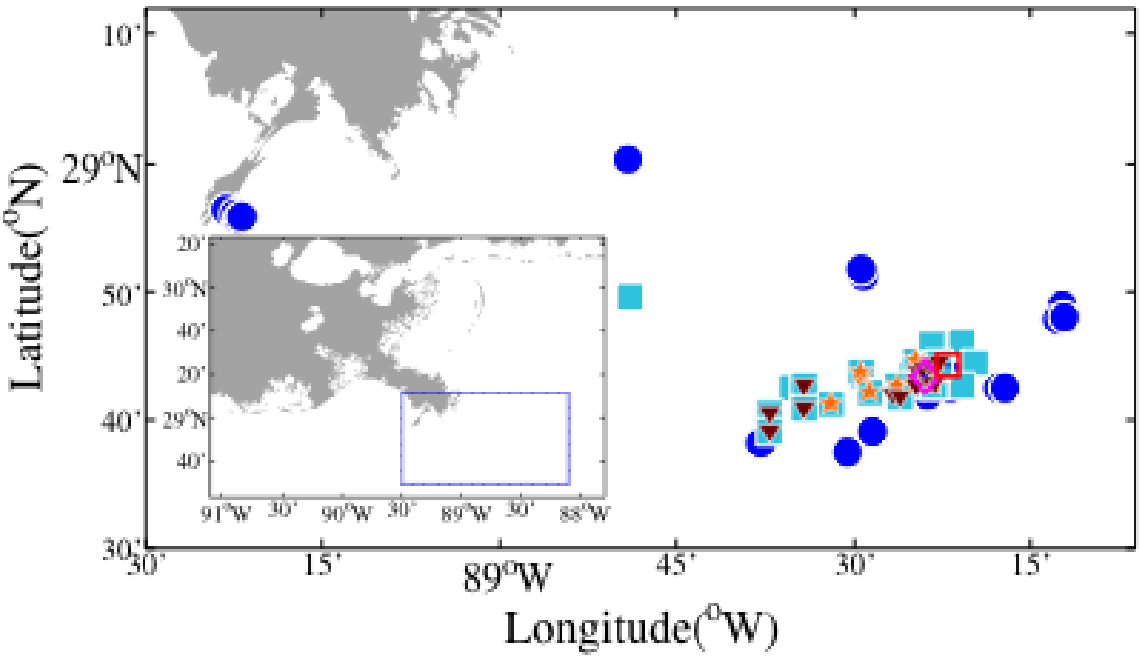

Figure 1. Sampling Locations In The Northern Gulf Of Mexico During Early May 2010 R/V Pelican Cruise (Blue Circles) And Late May/Early June 2010 R/V Walton Smith Cruise (Light Blue Squares). The Location Of The Macondo Well Is Shown By The Red Square. Another Set Of Markers (Orange Stars And Brown Triangles) Were Used To Denote Where The Two Specific Groups Of DOM Were Found In Deep Waters. The Inserted Rectangle Shows Sampling Locations Inside The Dashed Line Area.

Crude oil and dispersant samples were provided by BP. Weathered oil samples were collected with a basket from the sea surface as orimulsion at several stations close to the oil rig (e.g., stations 11 and 47). These oil samples were also measured for optical properties as an end-member reference for seawater samples after mixing with ultrafiltered seawater (<1 kDa) under ultrasound.

Table 1

Sampling Locations, Sampling Date, and Some Bulk DOM Parameters in Surface Waters

Station ID	Latitude (N)	Longitude (W)	Date	Surf. DOC (mg-C/L)	Surf. a_{254} (m^{-1})	Surf. $S_{275-295}$ (nm^{-1})
Wellhead	28˚44.312′	88°21.924′	-			
P-St1	28°56.325′	89°23.114′	05/10/10			
P-St2	28°55.940′	89°22.352′	05/10/10			
P-St3	28°55.736′	89°22.002′	05/10/10			
P-St4	28°55.819′	89°21.726′	05/10/10			
P-St5	29°00.194′	88°49.097′	05/10/10			
P-St6-1	28°51.243′	88°29.105′	05/10/10	1.23	3.84	.0227
P-St6	29°16.261′	88°16.152′	05/10/10			
P-St6-2	28°51.649′	88°29.344′	05/10/10	1.20	3.87	.0231
P-St7	28°48.892′	88°12.372′	05/11/10	1.15	3.32	.0235
P-St8	28°47.876′	88°12.600′	05/11/10	1.17	4.07	.0230
P-St9	28°48.036′	88°12.123′	05/11/10	7.94	3.78	.0235
P-St10	28°42.498′	88°17.692′	05/11/10	1.00	3.52	.0199
P-St11	28°42.455′	88°17.200′	05/11/10	1.02	2.74	.0229

Table 1 (continued).

Station ID	Latitude (N)	Longitude (W)	Date	Surf. DOC (mg-C/L)	Surf. a_{254} (m^{-1})	Surf. $S_{275-295}$ (nm^{-1})
P-St12	28°43.383′	88°21.556′	05/11/10	.87	1.58	.0274
P-St13	28°42.533′	88°21.776′	05/11/10			
P-St14	28°41.988′	88°26.698′	05/12/10	1.05	3.18	.0223
P-St15	28°42.969′	88°24.612′	05/12/10			
P-St16	28°43.520′	88°23.231′	05/12/10			
P-St17	28°42.953′	88°23.390′	05/12/10			
P-St19	28°43.965′	88°23.419′	05/12/10			
P-St20	28°44.739′	88°23.320′	05/12/10			
P-St21	28°41.924′	88°23.682′	05/12/10			
P-St22	28°39.156′	88°28.442′	05/13/10	.98	2.34	.0244
P-St23	28°37.401′	88°30.477′	05/13/10	1.02	2.55	.0239
P-St24	28°38.126′	88°37.742′	05/13/10	.91	1.82	.0267
P-St25	28°42.847′	88°23.075′	05/14/10			

Table 1 (continued).

Station ID	Latitude (N)	Longitude (W)	Date	Surf. DOC (mg-C/L)	Surf. a_{254} (m^{-1})	Surf. $S_{275-295}$ (nm^{-1})
P-St26	28°43.558′	88°23.450′	05/14/10	1.14	3.55	.0247
P-St27	28°42.998′	88°25.113′	05/14/10			
WS-St2	28°43.807′	88°24.575′	05/26/10			
WS-St2-1	28°43.651′	88°24.774′	05/26/10	1.00	2.13	.0269
WS-St2-2	28°43.483′	88°25.096′	05/26/10			
WS-St3	28°44.675′	88°24.739′	05/26/10	6.98	2.03	.0267
WS-St7-B	28°43.410′	88°29.041′	05/27/10			
WS-St13	28°49.571′	88°48.955′	05/27/10	6.35	2.11	.0284
WS-St26	28°42.524′	88°35.058′	05/28/10			
WS-St27	28°42.595′	88°34.080′	05/28/10			
WS-St29	28°43.688′	88°29.272′	05/28/10			
WS-St30	28°45.852′	88°23.263′	05/30/10	.83	1.49	.0310
WS-St31	28°46.002′	88°20.844′	05/30/10	.82	1.50	.0313
WS-St32	28°44.394′	88°19.611′	05/30/10	.79	1.66	.0315

Table 1 (continued).

Station ID	Latitude (N)	Longitude (W)	Date	Surf. DOC (mg-C/L)	Surf. a_{254} (m^{-1})	Surf. $S_{275-295}$ (nm^{-1})
WS-St33	28°42.585′	88°20.862′	05/30/10	.78	1.60	.0311
WS-St34	28°42.703′	88°23.372′	05/30/10	.71	1.51	.0283
WS-St34-B	28°42.721′	88°23.148′	05/30/12			
WS-St36	28°42.616′	88°24.602′	05/30/12			
WS-St37	28°42.622′	88°26.281	05/30/10			
WS-St39	28°42.193′	88°28.455′	05/30/10			
WS-St40	28°41.268′	88°31.891′	05/30/10			
WS-St41	28°40.951′	88°34.170′	05/30/10			
WS-St42	28°40.440′	88°37.038′	05/30/10			
WS-St43	28°39.024′	88°37.082′	05/31/10			
WS-St46	28°41.762′	88°25.952′	05/31/10			
WS-St47	28°43.302′	88°23.837′	05/31/10			
WS-St48	28°43.982′	88°24.033′	05/31/10			

Table 1 (continued).

Station ID	Latitude (N)	Longitude (W)	Date	Surf. DOC (mg-C/L)	Surf. a_{254} (m^{-1})	Surf. $S_{275-295}$ (nm^{-1})
WS-St53	28°44.010′	88°22.981′	06/01/10			
WS-St57	28°44.190′	88°23.603′	06/01/10			
WS-St58	28°44.337′	88°23.141′	06/01/10			
WS-St59	28°44.514′	88°22.714′	06/01/10			
WS-St57	28°44.190′	88°23.603′	06/01/10			
WS-St58	28°44.337′	88°23.141′	06/01/10			

Measurements of DOC and UV-vis Absorption

Concentrations of DOC were measured with a Shimadzu TOC-V total organic carbon analyzer using the high temperature combustion method (Guo et al., 1995). Samples were acidified with concentrated HCl to a pH<2 before analysis. Three to five replicate measurements each with 150 µL were made, with a coefficient of variance <2%. Calibration curves were generated before sample analysis. Nanopure water, working standard and certified DOC standard solutions (from Dr. Hansell's Lab at the University of Miami) were measured every eight samples to check the performance of the instrument.

UV-vis absorption spectra of samples were measured using a Cary UV-visible spectrophotometer (300 Bio) and a 10-cm path-length quartz cuvette over

the 190-900 nm wavelength ranges with 0.2 nm increments. The water blank was subtracted, and the refractive index effect was corrected by subtracting the averaged absorbance between 650 and 800 nm (Stedmon et al., 2000). Specific UV absorbance (SUVA) values were calculated from the UV absorbance at 254 nm (or others such as 225 and 240 nm) and DOC concentration (mg-C/L). Spectral slopes were determined by nonlinear regression (MATLAB software) over the 275-295 nm wavelength rage using the following equation: $y = Ae^{-S_o l} + C$ (Guéguen and Cuss, 2011; Helms et al., 2008; Moran et al., 2000; Twardowski et al., 2004).

Measurements of Fluorescence EEMs

Fluorescence signatures of seawater samples were acquired using a Shimadzu RF-5301PC spectrofluorometer and a 1 cm path-length quartz cuvette at 20 ˚C. Ninety-one separate fluorescence emission spectra were scanned from 240 to 680 nm with 1 nm interval under excitation wavelengths from 220 to 400 nm with a 2 nm step and concatenated to generate an excitation-emission matrix that is able to provide DOM component information for the water sample quantitatively and qualitatively (Coble, 1996; Green and Blough, 1994).

A water blank was scanned daily and its EEM was subtracted from each sample's EEM. Emission correction spectra were generated using rhodamine B and barium sulfate with the correction package from Shimadzu and multiplied to the EEM spectra (Stedmon et al., 2003). Quinine sulfate standards were also scanned daily for calibration and for checking instrument performance. Data in two triangle areas, corresponding to the Rayleigh and Raman scattering peaks

were eliminated in the PARAFAC analysis to acquire better mathematical results (Andersen and Bro, 2003; Christensen et al., 2005). All fluorescence intensities were converted to ppb-QSE units (Coble, 1996).

PARAFAC Modeling

Fluorescence PARAFAC modeling was used to investigate the spatial and temporal changes in DOM fluorescence components (Stedmon and Bro, 2008). PARAFAC modeling was applied to all 94 seawater samples from the two sampling cruises, using MATLAB software (MathWorks R2010b) and DOMFluor Toolbox (Stedmon and Bro, 2008). Seventeen samples were picked out as outlier samples after close examination of their EEMs and a non-negativity outlier test. Then the model was further validated by split-half analysis (Harshman and Lundy, 1984; Stedmon and Bro, 2008).

The fluorescence intensities of each component in every sample were quantified as outputs of the PARAFAC modeling, and were used as inputs to generate contour maps of the differentiated components in the study area.

Contour Map Generation

All contour maps were generated using MATLAB software (MathWorks R2010b) and m_map Toolbox (http://www.mathworks.com/MATLABcentral/linkexchange/links/ 993-mmap-a-mapping-package-for-MATLAB). The triangle-based cubic interpolation method was used to generate grid data for mapping.

Results and Discussion

Distributions of DOC and CDOM

Both bulk dissolved organic carbon (DOC) and CDOM concentrations in the surface waters near the Deepwater Horizon site during the two cruises were greatly influenced by oil released from the Macondo well. Concentrations of DOC were as high as 6 mg-C/L, which is considerably higher than the baseline values in the northern Gulf of Mexico (~1 mg-C/L) (Guo et al., 1994; Guo et al., 1995) and even the Mississippi River (Duan et al., 2007; Guo et al., 2009). These high DOC concentrations coincided with higher UV absorbance and lower spectral slope values and were found in surface waters around stations near 28˚44´ N 88˚25´ W and 28˚48´ N 88˚12´ W (Figure 2), indicating the presence of the released oil and its influence on the composition of DOM. Because the spectral slope $S_{275\text{-}295}$ is inversely related to DOM molecular weight (Helms et al., 2008; Twardowski et al., 2004), this suggests that higher molecular weight materials dominated the DOM found in surface waters near the Macondo well. Nevertheless, lower DOC concentrations, less optically active DOM, and lower molecular weight DOM were found at stations between the above stated areas covering the exploded oil rig, showing a patchy distribution of oil. Elevated DOC concentrations were also found at ~28˚49´ N 88˚49´ W, suggesting also the influence of oil at the northwest corner of the study area, since mere natural organic matter from river waters would not cause such high DOC concentration in the coastal waters of the Gulf of Mexico (Guo et al., 2009; Wang et al., 2004). In deep waters between 1100 and 1400 m, a region of elevated DOC

concentrations was found in the area located at 28˚41´- 28˚44´ N 88˚24´- 88˚33´ W (Figure 2), consistent with the presence of oil plume reported by other studies (Diercks et al., 2010; Hazen et al., 2010). However, no clear relationship was observed between the distribution pattern of DOC and other optical properties in the deep waters.

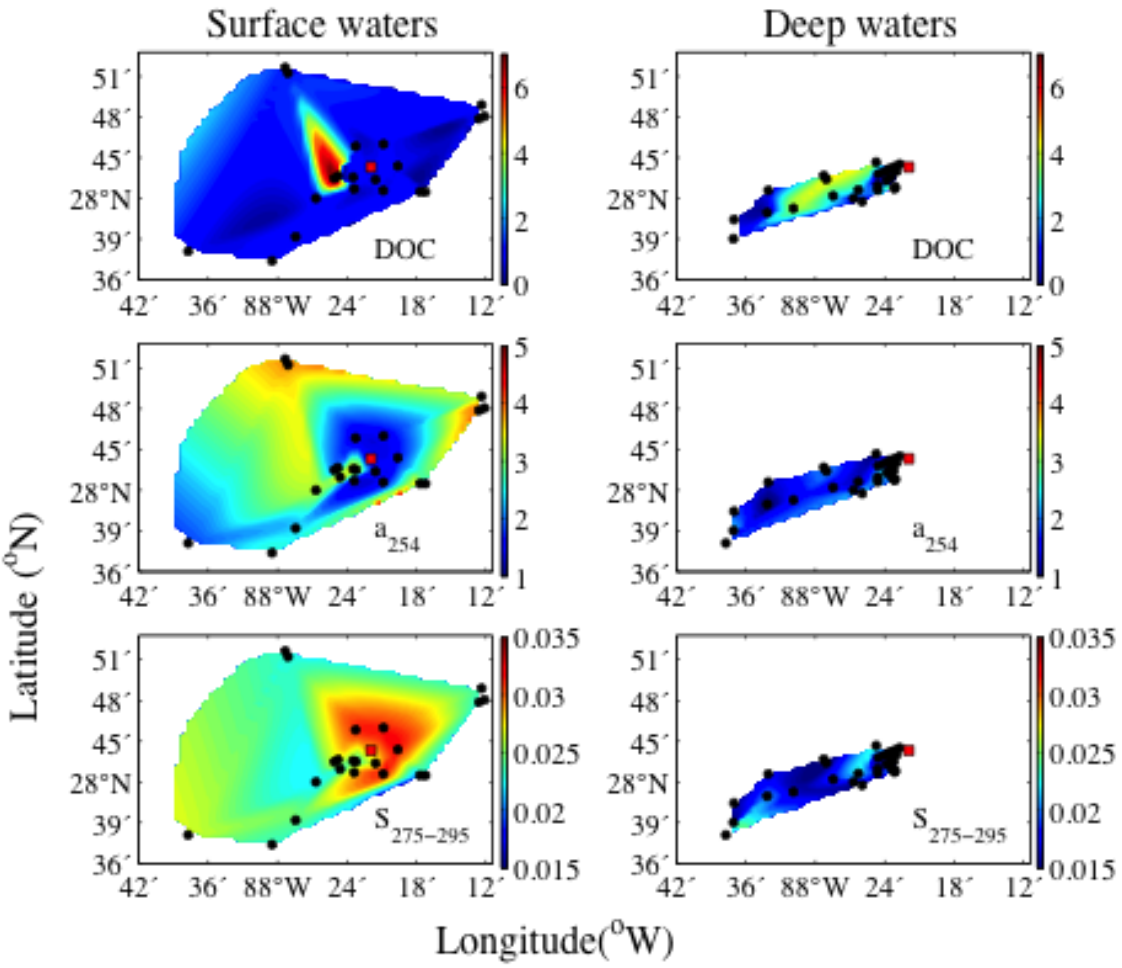

Figure 2. Distributions Of DOC Concentration (mg-C/L), UV-Vis Absorption (M-1) At 254 nm And Spectral Slope (S) In Surface (Left Column) And Deep Waters Between 1,100 – 1,400 m (Right Column) In The Northern Gulf Of Mexico.

Optical properties such as fluorescence and UV-vis absorbance can be used as a general proxy for DOM abundance in seawater, with a specific

correlation slope value between DOC concentration and optical properties when sources of DOM are constant (Chen and Gardner, 2004; Kowalczuk et al., 2010; Stedmon and Markager, 2003; Vodacek et al., 1997). Similarly, changes in SUVA values can be linked to sources and composition of DOM in the aquatic system (Weishaar et al., 2003). In this study, the correlations between DOC and $SUVA_{254}$ are dispersed and suggested the presence of two major types of DOM with distinctly different fluorescence/absorbance yields (Figure 3). Samples with high DOC concentrations but low $SUVA_{254}$ values seemed to have a quasi-positive correlation between SUVA and DOC or a_{254} values in deep waters (Figure 3) suggesting a similar DOM source. In addition, DOC concentrations (or a_{254}) and $SUVA_{254}$ are positively correlated for samples with lower DOC concentrations (0.6-1.3 mg-C/L) and higher $SUVA_{254}$ values ($P<0.0001$ for surface water samples and $P<0.12$ for deep water samples, Figure 3). The slope value of the regression line derived from low DOC samples is considerably higher than that derived from high DOC concentration samples, suggesting the existence of highly optically active DOM components in deep water samples (Figure 3).

Since oil components characterized by fluorescence spectroscopy also had lower excitation wavelengths such as 225 and 240 nm (see section 3.2), the correlations between DOC and optical properties at these wavelengths were also examined. Lower p-values and higher correlation coefficients were found for correlations between DOC and $SUVA_{225}$ or $SUVA_{240}$ (not shown) for deep-water samples, as compared to its counterparts at 254 nm. However, the overall

conclusions are the same regardless of wavelengths used to derive absorbance or spectral slope values. The decoupling between DOC concentration and optical yield might result from fractionation of DOM constituents under the influence of dispersants and preferential residence of higher molecular weight and more optically active DOM in large droplets in the deep water.

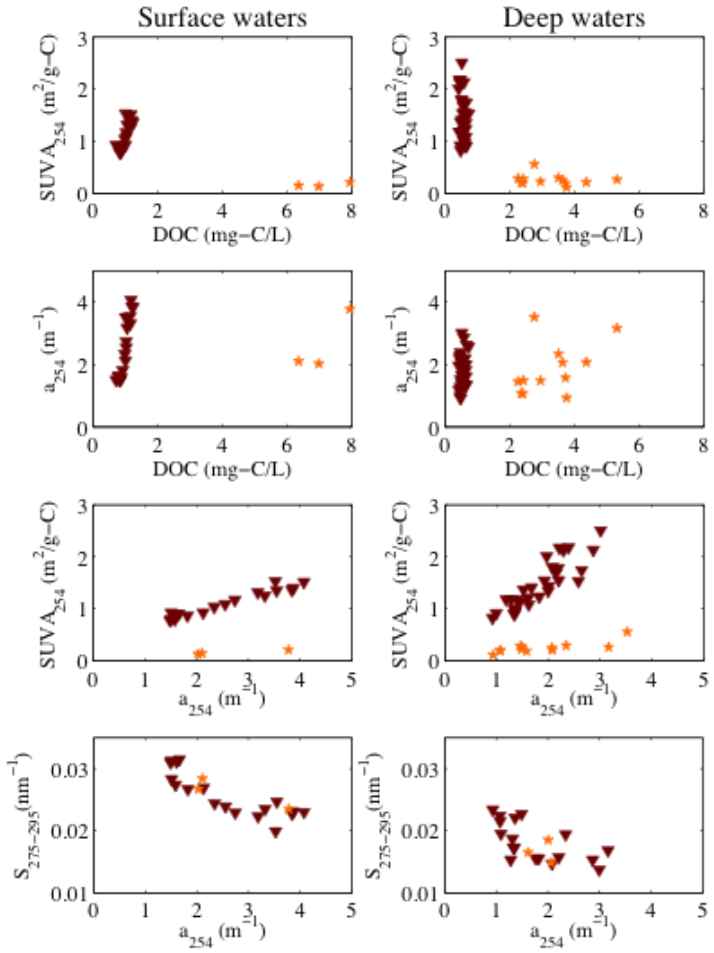

Figure 3. Relations Among DOC Concentration, UV-Vis Absorption At 254 Nm, Specific UV Absorbance At 254 nm, Spectral Slope (S) From Nonlinear Regression Over 290-400 nm, And Oil Fluorescence Intensity In Surface Waters (Left Panels) And Deep Waters (Right Panels). Samples With High DOC Concentrations But Low $SUVA_{254}$ Values Are Represented By Orange Stars, While Samples With Lower DOC Concentrations But Higher Optical Activities Are Shown With Brown Triangles. The Same Marker Types Used Here Were Also Followed In Figure 1, Where High DOC Concentration Samples Were Found

Around ~28˚42'N 88˚28'W In The Deep Water. Similar Property Correlations Were Also Found For Derived Optical Data At 225 Or 240 nm (Not Shown).

In addition, it is also likely caused by the filtration of seawater samples with 0.2 µm membranes, which may preferentially retain highly soluble low molecular weight DOM with a low optical yield, but reject less soluble large molecular weight DOM with a high optical yield. Nevertheless, methods do not seem available for filtration of oil-contaminated water samples without causing possible fractionation.

As shown in Figure 3, there are negative correlations between a_{254} and spectral slope (S) in both surface and deep waters, indicating samples with higher a_{254} values also contained higher molecular weight DOM components. This again suggests the influence of oil on the water column during the sampling time periods. Higher values of $SUVA_{254}$ (up to 2.2 m^2/g-C) and lower S values (0.01-0.025 nm^{-1}) were found in deep waters compared to surface waters, which had a high end $SUVA_{254}$ value of 1.5 m^2/g-C and S values ranging from 0.02 to 0.032 nm^{-1}. This suggests that the deep waters contained DOM component(s) with higher optical activity (yield) and lower spectral slope values or higher molecular weight from "fresher" crude oil components, which are subjected to biodegradation and photochemical degradation during their transport from deep to surface waters (Figure 3).

Fluorescence Characteristics of Oil, Dispersant and Chemically Dispersed Oil

Excitation-emission spectra of crude oil from the Macondo well, dispersant used during the oil spill, and chemically dispersed crude oil with an oil and dispersant ratio of 1:1 showed distinct fluorescence characteristics (Figure 4).

The crude oil sample had its maximum fluorescence intensities centered on 226/340 nm. Another fluorescence component of the crude oil had an emission maximum located at 322 nm over the excitation wavelength range of 260 – 280 nm (Figure 4A), which coincides with the fluorescence peak identified for other crude oils reported by Bugden et al. (2008). The dispersant was characterized with an intensity peak at Ex/Em 234/376 nm and another emission maximum at 370 nm over an excitation range of 260-290 nm (Figure 4B).

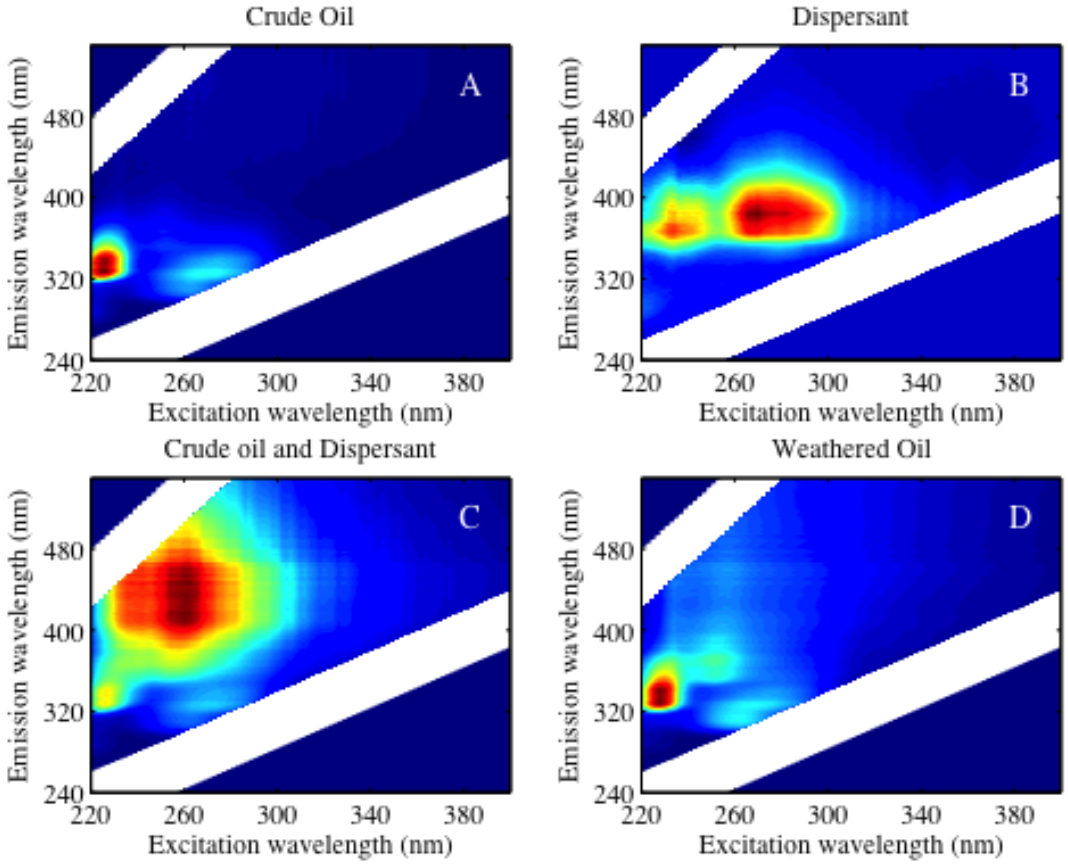

Figure 4. Fluorescence EEM Spectra Of End-member Crude Oil (Panel A), Dispersant (Panel B), Dispersed Crude Oil (1:1, panel C) And Weathered Oil Collected From Surface Seawater At Close Proximity Of The Oil Rig (Panel D).

Chemically dispersed oil showed a large increase in the fluorescence intensity of the emission band at 430 nm and was characterized with a peak at Ex/Em 260/430 nm (Figure 4C). Bugden et al. (2008) and Kepkay et al. (2002) also found similar effects of dispersant on the fluorescence spectra of crude oil. However, the fluorescence characteristics of dispersant were not easily discernable in the EEM of chemically dispersed oil. The different EEM spectra between crude oil, dispersant, and chemically dispersed oil should allow one to investigate the influence of both oil and dispersant on natural water samples.

Weathered oil samples collected from surface water during May/June 2010 cruise (e.g., station 47) showed very similar fluorescence EEM spectra to those of the crude oil sample from the Macondo well (Figure 4D). Nevertheless, their fluorescence EEM spectra also showed additional fluorescence components, for example, the one with a peak at Ex/Em ~240/355 nm. In addition, the spectral slope value of the weathered oil sample (0.0079 nm^{-1}) was larger than that found for the crude oil, 0.0019 nm^{-1}, suggesting overall smaller molecular weights for weathered oil samples. These differences are probably largely derived from rapid microbial and photochemical degradation of oil in the water column, as also observed in laboratory degradation experiments using the Macondo crude oil (Zhou et al., 2012). The changes in the EEM spectra and other optical properties of oil samples might thus be used to evaluate the degradation status of oils and their fate and transport in the water column.

Fluorescence Characteristics of Seawater Samples

Examples of fluorescence EEMs of seawater samples from different depths at two stations are shown in Figure 5. These EEM spectra and Ex/Em maxima strongly resemble those of the crude oil as shown in Figure 4, indicating the dominance of oil on all samples regardless of water depth and station (Figure 5). Fluorometry has been used to screen oil presence in the subsurface plume during the DWH oil spill (Diercks et al., 2010; Wade et al., 2011). A strong correlation was found between fluorescence intensities and polycyclic aromatic hydrocarbon (PAH) concentration (Wade et al., 2011). Both *in-situ* fluorescence data (Diercks et al., 2010; Joye et al., 2011) and our bench-top spectrofluorometric measurements showed that most of the elevated oil fluorescence intensities were found at 1000 – 1400 m. However, maximal oil fluorescence signatures were measured either in surface waters or deep waters at different stations (see examples in Figure 5), indicating heterogeneous distributions of oil in the water column during the DWH oil spill.

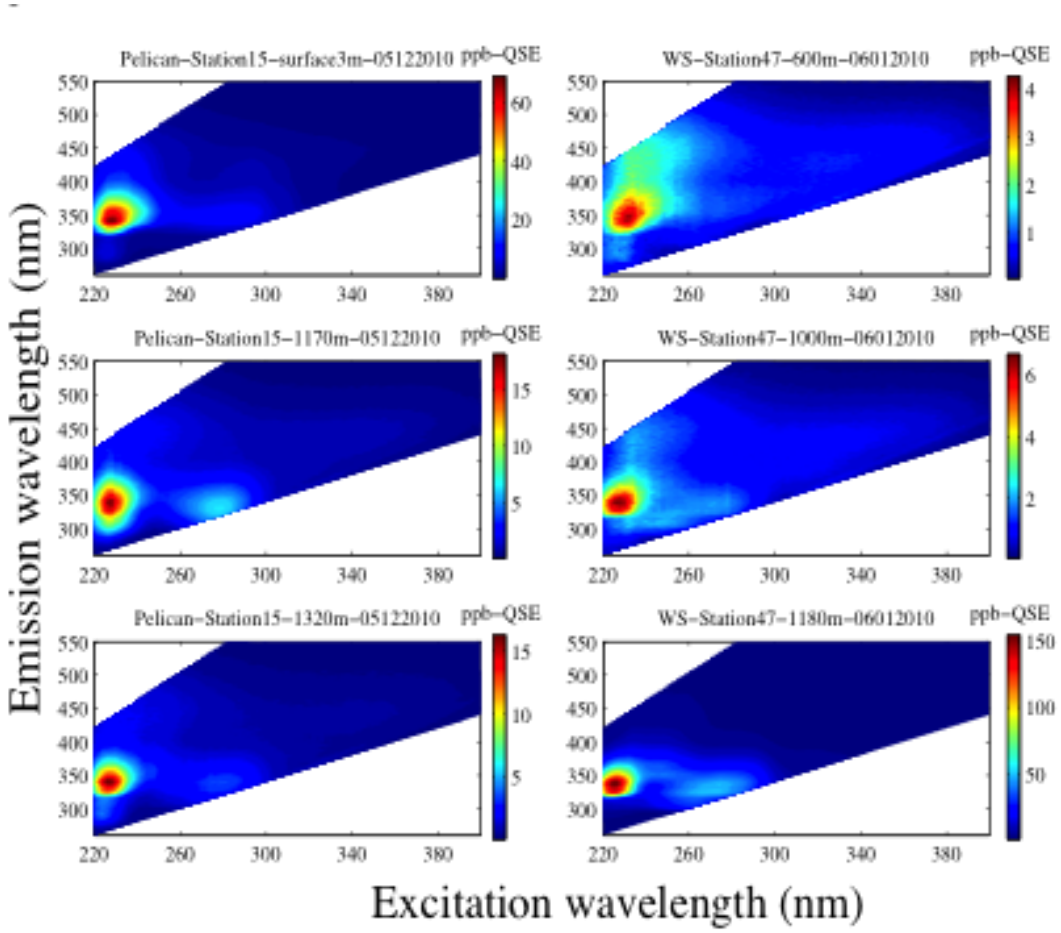

Figure 5. Examples Of Fluorescence EEMs Of Water Samples From Two Vertical Profiles Showing The Strong Presence Of Oil with Maximum Fluorescence Intensities Occurring Either In The Surface (Left Panels) Or Deep Waters (Right Panels).

While elevated fluorescence signatures identified by an *in situ* CDOM sensor faded away rapidly due to use of an unfavorable Ex/Em wavelength pair, identification and fingerprinting of oil components in seawater using 3D fluorescence spectroscopy are sensitive and reliable even several months after the oil spill event (Zhou and Guo, 2012) .

While the EEM spectra of seawater samples overwhelmingly contain the fingerprints of crude oil components (Figure 5), the fluorescence signatures of dispersant (Figure 4B) were not identifiable in seawater samples collected during

May/June 2010 due to its low optical activity compared to oil and its highly dispersive nature and rapid dilution by ambient seawater in the water column although the presence of dispersant was detected by other techniques (Kujawinski et al., 2011). Diminished emission peaks of pure dispersant in fluorescence EEM after the mixture of oil and dispersant also explain the absence of dispersant related fluorescence signatures in the water column. In contrast, the fluorescence peak at Ex/Em 260/430 nm, corresponding to chemically dispersed oil, was visually observable in seawater samples collected in June 2010.

Based on PARAFAC modeling, six fluorescence DOM components (C1 – C6) can be readily identified for seawater samples collected during the May/June 2010 cruises (Figure 6), and their specific Ex/Em maxima are listed in Table 2. The first fluorescence component (C1) with its Ex/Em maximum at 226/340 nm is the dominant component from the crude oil, and is probably the source of higher molecular weight DOM in deep waters. This component strongly resembles the PAH fluorescence (Beltrán et al., 1998; Christensen et al., 2005). The second component (C2) has its fluorescence Ex/Em intensity peak at 236/350 nm, resembling naphthalene/1-methyl naphthalane (Alostaz et al., 2008), but may also have originated from the degradation of crude oil based on changes in fluorescence component ratios (see discussion below). The third fluorescent component (C3), with two peaks at Ex/Em 256/460 and 340/460 nm, seems to have terrestrial humic characteristics showing widespread “A” and “C” peaks (Coble, 1996). In addition, the humic-like “A” peak also lies within close proximity

of the peak characteristic in chemically dispersed oil (Figure 4 and Bugden et al., 2008). Thus, it is likely that C3 is a mixture of natural humic-like DOM and chemically dispersed oil. The fourth component (C4), showing two peaks at Ex/Em ~240/324 and 280/324 nm, respectively, appears to consist of amino acid signals (Coble, 1996; Stedmon et al., 2007). The fifth component (C5) has two emission peaks at 290 and 477 nm over excitation at 224 nm, and appears to be a photochemical product of terrestrial organic matter, but its origin is yet uncertain (Stedmon et al., 2007). The sixth component (C6), with Ex/Em maximum at (260–280)/311 nm, shows a similar emission maximum as fluorene (Beltrán et al., 1998; Christensen et al., 2005), and is also likely a product of crude oil. The higher abundance of high molecular weight DOM in deep waters probably resulted from the preferential degradation or volatilization of lower molecular weight oil components in surface waters (Douglas et al., 2002).

Overall, four of the fluorescence DOM components (C1, C2, C3 and C6) are associated with the oil components found in the crude oil, weathered oil, and chemically dispersed oil samples. Thus, they are DOM components derived from Macondo oil.

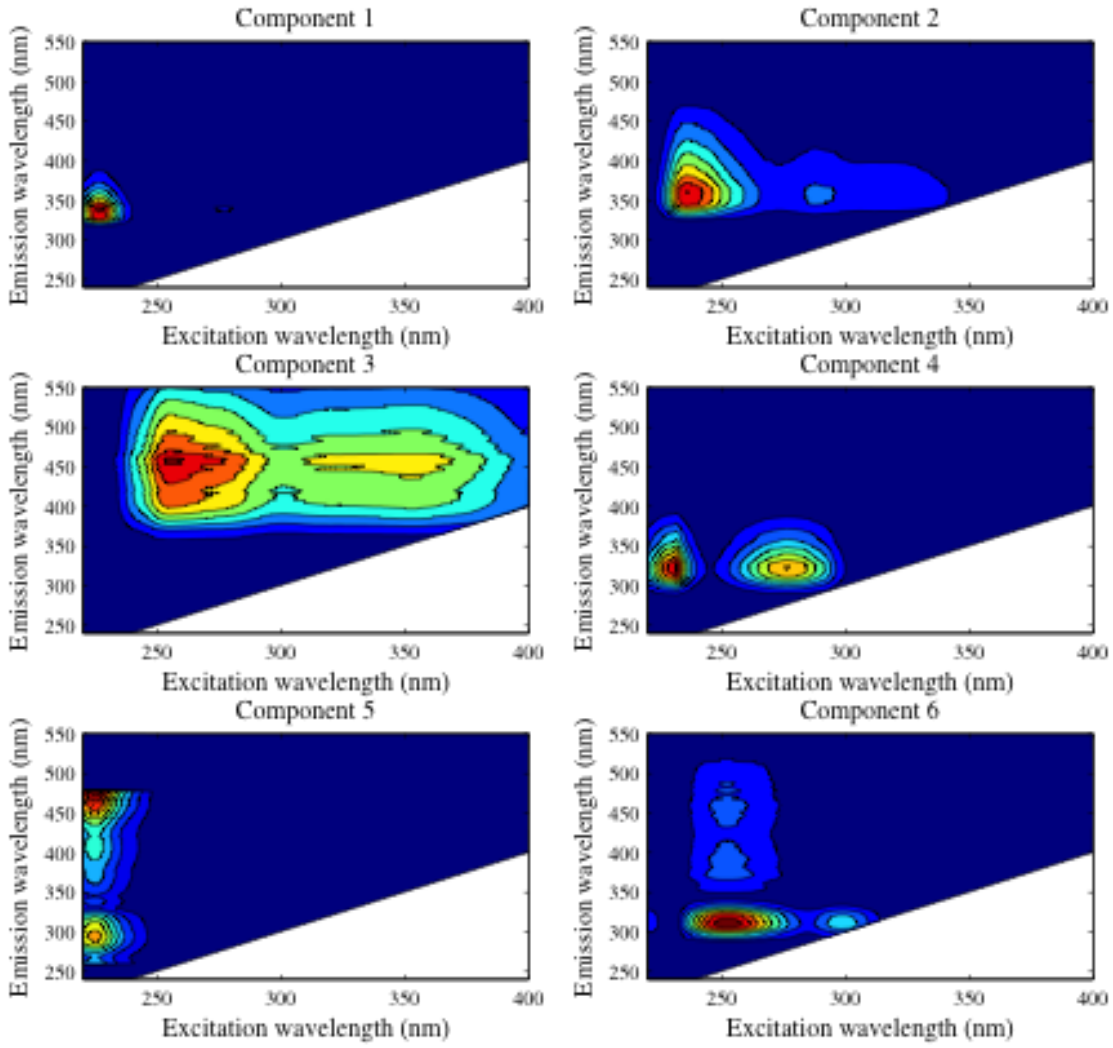

Figure 6. Characteristics Of Six Major DOM (Or Oil) Components Revealed By Fluorescence PARAFAC Modeling For Seawater Samples Collected During May 2010 In The Northern Gulf Of Mexico.

It is noteworthy that C3, has similar fluorescence characteristics to those previously reported for UV humic-like substances in natural seawater, as well as to the chemically dispersed oil. The C4 shows amino acid signals and C5 is likely to be a photochemical product of terrestrial organic matter (Table 2, Figure 6). However, as Christensen et al. (2005) noted, the alkylation of PAHs such as phenanthrene can also produce similar red-shifted emission spectra at longer wavelengths, while complex mixtures of PAHs having similar excitation and

emission spectra could produce broad, featureless components from PARAFAC modeling.

Table 2

Characteristics of the Six Fluorescence Components (C1 to C6) in Seawater Samples Identified by PARAFAC Modeling

Component	Excitation peak (nm)	Emission peak (nm)	Description
C1	226	340	Oil – related, dominant component
C2	236	350	Oil – related, degradation product
C 3	256, 340	460	Terrestrial humic substance, and chemically dispersed oil
C4	232, 275	324	Amino acids
C5	224	290, 477	Photochemical degradation product of terrestrial organic matter
C 6	252	311	Oil – related, degradation product

As shown in Figure 7, fluorescence intensity of oil components (e.g., component 1, C1) and a_{254} were positively correlated (P = 0.0011) in surface water samples. In contrast, the scattered relationship between oil fluorescence intensity and absorbance values of deep-water samples suggested that oil components in the deep water were more complex and diversified. For example, some samples from the deep water had high oil fluorescence signals but

intermediate absorbance values, while other samples had high absorbance but very low fluorescence intensities (Figure 7), consistent with the heterogeneous distribution of oil in the water column (Figure 5).

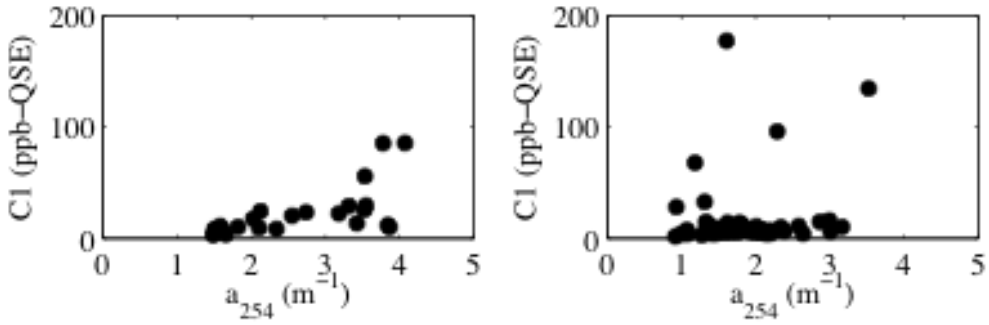

Figure 7. Correlation Between a254 (M-1) And Fluorescence Intensity Of Component 1.

I speculated that deep water samples contained mostly fresher oil derived from the Macondo well containing a wide spectrum of oil components with different optical characteristics and fluorescence quantum yields, while surface water samples contained oils which had undergone fractionation, degradation, and coagulation during their transport from the deep water to the surface. Furthermore, the oil-derived fluorescent substances detected in deep waters have the strongest absorption in the UV wavelength range <300 nm, as indicated from their primary excitation peaks at <300 nm (Figure 4). This in part explains the relationship of oil component C1 fluorescence to a_{254} in Figure 7. The differences in oil components between the surface and deep waters should be reflected in fluorescence components identified by PARAFAC analysis and the spatial and temporal changes in oil component ratios and will be discussed below.

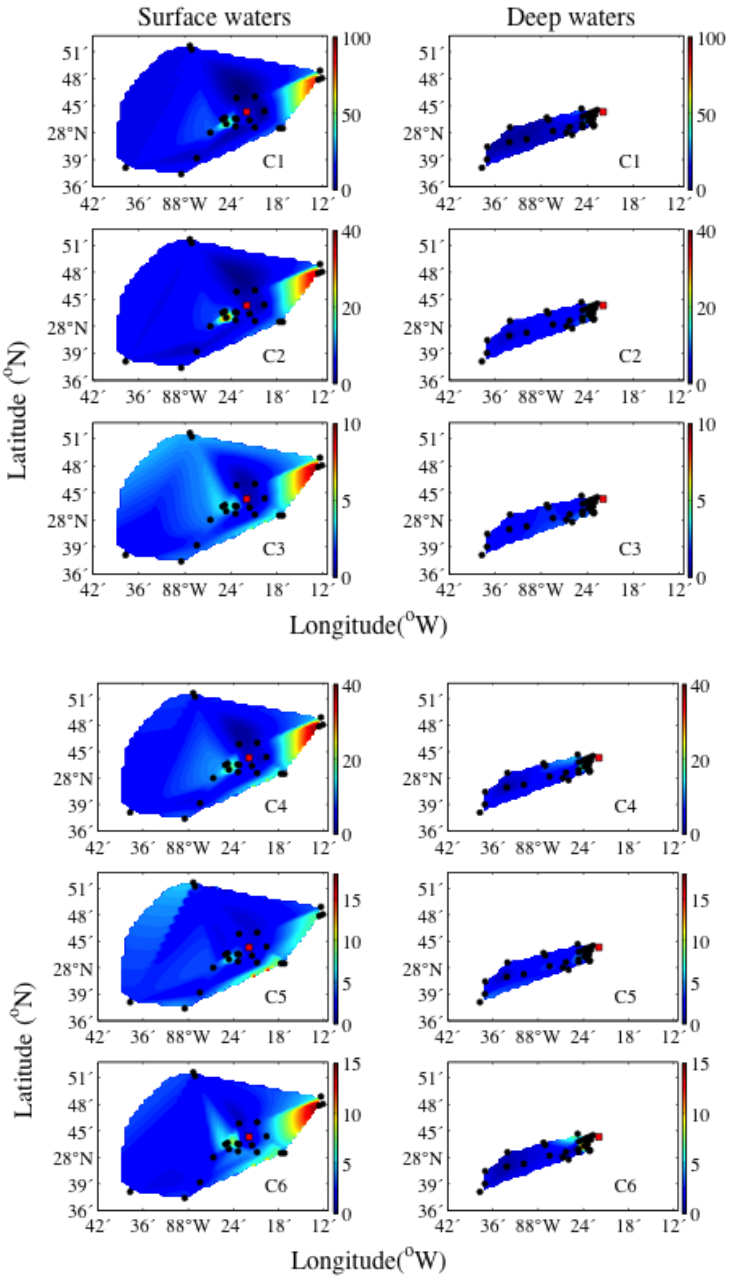

Figure 8. Distributions Of Fluorescence Intensities (Ppb-Qse) Of DOM Components Derived From PARAFAC Modeling In Surface (Left Panels) And Deep Waters Between 1,100 – 1,400 M (Right Panels) Near The Deepwater Horizon Site (Red Square).

Spatial Variability of PARAFAC Components

The distributions of the three oil components (C1, C2 and C6) and C3 that partially represents chemically dispersed oil in surface waters show a pattern of

dominance by a point source, with the highest oil fluorescence intensity close to the Macondo well, at 28˚43’N 88˚25’W (Figure 8). As the distance from the point source close to the oil rig increased, the fluorescence intensity decreased, consistent with the extent of oil influence. Another area of elevated oil fluorescence intensities was found at around 28°47’N 88°16’W. The spatial distribution pattern of oil components in the surface water is consistent with that observed for DOC concentration, UV-vis absorbance and spectral slope in the regions impacted by oil (Figure 2). Similar distribution patterns of oil has been observed through satellite imagery in the Gulf of Mexico (Hu et al., 2011), suggesting compatibility of circulation patterns and oil-derived component spatial distribution. The distribution pattern of C4, possibly comprising amino acids, also showed a response to the presence of oil, likely from induced growth of oil-degrading bacteria and breakdown of biota that are intolerant to the toxicity of crude oil (Figure 8). In contrast, the fifth fluorescent component, consisting of photochemical products of terrestrial organic matter, generally had a low fluorescence intensity and was more evenly distributed spatially (Figure 8), suggesting that the sources for C5 were different from the oil components. Although covering a smaller area, the distribution pattern of the four oil-related components in the deep water, showed again a distribution pattern with a point source from the Macondo well (Figure 8), but they had not been dispersed as far as in the surface water during the sampling time period. It seemed that lateral transport of oil in the deep water was limited during May/June 2010 compared to that in the surface water as shown in Figure 8.

Variations in Oil Component Ratios and Their Implications

Three of the fluorescence components, C1, C2 and C6, identified by PARAFAC modeling resemble those of crude oil and weathered oil. The absolute fluorescence intensity of them all seemed to decrease from crude oil to seawater samples. However, changes in the fluorescence component ratios, an intensive property, between crude oil and weathered oil in seawater, and between seawater samples and crude oil, would likely reflect the degradation status of oil and can be used as an index to examine the fate and transformation processes of oil in the Gulf of Mexico. For example, the ratio of C2 to C1 shows a general increase from crude oil to weathered oil and to the seawater samples (Figure 9). This suggests that the degradation rate of C1 could be much faster than C2 or that component C2 is largely a degraded product of crude oil. As the oil degraded, the C2/C1 ratio in seawater increased from early May to late May and to October 2010, regardless of surface or deep waters (Figure 9). For the component ratio of C6/C1, however, the crude oil had a similar ratio as the weathered oil collected from surface waters, and a higher C6/C1 ratio than the samples collected during early May 2010 when the extent of the oil spill was high. After the initial decrease, the C6/C1 ratio then increased with time in these series samples (Figure 9). This suggests that C6 could be an original crude oil component with a higher initial degradation rate compared to C1, and at the same time, it could also be a degradation-derived oil component, resulting in an initial decrease in the C6/C1 ratio, followed by an increase with time especially after the wellhead was capped (Figure 9). We hypothesize that C2 is largely

derived from the degradation of crude oil whereas C6 is an original oil component but also could be derived from oil degradation. Therefore, the dynamic changes in the fluorescence components of oil-affected seawater samples can be linked to the degradation and fractionation processes, and thus the fate and transport of crude oil during oil spill events.

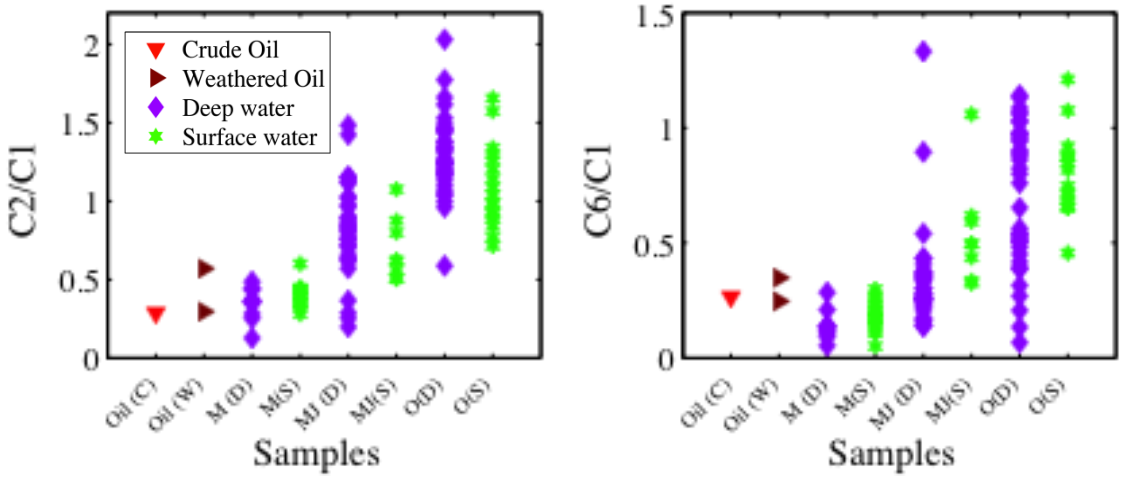

Figure 9. Variations In The Oil Component Ratio C2/C1 (Left Panel) And C6/C1 (Right Panel) Of Crude Oil [Oil(C)], Weathered Oil [Oil(W)], Deep Water Samples Taken In Mid-May [M(D)], Surface Samples Taken In Mid-May [M(S)], Deep Water Samples Taken In Late May - Early June, [Mj(D)], Surface Water Samples Taken During Late May-Early June [Mj(S)], Deep Water Samples Taken In October [O(D)], And Surface Water Samples Taken In October 2010 [O(S)] (Data of October 2010 Samples Are From The Next Chapter).

In addition, the fluorescence component ratios may represent a compelling alternative to other chemical analyses of oil in seawater. These results have important implications in oil spill research and environmental monitoring.

As shown in Figure 10, both the C2/C1 and C6/C1 ratios in surface water samples were positively correlated ($P< 0.001$ for both cases) with spectral slope value, which had an inverse relationship with the aromaticity and average molecular weight of DOM (Helms et al., 2008; Twardowski et al., 2004). Thus,

the positive correlation of C2/C1 or C6/C1 ratios with spectral slope values indicates that both C2 and C6 components contain more low molecular weight DOM materials with less aromaticity compared to crude oil.

As the oil degraded, both C2/C1 and C6/C1 ratios in the water column increased and the overall molecular weight tended to decrease. Similarly, the C6/C2 ratio was also positively correlated (P = 0.0013) with the spectral slope (Figure 10), suggesting that the average molecular weight of oil components decreased from C1 to C2 and C6.

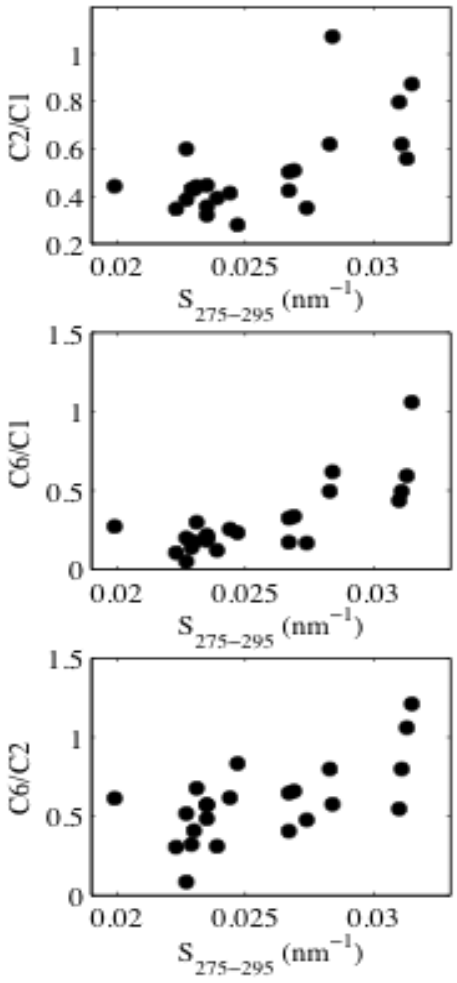

Figure 10. Relationships Between Spectral slope (S) And Oil Component Ratios (C2/C1, C6/C1, and C6/C2) in Surface Water Samples.

Conclusions

The Deepwater Horizon oil spill greatly changed the optical properties of DOM in seawater in the northern Gulf of Mexico, and provided a natural laboratory to study the fate and transformation processes of oil in marine environments. Elevated DOC concentration, higher absorption values, and lower spectral slope (i.e., higher molecular weight DOM) were found in the surface waters during May and early June 2010. There were two types of DOM in the water column, one with high optical activity but low in abundance and the other with low optical activity but high in DOC concentration. The fluorescence EEM spectra of both surface oil and seawater samples strongly resembled those of crude oil from the Macondo well, with maximum Ex/Em centered on 226/340 nm. Six fluorescence components were identified using PARAFAC analysis: three of them are components associated with crude or weathered oil, one represents partially UV humic-like DOM and partially chemically dispersed oil, one represents amino acid-like substances, and one is possibly a photochemical product of terrestrial DOM. Based on the dynamic changes between the fluorescence components in the water column, C2 and C6 contain mostly lower molecular weight materials and the oil component ratios such as C2/C1 and C6/C1 seem closely related to the degradation status of oil. The combined application of fluorescence EEM, PARAFAC modeling, and other optical properties can be used to effectively examine oil degradation pathways and mechanisms, and the fate and transport of oil components in the water column.

REFERENCES

Alostaz, M., Biggar, K., Donahue, R. and Hall, G., 2008. Petroleum contamination characterization and quantification using fluorescence emission-excitation matrices (EEMs) and parallel factor analysis (PARAFAC). Journal of Environmental Engineering & Science, 7(3): 183-197, doi: 10.1139/s07-049.

Andersen, C.M. and Bro, R., 2003. Practical aspects of PARAFAC modeling of fluorescence excitation-emission data. Journal of Chemometrics, 17(4): 200-215, doi: 10.1002/cem.790.

Beltrán, J.L., Ferrer, R. and Guiteras, J., 1998. Multivariate calibration of polycyclic aromatic hydrocarbon mixtures from excitation-emission fluorescence spectra. Analytica Chimica Acta, 373(2-3): 311-319.

Booksh, K.S., Muroski, A.R. and Myrick, M.L., 1996. Single-measurement excitation/emission matrix spectrofluorometer for determination of hydrocarbons in ocean water. 2. calibration and quantitation of naphthalene and styrene. Analytical Chemistry, 68(20): 3539-3544, doi: 10.1021/ac9602534.

Bugden, J.B.C., Yeung, C.W., Kepkay, P.E. and Lee, K., 2008. Application of ultraviolet fluorometry and excitation-emission matrix spectroscopy (EEMS) to fingerprint oil and chemically dispersed oil in seawater. Marine Pollution Bulletin, 56(4): 677-685, doi: 10.1016/j.marpolbul.2007.12.022.

Camilli, R. et al., 2010. Tracking hydrocarbon plume transport and biodegradation at deepwater horizon. Science, 330(6001): 201-204.

Chen, R.F. and Gardner, G.B., 2004. High-resolution measurements of chromophoric dissolved organic matter in the Mississippi and Atchafalaya River plume regions. Marine Chemistry, 89(1-4): 103-125.

Christensen, J.H., Hansen, A.B., Mortensen, J. and Andersen, O., 2005. Characterization and matching of oil samples using fluorescence spectroscopy and parallel factor analysis. Analytical Chemistry, 77(7): 2210-2217, doi: 10.1021/ac048213k.

Coble, P.G., 1996. Characterization of marine and terrestrial DOM in seawater using excitation-emission matrix spectroscopy. Marine Chemistry, 51(4): 325-346, doi: 10.1016/0304-4203(95)00062-3.

Coble, P.G., Green, S.A., Blough, N.V. and Gagosian, R.B., 1990. Characterization of dissolved organic matter in the Black Sea by fluorescence spectroscopy. Nature, 348(6300): 432-435.

Del Vecchio, R. and Blough, N.V., 2004. Spatial and seasonal distribution of chromophoric dissolved organic matter and dissolved organic carbon in the Middle Atlantic Bight. Marine Chemistry, 89(1-4): 169-187.

Diercks, A.-R. et al., 2010. Characterization of subsurface polycyclic aromatic hydrocarbons at the Deepwater Horizon site. Geophysical Research Letters, 37(20): L20602, doi: 10.1029/2010gl045046.

Dietrich, J.C. et al., 2012. Surface trajectories of oil transport along the Northern Coastline of the Gulf of Mexico. Continental Shelf Research, 41(0): 17-47.

Douglas, G.S., Owens, E.H., Hardenstine, J. and Prince, R.C., 2002. The OSSA II pipeline oil spill: the character and weathering of the spilled oil. Spill

Science and Technology Bulletin, 7(3): 135-148, doi: 10.1016/s1353-2561(02)00046-4.

Duan, S. et al., 2007. Variability in the bulk composition and abundance of dissolved organic matter in the lower Mississippi and Pearl rivers. Journal of Geophysical Research, 112(G2): G02024, doi: 10.1029/2006JG000206.

Ferreira, A.M., Micaelo, C. and Vale, C., 2003. Are coastal resources of NW Portugal fingerprinting hydrocarbons released from the Prestige accident? Ciencias Marinas, 29(1): 109-114.

González, J.J. et al., 2006. Spatial and temporal distribution of dissolved/dispersed aromatic hydrocarbons in seawater in the area affected by the Prestige oil spill. Marine Pollution Bulletin, 53(5-7): 250-259, doi: 10.1016/j.marpolbul.2005.09.039.

Green, S.A. and Blough, N.V., 1994. Optical absorption and fluorescence properties of chromophoric dissolved organic matter in natural waters. Limnology and Oceanography, 39(8): 1903-1916.

Guéguen, C. and Cuss, C.W., 2011. Characterization of aquatic dissolved organic matter by asymmetrical flow field-flow fractionation coupled to UV-Visible diode array and excitation emission matrix fluorescence. Journal of Chromatography A, 1218(27): 4188-4198, 10.1016/j.chroma.2010.12.038.

Guéguen, C., Guo, L., Yamamoto-Kawai, M. and Tanaka, N., 2007. Colored dissolved organic matter dynamics across the shelf-basin interface in the western Arctic Ocean. Journal of Geophysical Research, 112(C5): C05038, doi: 10.1029/2006jc003584.

Guo, L., Coleman Jr, C.H. and Santschi, P.H., 1994. The distribution of colloidal and dissolved organic carbon in the Gulf of Mexico. Marine Chemistry, 45(1-2): 105-119.

Guo, L., Santschi, P.H. and Warnken, K.W., 1995. Dynamics of dissolved organic carbon (DOC) in oceanic environments. Limnology and Oceanography, 40(8): 1392-1403.

Guo, L., White, D.M., Xu, C. and Santschi, P.H., 2009. Chemical and isotopic composition of high-molecular-weight dissolved organic matter from the Mississippi River plume. Marine Chemistry, 114(3-4): 63-71.

Harshman, R.A. and Lundy, M.E., 1984. The PARAFAC model for three-way factor analysis and multidimentional scaling. In: H.G. Law, C.W. Snyder Jr, J.A. Hattie and R.P. E McDonald (Editors), Research methods for multimode data analysis. Praeger, New York, pp. 112-215.

Hazen, T.C. et al., 2010. Deep-sea oil plume enriches indigenous oil-degrading bacteria. Science, 330(6001): 204-208, doi: 10.1126/science.1195979.

Hedges, J.I., 2002. Why dissolved organic matter? In: D.A. Hansell and C.A. Carlson (Editors), Biogeochemistry of marine dissolved organic matter. Academic Press: San Diego, London, UK., pp. 1-33.

Helms, J.R. et al., 2008. Absorption spectral slopes and slope ratios as indicators of molecular weight, source, and photobleaching of chromophoric dissolved organic matter. Limnology and Oceanography, 53(3): 955-969.

Hu, C. et al., 2011. Did the northeastern Gulf of Mexico become greener after the Deepwater Horizon oil spill? Geophysical Research Letters, 38(9): L09601, doi: 10.1029/2011GL047184.

Joye, S.B., MacDonald, I.R., Leifer, I. and Asper, V., 2011. Magnitude and oxidation potential of hydrocarbon gases released from the BP oil well blowout. Nature Geoscience, 4(3): 160-164, doi: org/10.1038/ngeo1067.

Kessler, J.D. et al., 2011. A persistent oxygen anomaly reveals the fate of spilled methane in the deep Gulf of Mexico. Science, 331(6015): 312-315, doi: 10.1126/science.1199697.

Kim, M. et al., 2010. Hebei Spirit oil spill monitored on site by fluorometric detection of residual oil in coastal waters off Taean, Korea. Marine Pollution Bulletin, 60(3): 383-389, doi: 10.1016/j.marpolbul.2009.10.015.

Kowalczuk, P. et al., 2010. Characterization of dissolved organic matter fluorescence in the South Atlantic Bight with use of PARAFAC model: Relationships between fluorescence and its components, absorption coefficients and organic carbon concentrations. Marine Chemistry, 118(1-2): 22-36.

Kowalczuk, P. et al., 2009. Characterization of dissolved organic matter fluorescence in the South Atlantic Bight with use of PARAFAC model: Interannual variability. Marine Chemistry, 113(3-4): 182-196.

Kujawinski, E.B. et al., 2011. Fate of dispersants associated with the Deepwater Horizon oil spill. Environmental Science and Technology, 45(4): 1298-1306, doi: 10.1021/es103838p.

Leifer, I. et al., 2012. State of the art satellite and airborne marine oil spill remote sensing: Application to the BP Deepwater Horizon oil spill. Remote Sensing of Environment, 124(0): 185-209.

Liu, Y., MacFadyen, A., Ji, Z.G. and Weisberg, R.H., 2011. Monitoring and modeling the Deepwater Horizon oil spill: a record-breaking enterprise. Geophys. Monogr. Ser., 195. AGU, Washington, DC, 271 pp.

Mascarelli, A., 2010. Deepwater Horizon: After the oil. Nature, 467: 22-24, doi: 10.1038/news.2010.378.

Moran, M.A., Sheldon, W.M., Jr. and Zepp, R.G., 2000. Carbon loss and optical property changes during long-term photochemical and biological degradation of estuarine dissolved organic matter. Limnology and Oceanography, 45(6): 1254-1264.

Murphy, K.R., Stedmon, C.A., Waite, T.D. and Ruiz, G.M., 2008. Distinguishing between terrestrial and autochthonous organic matter sources in marine environments using fluorescence spectroscopy. Marine Chemistry, 108(1-2): 40-58.

Patra, D. and Mishra, A.M., 2002. Total synchronous fluorescence scan spectra of petroleum products. Analytical and Bioanalytical Chemistry, 373(4): 304-309, doi: 10.1007/s00216-002-1330-y.

Reddy, C.M. et al., 2011. Composition and fate of gas and oil released to the water column during the Deepwater Horizon oil spill. Proceedings of the National Academy of Sciences: doi: 10.1073/pnas.1101242108.

Schrope, M., 2011. Oil cruise finds deep-sea plume. Nature, 465: 274-275, doi: 10.1038/465274a.

Sierra, M.M.D., Giovanela, M., Parlanti, E. and Soriano-Sierra, E.J., 2006. 3D-fluorescence spectroscopic analysis of HPLC fractionated estuarine fulvic and humic acids. Journal of the Brazilian Chemical Society, 17: 113-124.

Stedmon, C.A. and Bro, R., 2008. Characterizing dissolved organic matter fluorescence with parallel factor analysis: a tutorial. Limnology and Oceanography - Methods 6: 572-579, doi: 10.4319/lom.2008.6.572.

Stedmon, C.A. and Markager, S., 2003. Behaviour of the optical properties of coloured dissolved organic matter under conservative mixing. Estuarine, Coastal and Shelf Science, 57(5-6): 973-979.

Stedmon, C.A., Markager, S. and Bro, R., 2003. Tracing dissolved organic matter in aquatic environments using a new approach to fluorescence spectroscopy. Marine Chemistry, 82(3-4): 239-254, doi: 10.1016/s0304-4203(03)00072-0.

Stedmon, C.A., Markager, S. and Kaas, H., 2000. Optical properties and signatures of chromophoric dissolved organic matter (CDOM) in Danish coastal waters. Estuar. Coast. Shelf. S., 51: 267-278.

Stedmon, C.A. et al., 2007. Photochemical production of ammonium and transformation of dissolved organic matter in the Baltic Sea. Marine Chemistry, 104(3-4): 227-240, doi: 10.1016/j.marchem.2006.11.005.

Stolpe, B., Guo, L., Shiller, A.M. and Hassellöv, M., 2010. Size and composition of colloidal organic matter and trace elements in the Mississippi River,

Pearl River and the northern Gulf of Mexico, as characterized by flow field-flow fractionation. Marine Chemistry, 118(3-4): 119-128.

Turner, A. and Mawji, E., 2004. Hydrophobicity and octanol-water partitioning of trace metals in natural waters. Environmental Science and Technology, 38(11): 3081-3091.

Twardowski, M.S., Boss, E., Sullivan, J.M. and Donaghay, P.L., 2004. Modeling the spectral shape of absorption by chromophoric dissolved organic matter. Marine Chemistry, 89(1-4): 69-88.

Valentine, D.L. et al., 2010. Propane respiration jump-starts microbial response to a deep oil spill. Science, 330(6001): 208-211.

Vodacek, A., Blough, N.V., DeGrandpre, M.D., Peltzer, E.T. and Nelson, R.K., 1997. Seasonal variation of CDOM and DOC in the Middle Atlantic Bight: terrestrial inputs and photooxidation. Limnology and Oceanography, 42(4): 674-686.

Wade, T.L. et al., 2011. Analyses of water samples from the Deepwater Horizon oil spill: documentation of the subsurface plume, Monitoring and Modeling the Deepwater Horizon Oil Spill: A Record-Breaking Enterprise. Geophys. Monogr. Ser. AGU, Washington, DC, pp. 77-82, doi: 10.1029/2011gm001103.

Walker, S.A., Amon, R.M.W., Stedmon, C., Duan, S. and Louchouarn, P., 2009. The use of PARAFAC modeling to trace terrestrial dissolved organic matter and fingerprint water masses in coastal Canadian Arctic surface waters. Journal of Geophysical Research, 114: G00F06.

Wang, Z. et al., 2004. Characterization and identification of the Detroit River mystery oil spill (2002). Journal of Chromatography A, 1038(1-2): 201-214, doi: 10.1016/j.chroma.2004.03.004.

Weishaar, J.L. et al., 2003. Evaluation of specific ultraviolet absorbance as an indicator of the chemical composition and reactivity of dissolved organic carbon. Environmental Science and Technology, 37(20): 4702-4708, doi: 10.1021/es030360x.

Yamashita, Y., Jaffé, R., Maie, N. and Tanoue, E., 2008. Assessing the dynamics of dissolved organic matter (DOM) in coastal environments by excitation emission matrix fluorescence and parallel factor analysis (EEM-PARAFAC). Limnology and Oceanography, 53(5): 1900-1908.

Zhou, Z. and Guo, L., 2012. Evolution of the optical properties of seawater influenced by the Deepwater Horizon oil spill in the Gulf of Mexico. Environmental Research Letters, 7(2): 025301, doi: 10.1088/1748-9326/7/2/025301.

Zhou, Z., Liu, Z. and Guo, L., 2012. Chemical evolution of Macondo crude oil during laboratory degradation as characterized by fluorescence EEMs and hydrocarbon composition. Marine Pollution Bulletin, (in press).

CHAPTER V

EVOLUTION OF OPTICAL PROPERTIES OF SEAWATER INFLUENCED BY DWH OIL SPILL IN THE GULF OF MEXICO*

Introduction

The Deepwater Horizon (DWH) oil spill in the Gulf of Mexico from April to July 2010 is an unprecedented marine oil spill event in which over 800 million liters of crude oil gushed from the seafloor at ~1500 m depth, and a total of ~7 million liters of dispersants were released in surface waters and deep waters (Camilli et al., 2010; Hazen et al., 2010; Kessler et al., 2011; Kujawinski et al., 2011; Mascarelli, 2010; National Commission on the BP Deepwater Horizon Oil Spill and Offshore Drilling (National Commission), 2010; Schrope, 2011; Valentine et al., 2010). Massive studies have been carried out to investigate the impacts of oil on ecosystems and factors and processes that regulate the weathering and change of oil composition in the water column of natural systems (Boehm et al., 1982; Camilli et al., 2010; Harrison et al., 1975; Mansour and Sassen, 2011; Valentine et al., 2010) and in the laboratory (Delille et al., 1998; Wang et al., 2011). Recent studies have reported the extent and transport of oil, methane and dispersants in the Gulf of Mexico since the DWH oil spill (Diercks et al., 2010; Hazen et al., 2010; Joye et al., 2011; Kessler et al., 2011; Kujawinski et al., 2011). However, there are no published results on the characterization of oil

---

* This chapter of the dissertation has been published in the Journal of Environmental Research Letters.
Zhou, Z. and Guo, L., 2012. Evolution of the optical properties of seawater influenced by the Deepwater Horizon oil spill in the Gulf of Mexico. Environmental Research Letters 7(2), 025301, doi: 10.1088/1748-9326/7/2/025301.

from seawater samples using fluorescence excitation emission matrix (EEM) techniques coupled with parallel factor (PARAFAC) analysis. The fate and degradation pathways of oil from the DWH oil spill remain poorly understood. How oil interacts with natural organic matter and the subsequent dynamic changes in chemical and optical properties in the water column after the DWH oil spill in the Gulf of Mexico is largely unknown.

Crude oil contains diverse hydrocarbons and organic molecules that could contribute to UV absorbance and fluorescence signatures in seawater and could be readily determined and characterized by UV-vis spectroscopy and fluorescence spectroscopy techniques (Bidleman et al., 1990; Bugden et al., 2008; Patra and Mishra, 2002; Vandermeulen et al., 1979; Von Der Dick and Kalkreuth, 1986; Wakeham, 1977). Similarly, composition and sources of DOM in aquatic environments can be effectively characterized by its optical properties, including UV-vis absorbance and fluorescence EEMs spectra (Chen and Gardner, 2004; Coble, 2007; Coble et al., 1990; Del Vecchio and Blough, 2004; Guéguen et al., 2007; Helms et al., 2008; Sierra et al., 2006; Vodacek et al., 1997; Weishaar et al., 2003), especially when combing the application of PARAFAC modeling (Kowalczuk et al., 2009; Murphy et al., 2008; Stedmon and Bro, 2008; Stedmon et al., 2003; Walker et al., 2009; Yamashita et al., 2008). Indeed, fluorescence EEM and PARAFAC techniques have been used in many previous studies to characterize, fingerprint and monitor oil in coastal and marine environments (Alostaz et al., 2008; Booksh et al., 1996; Bugden et al., 2008; Ferreira et al., 2003; González et al., 2006; Kim et al., 2010; Østgaard and

Jensen, 1983; Patra and Mishra, 2002; Santos-Echeandía et al., 2008). Few studies have been conducted for the DWH oil spill in the northern Gulf of Mexico using the fluorescence EEM technique and PARAFAC modeling to track the fate, transport, and transformation of oil in the water column. Our hypothesis was that oil from DWH would significantly alter the optical properties of DOM in the water column and the degradation and transformation processes of oil components could be effectively traced by their dynamic changes in optical properties.

The objective of this study was to examine the dynamic changes in time series bulk organic matter, UV-vis absorbance, fluorescence EEM spectra in the water column near the Macondo well in the Gulf of Mexico through cruises from 2010 to 2011 after the oil spill using UV-vis and 3D fluorescence spectroscopy coupled with PARAFAC modeling. Together with data obtained during the oil spill, the variation in oil components and DOM optical properties in the water column over the 15-month time period was used to derive indices for tracking the degradation and transformation processes, and thus the fate and transport of oil in the Gulf of Mexico.

Materials and Methods

Study site and Sampling

Water samples were collected from stations around the Deepwater Horizon oilrig in the northern Gulf of Mexico during two cruises in October 2010 and October 2011 (Figure 1). Both cruises was accomplished onboard the R/V Cape Hatteras and covered 24 and 27 stations during October 2010 and October

2011, respectively. Detailed sampling locations and selected hydrographic data are listed in table 1.

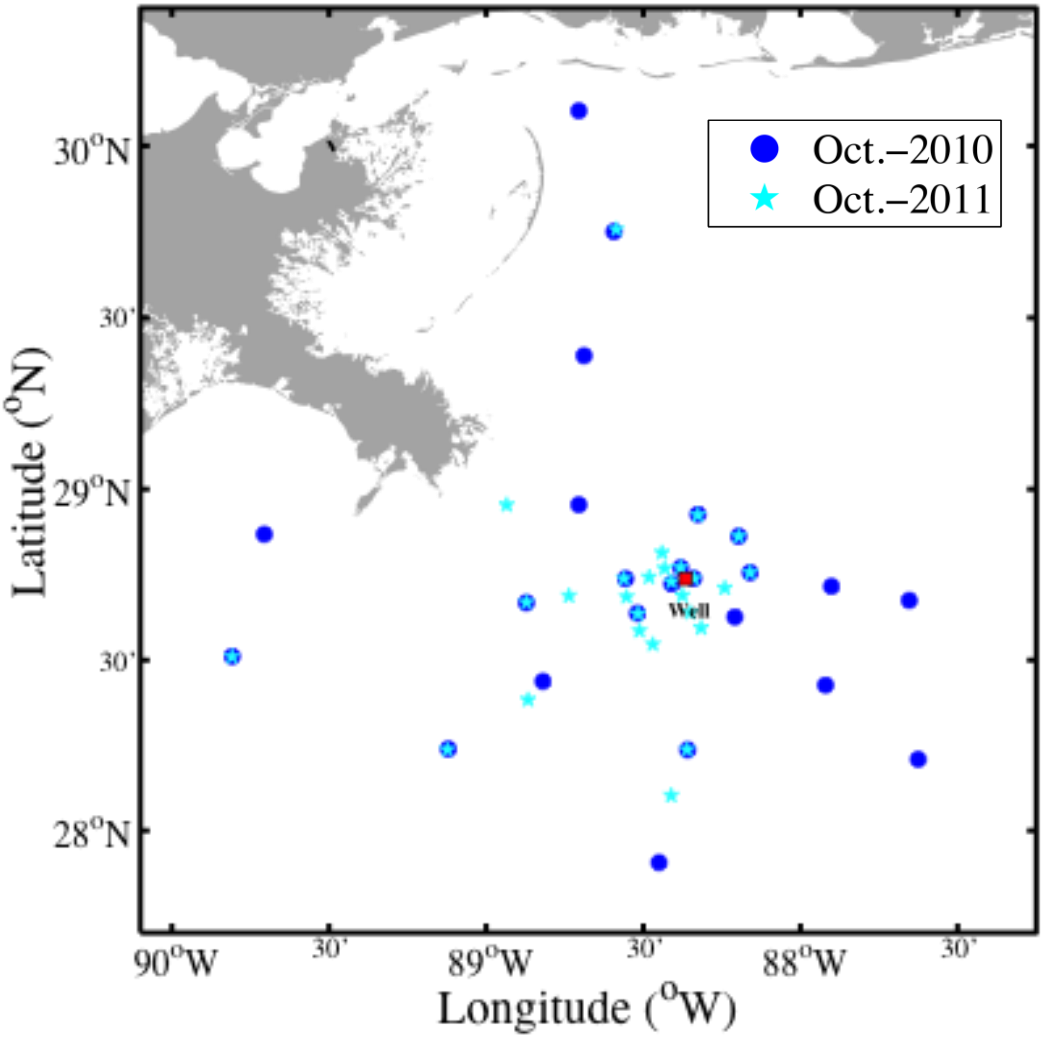

Figure 1. Sampling Locations In The Northern Gulf of Mexico During October 2010 (Blue circle) And October 2011 (Teal Pentacle) Onboard R/V Cape Hatteras.

Water samples from different depths at each station were collected with Niskin or Go-flo bottles mounted on a CTD rosette system, including surface waters at ~ 2-5 m depth and Chlorophyll a maximum layer, deep water samples between 1100 m and 1400 m, and bottom water samples (Table 1). Immediately

after sample collection, water samples were filtered through pre-combusted glass fiber filters (0.7 µm, Whatman).

Table 1

Sampling Locations, Sampling Dates, and Hydrographic Data for Stations Occupied During October 2010 and October 2011 in the Gulf of Mexico

Station ID	Latitude (˚N)	Longitude (˚W)	Date	Water Depth (m)	Surface Water Temp. (˚C)	Surface Water Salinity
Oct 2010						
GIP 01	30° 6.113′	88°42.328′	10/12/10	16	24.42	31.64
GIP 02	29°45.038′	88°35.618′	10/12/10	28	25.46	32.92
GIP 03	29°23.384′	88°41.304′	10/12/10	53	25.62	30.77
GIP 04	28°57.278′	88°56'.103′	10/14/10	126	26.30	30.26
GIP 05	28°52.122′	89°38'.413′	10/13/10	72	26.17	30.52
GIP 06	28°30.663′	89°48.499′	10/13/10	530	27.11	35.36
GIP 07	28°14.383′	89°7.240′	10/13/10	1136	27.43	35.62
GIP 08	27°54.370′	88°27.001′	10/14/10	2360	25.83	33.48
GIP 09	28°12.581′	87°37.515′	10/15/10	2530	27.27	36.41
GIP 10	28°25.614′	87°55.219′	10/15/10	2315	26.95	36.30
GIP 11	28°14.216′	88°21.528′	10/16/10	1973	26.17	35.62

Table 1 (continued).

Station ID	Latitude (˚N)	Longitude (˚W)	Date	Water Depth (m)	Surface Water Temp. (˚C)	Surface Water Salinity
GIP 12	28°26.275′	88°49.166′	10/16/10	1210	25.96	32.70
GIP 13	28°40.100′	88°52.327′	10/14/10	1025	26.63	32.36
GIP 15	28°44.315′	88°33.390′	10/16/10	1207	25.44	33.00
GIP 16	28°43.383′	88°24.577′	10/17/10	1560	25.66	34.26
GIP 17	28°38.237′	88°31.128′	10/18/10	1595	25.99	34.38
GIP 18	28°44.336′	88°20.416′	10/17/10	1,570	26.49	35.82
GIP 19	28°37.587′	88°12.515′	10/20/10	2,010	26.99	36.43
GIP 20	28°45.393′	88°9.595′	10/20/10	1,760	26.83	36.35
GIP 21	28°42.960′	87°54.086′	10/20/10	2,180	26.97	36.35
GIP 22	28°40.502′	87°39.250′	10/19/10	2,370	26.97	36.28
GIP 23	28°51.774′	88°11.835′	10/20/10	1,350	25.90	34.66
GIP 24	28°46.235′	88°22.874′	10/18/10	1,418	26.11	35.56
GIP 25	28°55.602′	88°19.579′	10/21/10	1,160	26.05	34.99

Table 1 (continued).

Station ID	Latitude (˚N)	Longitude (˚W)	Date	Water Depth (m)	Surface Water Temp. (˚C)	Surface Water Salinity
Oct 2011						
GIP 02	29º45.423′	88º35.125′	10/20/11	20	25.28	34.58
GIP 04	29º45.423′	88º35.125′	10/20/11	126	23.94	32.27
GIP 06	28º57.252′	88º56.095′	10/21/11	520	26.44	36.47
GIP L	28º30.633′	89º48.488′	10/21/11	1,130	26.33	35.08
GIP 7	28º06.175′	88º24.657′	10/21/11	1,150	26.24	35.34
GIP K	28º14.264′	89º07.380′	10/21/11	1,332	26.26	35.17
GIP 11	28º23.047′	88º52.007′	10/22/11	1,984	26.20	35.39
GIP I	28º14.255′	88º21.631′	10/22/11	1,734	26.19	35.51
GIP H	28º32.779′	88º28.153′	10/22/11	1,697	26.21	35.47
GIP 17b	28º35.169′	88º30.717′	10/23/11	1,577	26.11	35.47
GIP 13	28º38.186′	88º31.018′	10/23/11	1,017	26.03	35.86
GIP M	28º40.153′	88º52.284′	10/23/11	1,207	26.24	35.34
GIP G	28º41.288′	88º44.181′	10/23/11	1,395	26.13	35.14
GIP 15	28º41.113′	88º33.161′	10/24/11	1,178	26.12	35.35

Table 1 (continued).

Station ID	Latitude (˚N)	Longitude (˚W)	Date	Water Depth (m)	Surface Water Temp. (˚C)	Surface Water Salinity
GIP B	28º44.331′	88º33.668′	10/24/11	1,480	26.11	35.32
GIP A	28º44.593′	88º28.894′	10/24/11	1,237	26.22	35.40
GIP C	28º48.874′	88º26.403′	10/25/11	1,378	26.03	35.42
GIP 24	28º46.135′	88º25.902′	10/25/11	1,400	25.97	35.35
GIP 18	28º46.258′	88º22.852′	10/25/11	1,554	25.97	35.27
GIP 16b	28º44.304′	88º20.326′	10/25/11	1,554	25.88	35.27
GIP D	28º43.788′	88º24.619′	10/26/11	1,618	25.84	35.23
GIP E	28º41.365′	88º22.549′	10/26/11	1,708	25.89	35.28
GIP J	28º38.349′	88º21.051′	10/26/11	1,847	26.15	35.34
GIP 23	28º35.657′	88º18.951′	10/27/11	1,345	25.98	35.45
GIP 20	28º51.770′	88º11.777′	10/27/11	1,752	25.99	35.41
GIP F	28º45.374′	88º09.595′	10/28/11	1,729	26.24	35.62
GIP 25	28º42.65′	88º14.45′	10/28/11	1150	26.09	35.46

Filtered water samples for dissolved organic carbon (DOC) were collected in 30 ml HDPE bottles and stored frozen, while samples for optical measurements, including UV-vis absorbance and fluorescence EEMs, were

collected with pre-combusted (550°C) 125 ml amber bottles and stored in the dark at 4˚C.

Measurements of DOC and UV-vis Absorption

Concentrations of DOC were measured on a Shimadzu TOC-V total organic carbon analyzer using the high temperature combustion method (Guo et al., 1995). For DOC measurements, samples were acidified with concentrated HCl to pH<2 before analysis. Three to five replicate measurements, each using 150 µL sample were made, with a coefficient of variance <2%. Calibration curves were generated before sample analysis. Nanopure water, working standards and certified DOC standards (University of Miami) were measured as a sample every eight seawater samples to check the performance of the instrument. Total DOC blank, including water and instrument blanks, was normally less than 2-6 µM (Guo et al., 1995).

UV-vis absorption spectra of samples were measured using an Agilent 8453 UV-visible spectrophotometer and a 1-cm path-length quartz cuvette over the 200-1100 nm wavelength ranges with 0.1 nm increments. The water blank was subtracted, and the refractive index effect was corrected by subtracting the averaged absorbance between 650 and 800 nm (Stedmon et al., 2000). Specific UV absorbance at 254 nm ($SUVA_{254}$) values was calculated by dividing absorption coefficient (m^{-1}) at 254 nm (a_{254}) by the DOC concentration (mg-C/L). Non-linear spectral slopes between 290-400 nm were calculated to provide information on the overall molecular weight of DOM (Helms et al., 2008; Twardowski et al., 2004; Zhou and Guo, 2010).

Measurements of Fluorescence EEMs

A Shimadzu RF-5301PC spectrofluorometer was used to measure fluorescence signatures of water samples in a 1 cm path-length quartz cuvette. Each sample was scanned from 240 to 680 nm with 1 nm interval under excitation wavelengths from 220 to 400 nm with a 2 nm step. Ninety-one separate fluorescence emission spectra were concatenated to generate an excitation-emission matrix that is able to provide DOM component information for the water sample qualitatively and quantitatively (Coble, 1996; Green and Blough, 1994). PARAFAC modeling was used to derive DOM fluorescence components (Stedmon and Bro, 2008) and to examine the spatial and temporal changes in DOM components in the Gulf of Mexico.

A water blank was scanned daily before sample analysis and its EEM was subtracted from each sample's EEM. Emission correction spectrum was generated using Rhodamin B and barium sulfate with the correction package from Shimadzu and multiplied to the EEM spectra. Quinine sulfate standards were also scanned daily for fluorescence calibration and for checking the instrument performance. All fluorescence intensities were converted to ppb-QSE units (Coble, 1996). Data in two triangle areas, corresponding to the Rayleigh and Raman scattering peaks were eliminated in the PARAFAC analysis to acquire better mathematical results.

PARAFAC Modeling

PARAFAC modeling was applied to all field seawater samples collected from 2010 to 2011, using the MATLAB software (MathWorks R2010b) and the

DOMFluor Toolbox (Stedmon and Bro, 2008). Sample matrices were calibrated and corrected before running the PARAFAC analysis. A non-negativity outlier test was performed and no outlier sample was chosen for removal. Thus, no sample was removed before split-half analysis and model validation. The fluorescence intensities of each component in every sample were quantified as a result of the PARAFAC modeling.

Results and Discussion

Variations in Quantity and Quality of DOM in the Water Column

The spatial distributions of salinity, DOC concentration, UV absorption coefficient at 254 nm (a_{254}) and specific UV absorbance at 254 nm ($SUVA_{254}$) during October 2010 are showed in Figure 2. During October 2010, three months after the oil spill was capped, the DOC concentration and a_{254} in surface waters did not show an obvious influence of oil and their abundance dropped back to more naturally occurring levels, with the highest value found at stations close to the Mississippi River plume and a general decrease in DOC with increasing salinity (Figure 3).

These surface distribution patterns are distinctly different from those observed during the oil spill in the May and June cruises (Diercks et al., 2010; Zhou et al., 2012a), showing remarkable resilience of surface waters. The distribution of DOC and chromophoric dissolved organic matter (CDOM) in surface waters during the early stages of the oil spill in May and June 2010 showed a profound influence of oil released from the Macondo well in the northern Gulf of Mexico, with DOC concentrations as high as 6 mg-C/L found

around the oilrig, which were considerably higher than the baseline values in the northern Gulf of Mexico (Guo et al., 1994; Guo et al., 1995; Hansell and Carlson, 1998).

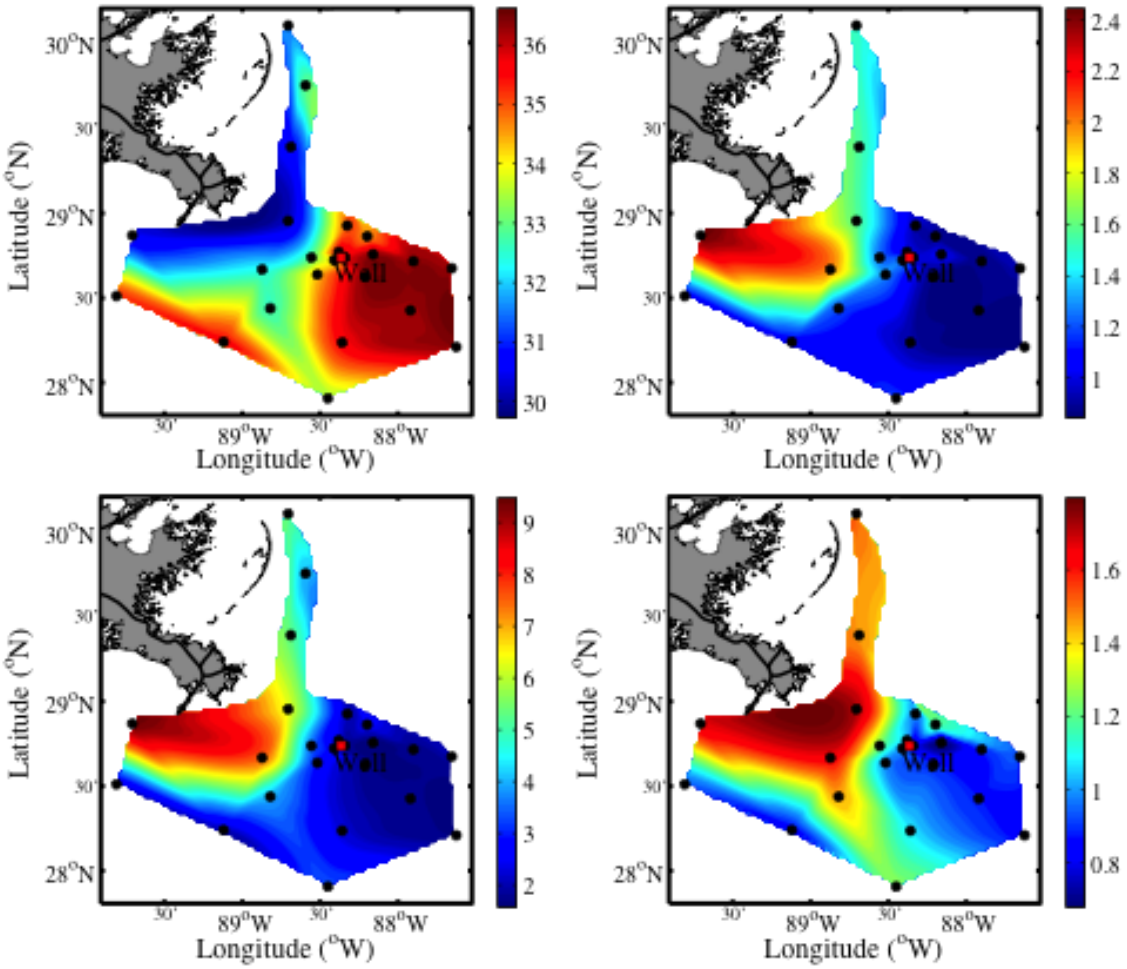

Figure 2. Distributions Of Salinity (Upper Left Panel), DOC Concentration (mg-C/L, Upper Right Panel), UV Absorption Coefficient At 254 nm (a254 in m-1, Lower Left Panel) And Specific UV Absorbance (SUVA254 In m2/g-C, Lower Right Panel) In The Surface Water From The Northern Gulf Of Mexico During October 2010 After Three Months Of The Oil Spill.

Similarly, elevated DOC concentrations and absorbance values in deep waters between 1100 and 1400 m were also observed during May/June 2010

(Zhou et al., 2012a), consistent with the presence of oil plume observed in the deep water (Camilli et al., 2010; Hazen et al., 2010; Schrope, 2011).

Even though surface water DOC and CDOM did not seem to have a significant oil signature by October 2010, as shown in Figure 2, the relationship between DOC concentration and salinity in all water samples throughout the water column shows an abnormal deviation from a general conservative DOC-salinity relationship as observed before the oil spill in the Gulf of Mexico and in other oceanic environments (Conmy et al., 2004; Guo et al., 1995; Kowalczuk et al., 2010; Stedmon and Markager, 2003; Weishaar et al., 2003). Surprisingly, some of the DOC concentrations from those abnormal deep-water samples were significantly lower than those observed previously from deep waters in the Gulf of Mexico and North Atlantic Ocean (Figure 3 and (Guo et al., 1994; Guo et al., 1995; Hansell and Carlson, 1998)). We hypothesized that the extremely low DOC concentrations measured for oil contaminated deep waters were the result of the scavenging or removal of DOC by oil droplets and subsequent sorption of oil on glass fiber filters during water sample filtration.

Based on the correlations between salinity, DOC, a_{254}, and $SUVA_{254}$, two major types of DOM could be identified in the water column during October 2010, three months after the oil spill (Figure 3). The first type of DOM, residing mostly in the upper water column, had natural DOM characteristics with a positive correlation between DOC concentration and $SUVA_{254}$ values. The second group of DOM, found exclusively in deep waters with a characteristic salinity of 34.96±0.03, had an anomalously high optical yield and a negative correlation

between $SUVA_{254}$ values and DOC concentrations, showing a strong influence of oil on deep waters in October 2010 (Figure 3) although rapid recovery was observed in surface waters.

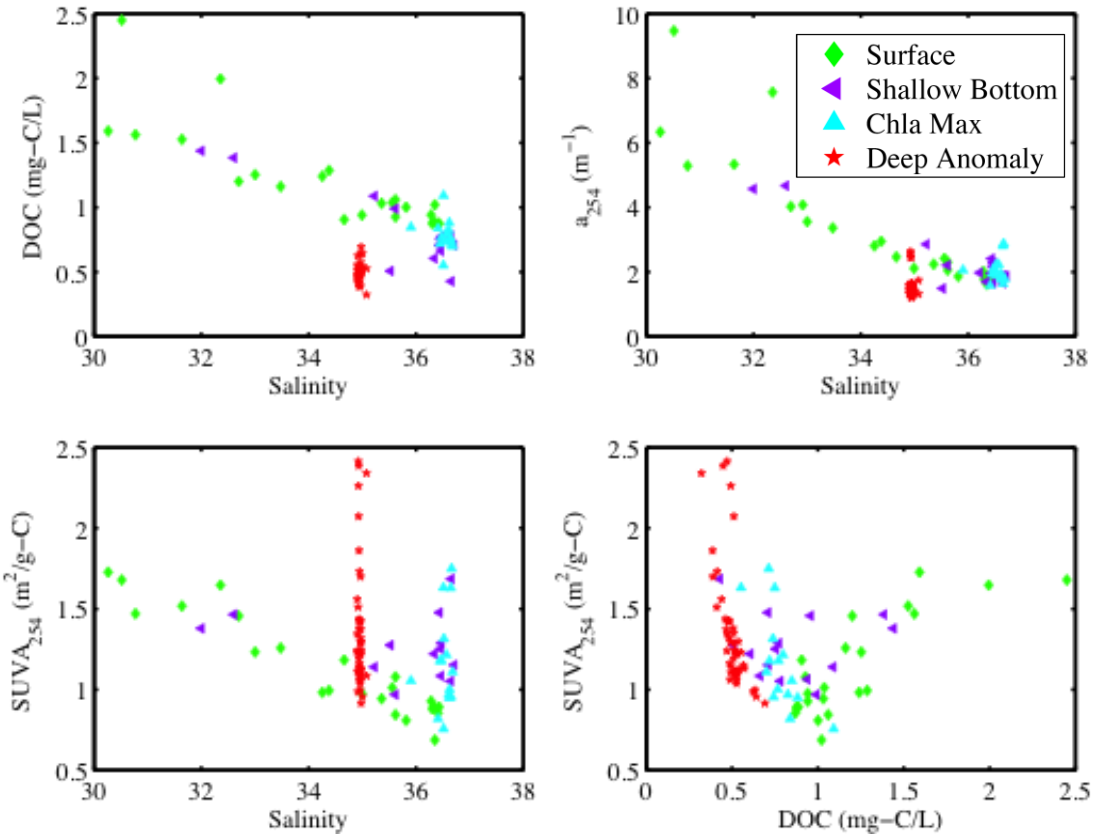

Figure 3. Relationships Between Salinity, DOC Concentration, a254, And SUVA254 In The Water Column Of The Northern Gulf of Mexico During October 2010.

Similar to the results observed during October 2010 (Figures 2 and 3), surface water samples collected during October 2011 (15 months after the oil spill) had undetectable oil signals (Figure 4), but deeper water samples again showed a strong presence of oil contaminated DOM (Figure 5). While the oil signatures in surface waters identified from optical properties faded away quickly, the presence of oil in the deep-water column persisted even 15 months after the

oil spill in the Gulf of Mexico was capped. Effective microbial and photochemical degradation in surface waters, water stratification in the deeper water column, as well as circulation in the Gulf of Mexico (North et al., 2011) are likely the major factors governing the distribution of oil and DOM and their fate and transport in the water column.

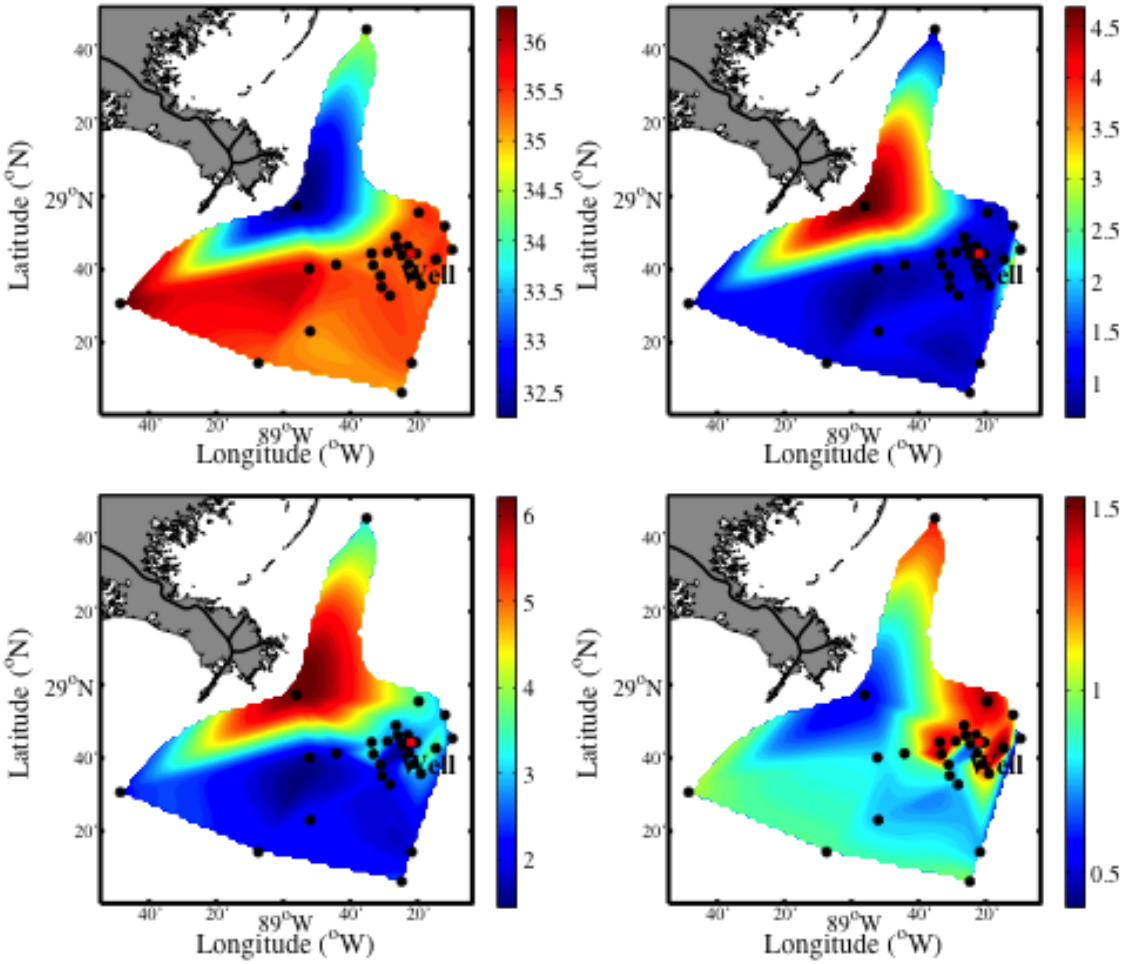

Figure 4. Distributions Of Salinity (Upper Left Panel), DOC Concentration (mg-C/L, Upper Right Panel), UV Absorption Coefficient At 254 nm (a254 in m-1, Lower Left Panel) And Specific UV Absorbance At 254 nm (SUVA254 in m2/g-C, Lower Right Panel) In The Surface Water In The Northern Gulf of Mexico During October 2011, After 15 Months Of The Oil Spill.

Fluorescence Characteristics of DOM in the Water Column

Fluorescence EEM spectra of crude oil and a time series of seawater samples taken from the same depth at ~1050 m in the Gulf of Mexico, from May 2010, October 2010 and October 2011 are shown in Figure 6. Crude oil had its maximum fluorescence emission at 320-360 nm over excitation of 220-240 nm, centering on Ex/Em 226/340 nm. Another peak in the crude oil EEM was located at an emission wavelength of 322 nm under excitation between 260-280 nm, similar to that reported by Bugden et al. (2008).

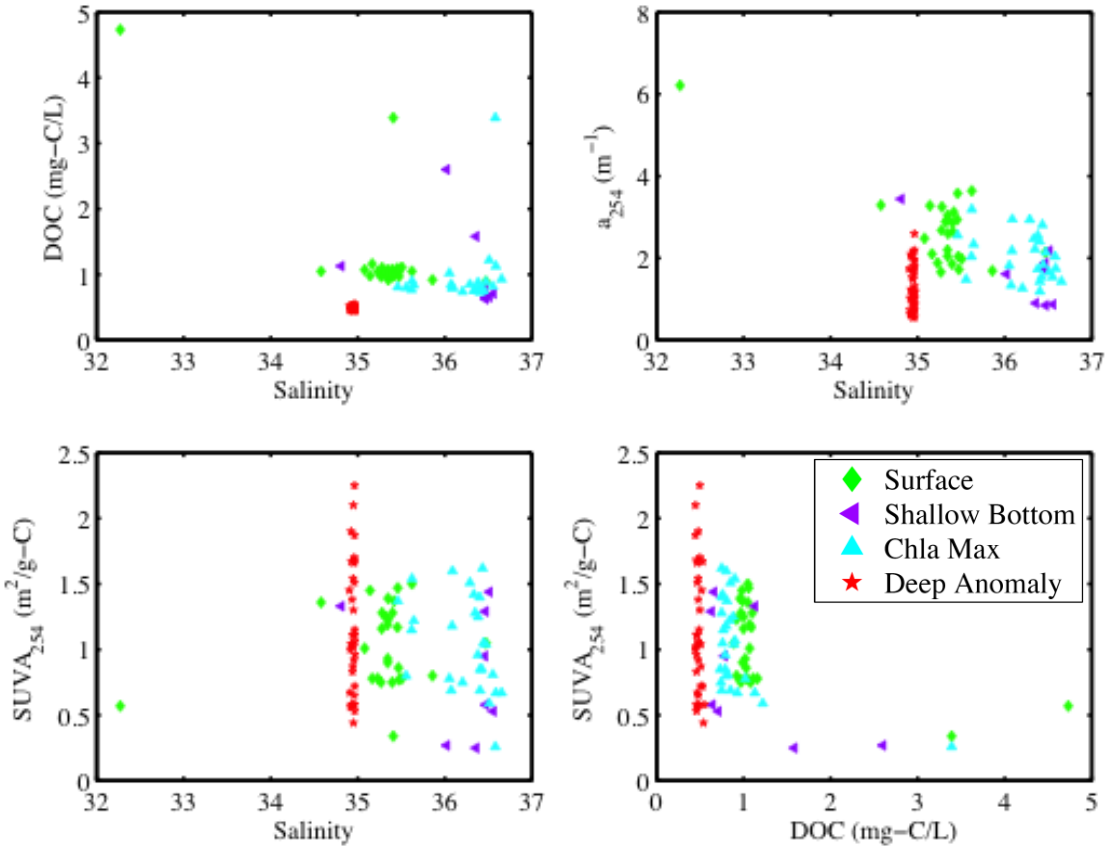

Figure 5. Relationships Between Salinity, DOC Concentration, a254, SUVA254 In The Water Column Of The Gulf of Mexico During October 2011.

As shown in Figure 6, the fluorescence EEM signatures of seawater samples taken in May 2010 strongly resemble those of the crude oil, indicating the presence of oil in the water column and its influence on seawater samples. However, oil fluorescence signatures derived from EEM spectra were weak in samples collected during October 2010 and October 2011 cruises, indicating effective dilution, degradation and transformation of oil in the water column.

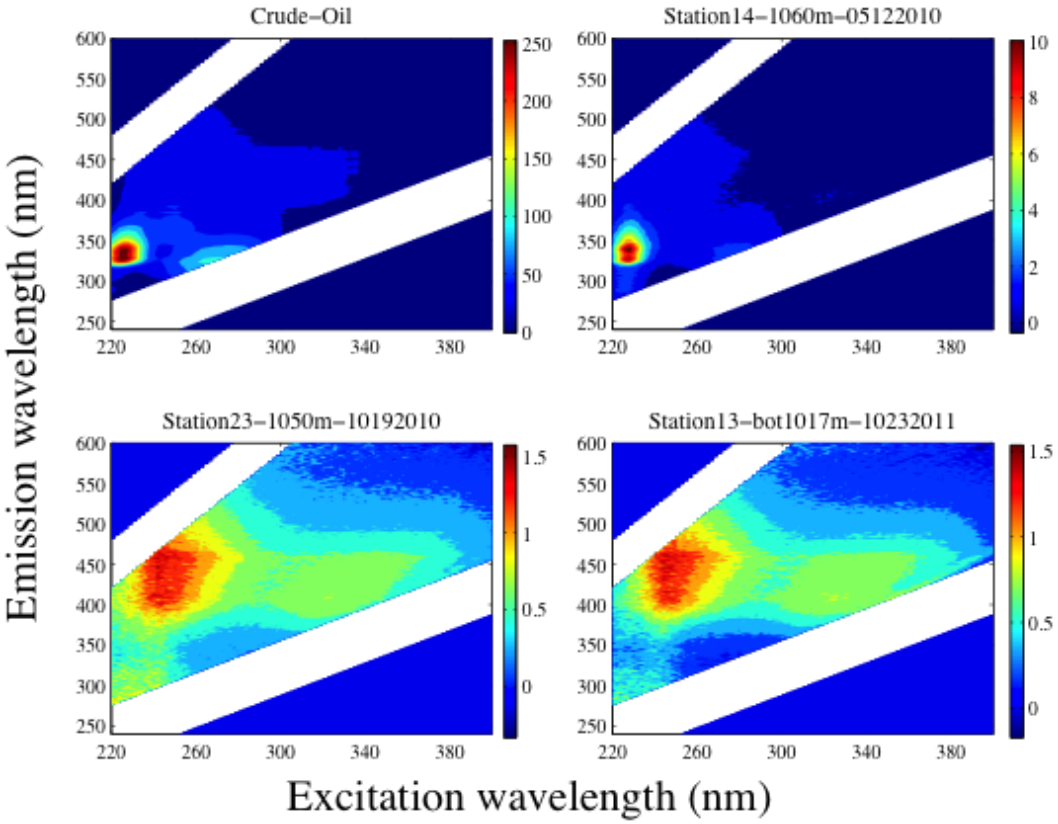

Figure 6. Fluorescence EEMs Of Crude Oil (Upper Left Panel) And Field Samples Taken In May 2010 (Upper Right Panel), October 2010 (Lower Left Panel) And October 2011 (Lower Right Panel).

Since data of DOC and other optical properties clearly demonstrated the presence of oil in deep waters even 15 months after capping the spill (see previous section), the weak oil fluorescence signatures observed after the oil spill likely also resulted from the application of vast quantity of dispersants during the

DWH oil spill and thus the interactions of oil with dispersants in the water column (Yamada et al., 2003; Yin et al., 1997). Indeed, significant alterations in oil EEMs spectra have been observed when dispersants were present with oil (Bugden et al., 2008; Guo et al., 2010). Other factors contributing to the weak fluorescence signatures included possible sorption effect during sample filtration processes since, in general, oil has a very low solubility in seawater, and can be readily removed on filters and sorbs on the bottle wall during sample processing.

Oil Components as Derived from PARAFAC Modeling

Despite low fluorescence oil signatures, oil components could be recognized from these seawater samples using PARAFAC modeling (Figure 7). As shown in table 2, four DOM fluorescence components had been identified using PARAFAC analysis of EEM data from seawater samples taken during and after the oil spill.

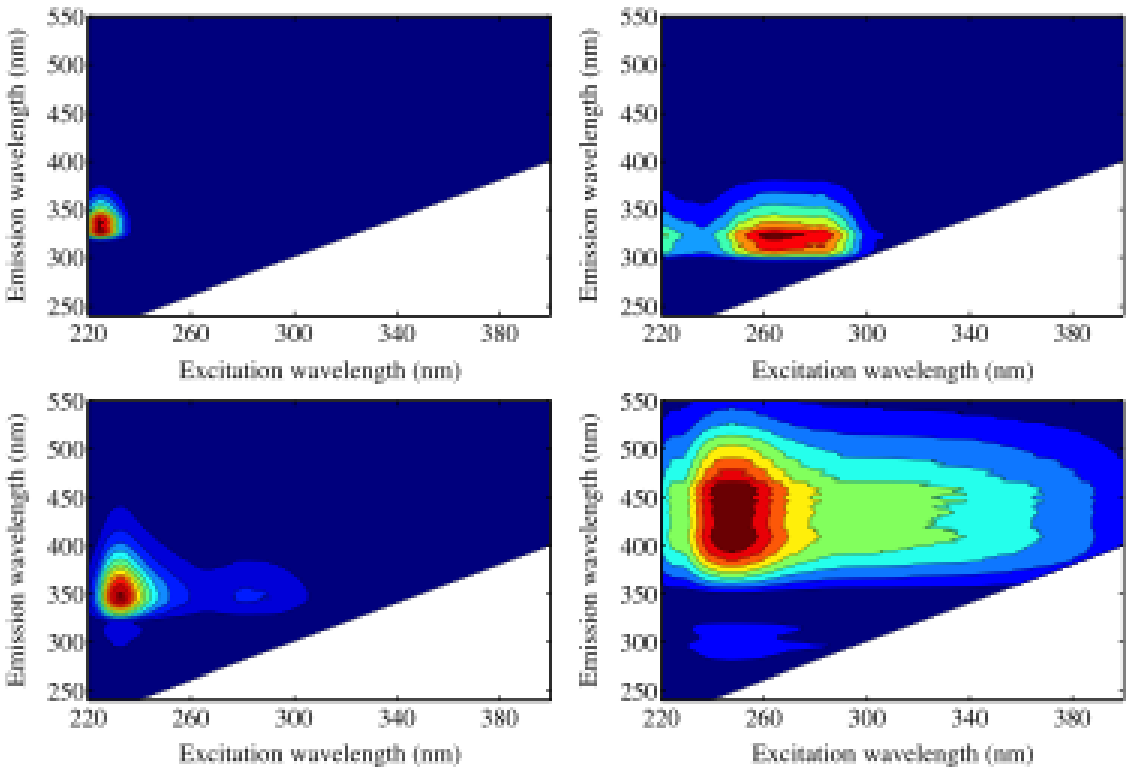

Figure 7. Characteristics Of Four Major DOM Components Identified By PARAFAC Analysis Based On Fluorescence EEMs Of All Field Samples Collected During Four Cruises From May 2010 During The Oil Spill To October 2011, After 15 Months Of The Oil Spill In The Northern Gulf of Mexico.

A total of 228 fluorescence emission matrices collected at wavelengths from 240 to 680 nm over excitation wavelengths from 220 to 400 nm were decomposed into a four-factor PARAFAC model, including three oil-related components (C1, C2 and C3) and one humic-like DOM component (C4). The first component, C1, having emission maximum at 224 nm under excitation wavelength of 328 nm, is the most prominent oil component. The second and third components were identified at Ex/Em maximum wavelengths of 264/324 and 232/346 nm, respectively. The fourth component, with its maximum Ex/Em of 248/446 nm, is characterized as naturally occurring humic-like DOM (Table 2, Figure 7). As shown in Figure 8, fluorescence intensities of the oil component C3

had a broad correlation with a_{254} in the Gulf of Mexico in October 2010, suggesting an oil component with similar quantum yields and optical activities.

Table 2

Fluorescent DOM Components Identified Using PARAFAC Analysis Based on EEM Spectra of All Field Seawater Samples Collected from the Gulf of Mexico

DOM component	Excitation wavelength (nm)	Emission wavelength (nm)	Description
Component-1	224	328	Oil
Component-2	264	324	Oil
Componnet-3	232	346	Oil
Component-4	248	446	Humic-like

A more scattered relationship between a_{254} and fluorescence intensities was observed for oil components C2 and C1 (Figure 8), suggesting that both C1 and C2 are more complex in composition and might have multiple production/degradation pathways.

Chemical Evolution of Oil as Characterized by its Component Ratios

Since the oil-related fluorescence components identified by PARAFAC modeling were derived from seawater samples collected at different times during and after oil spill, changes in the fluorescence intensities and component ratios between seawater samples would likely reflect the results of degradation and

transformation of oil in the water column. Additionally, the fluorescence component ratio is an intensive property, which is not related to quantity or abundance of oil, and should be an ideal parameter or index to evaluate time series samples in the same water column. As shown in Figure 9, even though the intensity/concentration of DOM fluorescence components decreased with time, the C2/C1 and C3/C1 ratios increased consistently in seawater samples from the middle of May to May/June to October 2010 and to October 2011, indicating that these oil component ratios are indeed correlated with oil degradation and can be used as an index for tracking the chemical evolution of oil during its degradation and transformation in the water column. The increase in the C2/C1 and C3/C1 ratios during oil degradation in the water column suggests that both oil components, C2 and C3, had significantly lower degradation rates as compared to the C1 oil component, or that C2 and C3 are also degraded products of crude oil. Independent controlled laboratory experiments on the degradation of crude oil also provided similar variation trends of oil component ratios with increasing C2/C1 and C3/C1 ratio during oil degradation (Zhou et al., 2012b), further supporting the use of C2/C1 and C3/C1 ratios as an index to trace weathered

degraded oil in marine environments.

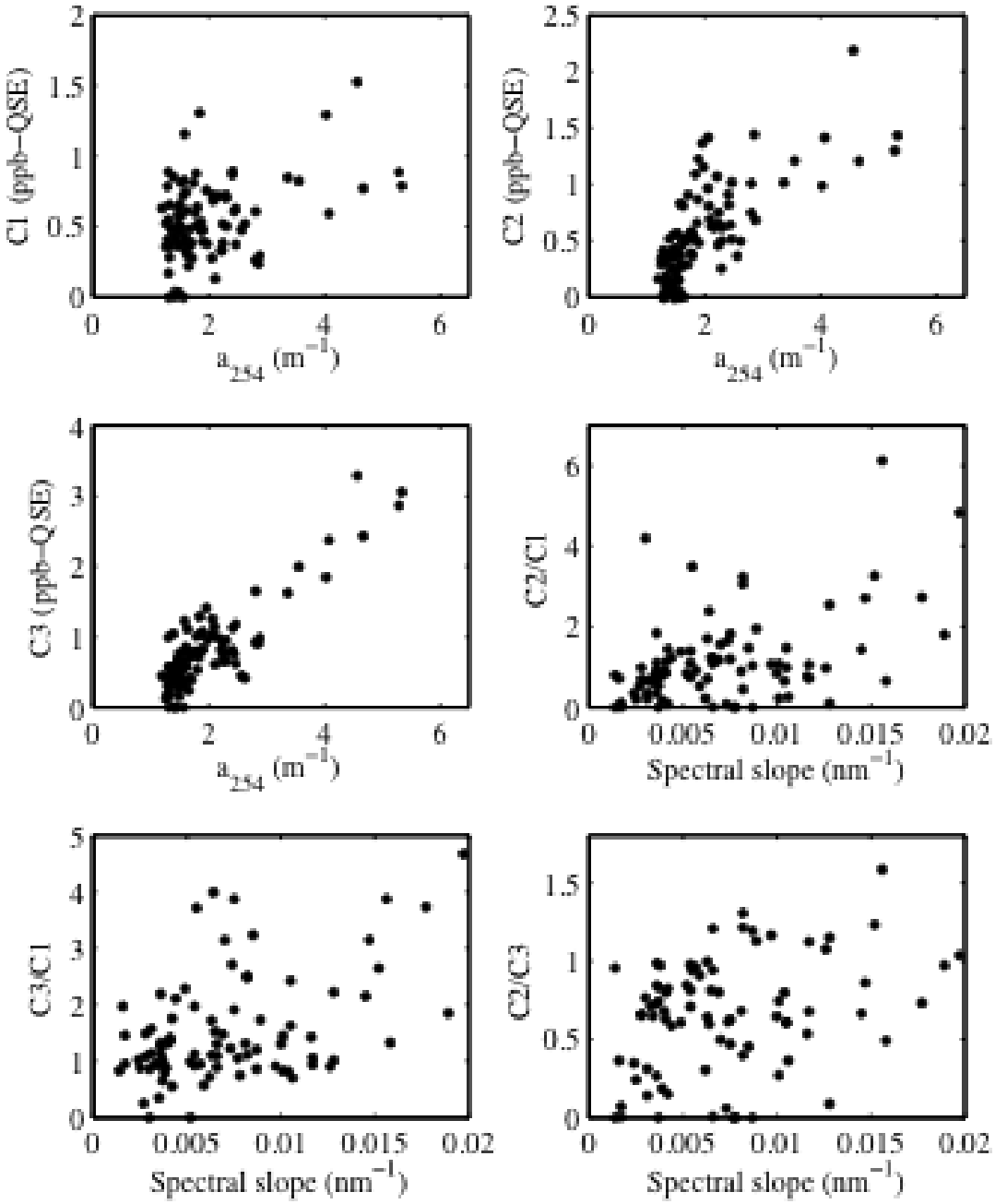

Figure 8. Relationships Between a254 And The Fluorescence Intensity Of Oil Components, C1, C2 And C3 And Between Spectral Slope (S) And Oil Component Ratio C2/C1, C3/C1and C2/C3 In The Water Column Of The Northern Gulf of Mexico During October 2010.

Data from the October 2010 cruise also showed a broad correlation between spectral slope values and oil component ratios such as C2/C1, C3/C1 and C2/C3, in the water column of the Gulf of Mexico, although the correlations are somewhat scattered (Figure 8).

Given that spectral slope values are inversely related with the aromaticity and average molecular weight of DOM (Helms et al., 2008; Twardowski et al., 2004), these positive correlations between oil components and spectral slope values suggest C2 and C3 are less aromatic and have lower inferred molecular weight components compared with crude oil. Thus, the overall molecular weight of DOM in the water column is expected to decrease as oil is degraded and as C2/C1 and C3/C1 ratios increase (Figure 9). Similar correlation between C2/C3 ratio and spectral slope (Figure 8) further suggest a decreasing trend of average molecular weight in oil components from C1 to C3 and then to C2. However, detailed analyses of hydrocarbon composition are needed to confirm this conclusion derived from spectral slope measurements.

Interestingly, the C2/C1 ratios in surface water samples were, in general, slightly higher than those of deep water samples regardless of sampling time, suggesting that the C2 component is either less sensitive to photochemical degradation, or its production rate from degradation is slightly higher than its degradation. In contrast, surface water C3/C1 ratios were in general lower than deep water samples except for May 2010 samples collected during oil spill (Figure 9), suggesting that production of C3 in the surface waters could be lower than its degradation. We hypothesize that C2 is mostly derived from

photochemical degradation and C3 is a degradation product from both microbial and photochemical degradation, while both of them are also subject to degradation in the water column.

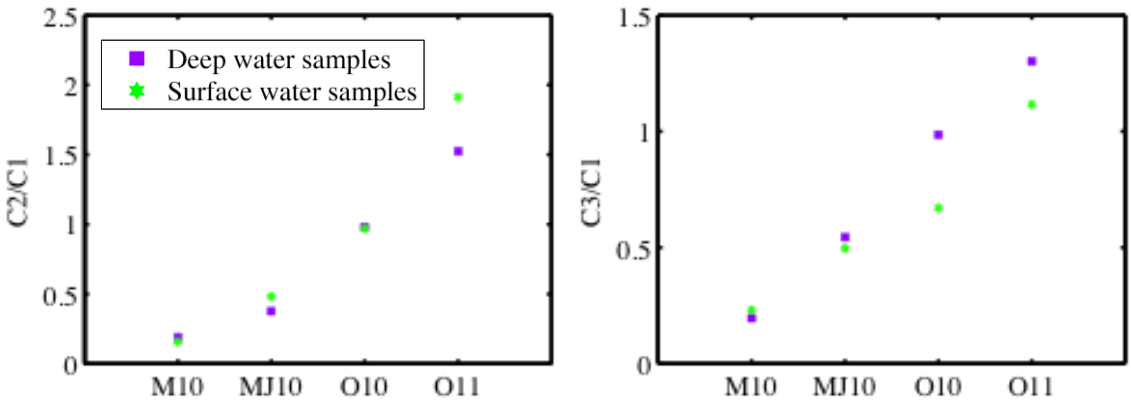

Figure 9. Variations In The Oil Component Ratios, C2/C1 and C3/C1, With Time Based On Field Samples Collected During Four Cruises At Different Time In The Gulf of Mexico, Including Samples Taken In Mid-May 2010 [M10] And Late May – Early June 2010 [MJ10] During The Oil Spill, October 2010 [O10] Three Months After The Oil Spill, And October 2011 [O11] 15 Months After The Oil Spill Was Capped. Deep-Water Samples Are Denoted With Purple Squares, While Surface Water Samples With Green Pentacles.

The inferred C2/C3 ratio was higher in surface water samples than in deep waters, and increased with time, further confirmed the degradation preference of C2 and C3. Thus, changes in oil component ratios in the water column could be quantitatively linked to the fate and degradation and transformation pathways of crude oil in the water column.

Conclusions

The Deepwater Horizon oil spill had a profound influence on the optical characteristics of DOM in the northern Gulf of Mexico. At the early stages of the oil spill during May-June 2010, more freshly released crude oil in the water column gave rise to elevated DOC concentration and optical reactivity, showing

two distinct types of DOM in the water column, with a strong influence of oil throughout the entire water column. During October 2010, three months after the oil spill was capped, DOM in the upper water column seemed to contain mostly natural organic matter. However, anomalous DOM with high optical yields still resided in deep waters, showing a persistent oil influence on optical properties. The strong presence and persistent influence of oil in the water column was also observed in deep waters surrounding the DWH Macondo well during October 2011, even 15 months after the oil spill was capped. Four DOM fluorescence components have been identified using PARAFAC modeling on EEMs data of seawater samples from the Gulf of Mexico. Three of them are oil components and one is UV humic-like DOM. The fluorescence component ratios, such as C2/C1 and C3/C1, showed a consistent increase with time from 2010 to 2011 in the Gulf of Mexico, and could be quantitatively linked to the degradation status of oil in the water column and thus, be used as indices to effectively track the fate and transport of oil in marine environments. These results have important implications in oil spill research, environmental monitoring, and the development of *in situ* sensors.

REFERENCES

Alostaz, M., Biggar, K., Donahue, R. and Hall, G., 2008. Petroleum contamination characterization and quantification using fluorescence emission-excitation matrices (EEMs) and parallel factor analysis (PARAFAC). Journal of Environmental Engineering & Science, 7(3): 183-197, doi: 10.1139/s07-049.

Bidleman, T.F., Castleberry, A.A., Foreman, W.T., Zaranski, M.T. and Wall, D.W., 1990. Petroleum hydrocarbons in the surface water of two estuaries in the Southeastern united states. Estuarine, Coastal and Shelf Science, 30(1): 91-109.

Boehm, P.D., Fiest, D.L., Mackay, D. and Paterson, S., 1982. Physical-chemical weathering of petroleum hydrocarbons from the IXTOC I blowout: chemical measurements and a weathering model. Environmental Science & Technology, 16(8): 498-505.

Booksh, K.S., Muroski, A.R. and Myrick, M.L., 1996. Single-measurement excitation/emission matrix spectrofluorometer for determination of hydrocarbons in ocean water. 2. calibration and quantitation of naphthalene and styrene. Analytical Chemistry, 68(20): 3539-3544, doi: 10.1021/ac9602534.

Bugden, J.B.C., Yeung, C.W., Kepkay, P.E. and Lee, K., 2008. Application of ultraviolet fluorometry and excitation-emission matrix spectroscopy (EEMS) to fingerprint oil and chemically dispersed oil in seawater. Marine Pollution Bulletin, 56(4): 677-685, doi: 10.1016/j.marpolbul.2007.12.022.

Camilli, R. et al., 2010. Tracking hydrocarbon plume transport and biodegradation at deepwater horizon. Science, 330(6001): 201-204.

Chen, R.F. and Gardner, G.B., 2004. High-resolution measurements of chromophoric dissolved organic matter in the Mississippi and Atchafalaya River plume regions. Marine Chemistry, 89(1-4): 103-125.

Coble, P.G., 1996. Characterization of marine and terrestrial DOM in seawater using excitation-emission matrix spectroscopy. Marine Chemistry, 51(4): 325-346, doi: 10.1016/0304-4203(95)00062-3.

Coble, P.G., 2007. Marine Optical Biogeochemistry: The Chemistry of Ocean Color. Chemical Reviews, 107(2): 402-418.

Coble, P.G., Green, S.A., Blough, N.V. and Gagosian, R.B., 1990. Characterization of dissolved organic matter in the Black Sea by fluorescence spectroscopy. Nature, 348(6300): 432-435.

Conmy, R.N., Coble, P.G., Chen, R.F. and Gardner, G.B., 2004. Optical properties of colored dissolved organic matter in the Northern Gulf of Mexico. Marine Chemistry, 89(1-4): 127-144.

Del Vecchio, R. and Blough, N.V., 2004. Spatial and seasonal distribution of chromophoric dissolved organic matter and dissolved organic carbon in the Middle Atlantic Bight. Marine Chemistry, 89(1-4): 169-187.

Delille, D., Bassères, A., Dessommes, A. and Rosiers, C., 1998. Influence of daylight on potential biodegradation of diesel and crude oil in Antarctic seawater. Marine Environmental Research, 45(3): 249-258.

Diercks, A.-R. et al., 2010. Characterization of subsurface polycyclic aromatic hydrocarbons at the Deepwater Horizon site. Geophysical Research Letters, 37(20): L20602, doi: 10.1029/2010gl045046.

Ferreira, A.M., Micaelo, C. and Vale, C., 2003. Are coastal resources of NW Portugal fingerprinting hydrocarbons released from the Prestige accident? Ciencias Marinas, 29(1): 109-114.

González, J.J. et al., 2006. Spatial and temporal distribution of dissolved/dispersed aromatic hydrocarbons in seawater in the area affected by the Prestige oil spill. Marine Pollution Bulletin, 53(5-7): 250-259, doi: 10.1016/j.marpolbul.2005.09.039.

Green, S.A. and Blough, N.V., 1994. Optical absorption and fluorescence properties of chromophoric dissolved organic matter in natural waters. Limnology and Oceanography, 39(8): 1903-1916.

Guéguen, C., Guo, L., Yamamoto-Kawai, M. and Tanaka, N., 2007. Colored dissolved organic matter dynamics across the shelf-basin interface in the western Arctic Ocean. Journal of Geophysical Research, 112(C5): C05038, doi: 10.1029/2006jc003584.

Guo, L., Coleman Jr, C.H. and Santschi, P.H., 1994. The distribution of colloidal and dissolved organic carbon in the Gulf of Mexico. Marine Chemistry, 45(1-2): 105-119.

Guo, L., Santschi, P.H. and Warnken, K.W., 1995. Dynamics of dissolved organic carbon (DOC) in oceanic environments. Limnology and Oceanography, 40(8): 1392-1403.

Guo, L., Zhou, Z., Shiller, A.M. and Lohrenz, S.E., 2010. Optical characterization of crude oils and dispersant used in the northern gulf of mexico by fluorescence EEM techniques, AGU Fall Meeting Abstracts, pp. B1471.

Hansell, D.A. and Carlson, C.A., 1998. Deep-ocean gradients in the concentration of dissolved organic carbon. Nature, 395(6699): 263-266.

Harrison, W., Winnik, M.A., Kwong, P.T.Y. and Mackay, D., 1975. Crude oil spills. Disappearance of aromatic and aliphatic components from small sea-surface slicks. Environmental Science & Technology, 9(3): 231-234.

Hazen, T.C. et al., 2010. Deep-sea oil plume enriches indigenous oil-degrading bacteria. Science, 330(6001): 204-208, doi: 10.1126/science.1195979.

Helms, J.R. et al., 2008. Absorption spectral slopes and slope ratios as indicators of molecular weight, source, and photobleaching of chromophoric dissolved organic matter. Limnology and Oceanography, 53(3): 955-969.

Joye, S.B., MacDonald, I.R., Leifer, I. and Asper, V., 2011. Magnitude and oxidation potential of hydrocarbon gases released from the BP oil well blowout. Nature Geoscience, 4(3): 160-164, doi: org/10.1038/ngeo1067.

Kessler, J.D. et al., 2011. A persistent oxygen anomaly reveals the fate of spilled methane in the deep Gulf of Mexico. Science, 331(6015): 312-315, doi: 10.1126/science.1199697.

Kim, M. et al., 2010. Hebei Spirit oil spill monitored on site by fluorometric detection of residual oil in coastal waters off Taean, Korea. Marine Pollution Bulletin, 60(3): 383-389, doi: 10.1016/j.marpolbul.2009.10.015.

Kowalczuk, P. et al., 2010. Characterization of dissolved organic matter fluorescence in the South Atlantic Bight with use of PARAFAC model: Relationships between fluorescence and its components, absorption coefficients and organic carbon concentrations. Marine Chemistry, 118(1-2): 22-36.

Kowalczuk, P. et al., 2009. Characterization of dissolved organic matter fluorescence in the South Atlantic Bight with use of PARAFAC model: Interannual variability. Marine Chemistry, 113(3-4): 182-196.

Kujawinski, E.B. et al., 2011. Fate of dispersants associated with the Deepwater Horizon oil spill. Environmental Science and Technology, 45(4): 1298-1306, doi: 10.1021/es103838p.

Mansour, A.S. and Sassen, R., 2011. Mineralogical and stable isotopic characterization of authigenic carbonate from a hydrocarbon seep site, Gulf of Mexico slope: Possible relation to crude oil degradation. Marine Geology, 281(1-4): 59-69.

Mascarelli, A., 2010. Deepwater Horizon: After the oil. Nature, 467: 22-24, doi: 10.1038/news.2010.378.

Murphy, K.R., Stedmon, C.A., Waite, T.D. and Ruiz, G.M., 2008. Distinguishing between terrestrial and autochthonous organic matter sources in marine environments using fluorescence spectroscopy. Marine Chemistry, 108(1-2): 40-58.

National Commission on the BP Deepwater Horizon Oil Spill and Offshore Drilling (National Commission), 2010. The use of surface and subsea

dispersants during the BP Deepwater Horizon oil spill, staff working paper no. 4.

North, E.W. et al., 2011. Simulating oil droplet dispersal from the Deepwater Horizon spill with a Lagrangian Approach. In: Y. Liu (Editor), Monitoring and Modeling the Deepwater Horizon Oil Spill: A Record-Breaking Enterprise. Geophysical Monograph Series. AGU, Washington, DC, pp. 217-226.

Østgaard, K. and Jensen, A., 1983. Evaluation of direct fluorescence spectroscopy for monitoring aqueous petroleum solutions. International Journal of Environmental Analytical Chemistry, 14(1): 55-72.

Patra, D. and Mishra, A.M., 2002. Total synchronous fluorescence scan spectra of petroleum products. Analytical and Bioanalytical Chemistry, 373(4): 304-309, doi: 10.1007/s00216-002-1330-y.

Santos-Echeandía, J., Prego, R. and Cobelo-García, A., 2008. Influence of the heavy fuel spill from the Prestige tanker wreckage in the overlying seawater column levels of copper, nickel and vanadium (NE Atlantic ocean). Journal of Marine Systems, 72(1-4): 350-357, doi: 10.1016/j.jmarsys.2006.12.005.

Schrope, M., 2011. Oil cruise finds deep-sea plume. Nature, 465: 274-275, doi: 10.1038/465274a.

Sierra, M.M.D., Giovanela, M., Parlanti, E. and Soriano-Sierra, E.J., 2006. 3D-fluorescence spectroscopic analysis of HPLC fractionated estuarine fulvic and humic acids. Journal of the Brazilian Chemical Society, 17: 113-124.

Stedmon, C.A. and Bro, R., 2008. Characterizing dissolved organic matter fluorescence with parallel factor analysis: a tutorial. Limnology and Oceanography - Methods 6: 572-579, doi: 10.4319/lom.2008.6.572.

Stedmon, C.A. and Markager, S., 2003. Behaviour of the optical properties of coloured dissolved organic matter under conservative mixing. Estuarine, Coastal and Shelf Science, 57(5-6): 973-979.

Stedmon, C.A., Markager, S. and Bro, R., 2003. Tracing dissolved organic matter in aquatic environments using a new approach to fluorescence spectroscopy. Marine Chemistry, 82(3-4): 239-254, doi: 10.1016/s0304-4203(03)00072-0.

Stedmon, C.A., Markager, S. and Kaas, H., 2000. Optical properties and signatures of chromophoric dissolved organic matter (CDOM) in Danish coastal waters. Estuarine, Coastal and Shelf Science, 51(2): 267-278.

Twardowski, M.S., Boss, E., Sullivan, J.M. and Donaghay, P.L., 2004. Modeling the spectral shape of absorption by chromophoric dissolved organic matter. Marine Chemistry, 89(1-4): 69-88.

Valentine, D.L. et al., 2010. Propane respiration jump-starts microbial response to a deep oil spill. Science, 330(6001): 208-211.

Vandermeulen, J.H. et al., 1979. Sediment penetration of Amoco Cadiz oil, potential for future release, and toxicity. Marine Pollution Bulletin, 10(8): 222-227, doi: 10.1016/0025-326x(79)90294-7.

Vodacek, A., Blough, N.V., DeGrandpre, M.D., Peltzer, E.T. and Nelson, R.K., 1997. Seasonal variation of CDOM and DOC in the Middle Atlantic Bight:

terrestrial inputs and photooxidation. Limnology and Oceanography, 42(4): 674-686.

Von Der Dick, H. and Kalkreuth, W., 1986. Synchronous excitation and three-dimensional fluorescence spectroscopy applied to organic geochemistry. Organic Geochemistry, 10(1-3): 633-639, doi: 10.1016/0146-6380(86)90060-4.

Wakeham, S.G., 1977. Synchronous fluorescence spectroscopy and its application to indigenous and petroleum-derived hydrocarbons in lacustrine sediments. Environmental Science and Technology, 11(3): 272-276, doi: 10.1021/es60126a012.

Walker, S.A., Amon, R.M.W., Stedmon, C., Duan, S. and Louchouarn, P., 2009. The use of PARAFAC modeling to trace terrestrial dissolved organic matter and fingerprint water masses in coastal Canadian Arctic surface waters. Journal of Geophysical Research, 114: G00F06.

Wang, X.B. et al., 2011. Degradation of petroleum hydrocarbons (C6-C40) and crude oil by a novel Dietzia strain. Bioresource Technology, 102(17): 7755-7761.

Weishaar, J.L. et al., 2003. Evaluation of specific ultraviolet absorbance as an indicator of the chemical composition and reactivity of dissolved organic carbon. Environmental Science and Technology, 37(20): 4702-4708, doi: 10.1021/es030360x.

Yamada, M. et al., 2003. Study on the fate of petroleum-derived polycyclic aromatic hydrocarbons (PAHs) and the effect of chemical dispersant using

an enclosed ecosystem, mesocosm. Marine Pollution Bulletin, 47(1-6): 105-113, doi: 10.1016/s0025-326x(03)00102-4.

Yamashita, Y., Jaffé, R., Maie, N. and Tanoue, E., 2008. Assessing the dynamics of dissolved organic matter (DOM) in coastal environments by excitation emission matrix fluorescence and parallel factor analysis (EEM-PARAFAC). Limnology and Oceanography, 53(5): 1900-1908.

Yin, Z. et al., 1997. Application of soft X-ray absorption spectroscopy in chemical characterization of antiwear films generated by ZDDP Part II: the effect of detergents and dispersants. Wear, 202(2): 192-201.

Zhou, Z. and Guo, L., 2010. Variations in composition and size of dissolved and colloidal organic matter in the Bay of St. Louis estuary, Goldschmidt Conference, Knoxville, TN, pp. 1231.

Zhou, Z. et al., 2012a. Characterization of oil components from the Deepwater Horizon oil spill in the Gulf of Mexico using fluorescence EEM techniques. Marine Chemistry: (in press).

Zhou, Z., Liu, Z. and Guo, L., 2012b. Chemical evolution of Macondo crude oil during laboratory degradation as characterized by fluorescence EEMs and hydrocarbon composition. Marine Pollution Bulletin: (in press).

CHAPTER VI

CHEMICAL EVOLUTION OF MACONDO CRUDE OIL DURING LABORATORY DEGRADATION AS CHARACTERIZED BY FLUORESCENCE EEMS AND HYDROCARBON COMPOSITION*

Introduction

During the Deepwater Horizon oil spill in the Gulf of Mexico between April 20 and July 15, 2010, over 800 million liters of crude oil were released from the Macondo well to the water column, exerting great adverse effects on the marine life, human health, and natural resources in the northern Gulf of Mexico (Mascarelli, 2010; Schrope, 2011). Many weathering processes, including dissolution, dispersion, evaporation, and photochemical and biological degradation, would affect the distribution and transport of crude oil in the Gulf of Mexico. Studies related to the Deepwater Horizon oil spill have been focused mostly on the extent and transport of oil, methane, and dispersant in the water column (Diercks et al., 2010; Hazen et al., 2010; Joye et al., 2011; Kessler et al., 2011; Kujawinski et al., 2011). Although oil in surface waters seemed to be weathered rapidly right after the oil spill, recent studies have shown the persistence of oil signatures in the deeper water column in the northern Gulf of Mexico, even 15 months after the oil spill (Ryerson et al., 2012; Zhou and Guo, 2012). The fate, transport, and transformation of oil components and their

---

* This chapter of the dissertation has been accepted for publication in the Journal of Marine Pollution Bulletin.
Zhou, Z., Liu, Z. and Guo, L., 2012. Chemical evolution of Macondo crude oil during laboratory degradation as characterized by fluorescence EEMs and hydrocarbon composition. Marine Pollution Bulletin, (in press).

degradation pathways and mechanisms in the water column remain poorly understood. The relative importance between photochemical and biological degradation, and the chemical evolution and molecular fractionation of Macondo crude oil during degradation are largely unknown. Therefore, in addition to field studies, controlled laboratory experiments are critically needed to better understand the degradation pathways and mechanisms of crude oil in marine environments.

Polycyclic aromatic hydrocarbons (PAHs), as well as some other aromatic constituents, are the components in crude oil responsible for its optical properties, especially its fluorescence characteristics (Barron et al., 2003; Booksh et al., 1996; Patra and Mishra, 2002; Yamada et al., 2003). The existence of these compounds allows the use of optical properties to examine the composition and transformation of oil. Fluorescence EEM techniques coupled with PARAFAC modeling have been used in previous studies for characterizing, fingerprinting, and monitoring of oil in marine environments (Alostaz et al., 2008; Booksh et al., 1996; Bugden et al., 2008; Ferreira et al., 2003; González et al., 2006; Kim et al., 2010; Patra and Mishra, 2002; Santos-Echeandía et al., 2008; Vandermeulen et al., 1979; Von Der Dick and Kalkreuth, 1986; Wakeham, 1977). In addition, gas chromatography with flame ionization detection (GC-FID) and gas chromatography-mass spectrometry (GC-MS) techniques have also been used to examine the chemical composition of crude oil during degradation (Bence et al., 1996; Boehm et al., 1983; Christensen and Tomasi, 2007; Douglas et al., 2002; Liu et al., 2012; Magi et al., 2002; Overton et al., 1981; Wakeham, 1996;

Wang et al., 2004; Yan et al., 2006). However, laboratory studies on oil degradation using both fluorescence EEMs and GC-MS techniques are still few (D'Auria et al., 2008; Ziolli and Jardim, 2003), especially for the degradation of Macondo crude oil from the Gulf of Mexico. The combination of fluorescence EEMs and GC-MS techniques should allow us to link fluorescence signatures and hydrocarbon composition to reveal the evolution of the oil's composition and fingerprint during degradation.

In this study, laboratory experiments were conducted to examine the chemical evolution, the degradation and transformation pathways and mechanisms of oil components during photochemical and biological degradation of the Macondo crude oil. Measurements included the bulk dissolved organic carbon (DOC) concentration, UV-vis absorbance, fluorescence EEMs, and hydrocarbon composition, including analysis of *n*-alkanes and PAHs using GC-FID and GC-MS. The major objectives of this study were to (1) examine the chemical fractionation of oil components during their degradation in terms of their fluorescence characteristics and hydrocarbon composition, (2) establish a linkage between hydrocarbon composition and fluorescence signatures, and (3) develop potential indices based on fluorescence EEMs for tracking the fate and transport of oil in the water column in the northern Gulf of Mexico.

Materials and Methods

Degradation Experiments

Macondo crude oil (MC252), acquired from BP, was dispensed into pre-combusted amber glass bottles and acid-cleaned Teflon bottles containing

seawater or deionized water. All degradation experiments and amounts of oil and dispersant used are listed in Table 1. Seawater collected from the Gulf of Mexico was filtered through a 0.45 µm Nuclepore filter cartridge (Osmotics). Deionized water was used to represent freshwater for the comparison with seawater to examine the difference in oil degradation between freshwater and seawater. Additional experimental treatments occurred with and without the addition of dispersants to determine the effect of dispersants on the degradation of crude oil.

Table 1

Oil and Dispersant Concentrations in Degradation Experiments (DW=deionized water, SW=seawater)

Sample ID	Oil conc. (µl/l)	Dispersant conc. (µl/l)	Incubation medium	Treatment
DW-dark	20	0	Deionized water	Dark
DW-light	20	0	Deionized water	Light
SW-dark	20	0	Sea water	Dark
SW-light	20	0	Sea water	Light
SW-dispersant-dark	10	10	Sea water	Dark
SW-dispersant-light	10	10	Sea water	Light

Teflon bottles (Thermo Scientific) were used for light treatments (photo-degradation plus microbial degradation), while amber glass bottles wrapped with aluminum foil were used for dark control treatments (microbial degradation only). All the bottles were placed in an incubator filled with running water to maintain a consistent temperature. During the 105-d experimental period, the average temperature was 30 °C, and the average temperature in August was 35 °C (Table 2). The degradation incubator was placed outdoors to receive natural solar radiation. Two temperature/radiation data loggers were used to monitor the variability of both temperature and radiation during oil degradation. Average light intensity ranged from 59021 to 69179 lux from June to October. A maximum light intensity as high as ~330,667 lux was found in August 2011, and the daytime average was ~ 69,179 lux (Table 2).

Immediately after oil was added and mixed, an initial water sample (t = 0 d) was collected from each treatment. After that, samples were taken at different frequencies and time intervals to track oil degradation at both short-term (15 d) and longer-term time scales (up to 150 d). Before each sampling, bottles were taken from the water bath incubator, shaken vigorously for 5 minutes and then allowed to calm for 5 minutes. Duplicate samples were collected for measurements of DOC, dissolved inorganic carbon (DIC), UV-vis absorbance, fluorescence EEM, and hydrocarbons (see below for detailed methods).

Measurements of DOC and UV-vis Absorption

Concentrations of DOC and DIC of the time-series samples were measured with a Shimadzu TOC-V total organic carbon analyzer using a high

temperature combustion method (Guo et al., 1995). For DOC measurements, samples were acidified with concentrated HCl to pH < 2 before analysis.

Table 2

Light Intensity and Temperature during Oil Degradation Experiments

Month	Light intensity daytime mean (lux)	Light intensity daytime max (lux)	Temp. daytime mean (°C)	Temp. nighttime mean (°C)
June	62,882	264,534	33.5	28.8
July	59,021	264,534	33.0	29.2
Aug.	69,179	330,667	34.6	29.9
Sep.	59,418	297,601	31.4	26.9
Oct.	62,398	231,467	28.5	23.2
Nov.	32,747	159,823	24.0	21.1

Three to five replicate measurements, each using 150 µL sample, were made with a preset coefficient of variance <2%. Calibration curves were generated before sample analysis. Concentrations of nanopure water, working standards and certified DOC standards (from Dr. Hansell's Lab at the University of Miami) were measured every eight samples to check the performance of the instrument and ensure data quality. The concentration of DIC was calculated from the difference between total dissolved carbon (TDC) and DOC concentrations, DIC =

TDC-DOC (Guo and Macdonald, 2006) .

The UV-vis absorption spectra of samples were measured using an Agilent 8453 UV-visible spectrophotometer and a 1-cm path-length quartz cuvette over 200-1100 nm with 1 nm increments. The water blank was subtracted, and the refractive index effect was corrected by subtracting the average absorbance between 650 and 800 nm (Stedmon and Bro, 2008). Values of specific UV absorbance ($SUVA_{254}$) were calculated by dividing UV absorbance at 254 nm (m^{-1}) by the DOC concentration (mg-C/L). Non-linear spectral slopes between 290-400 nm and 350-550 nm were calculated.

Measurements of Fluorescence EEMs

A Shimadzu RF-5301PC spectrofluorometer was used to measure fluorescence signatures of water samples in a 1 cm path-length quartz cuvette (Zhou and Guo, 2012). Ninety-one separate fluorescence emission spectra were scanned from 240 to 680 nm with 1 nm intervals under excitation wavelengths from 220 to 400 nm with a 2 nm step and concatenated to generate an excitation-emission matrix that provides DOM component information for the water sample quantitatively and qualitatively (Coble, 1996; Green and Blough, 1994). PARAFAC modeling was used to investigate the spatial and temporal changes in DOM fluorescence components (Stedmon and Bro, 2008).

A water blank was scanned daily and its signatures were subtracted from each sample's EEM. The emission correction spectrum was generated using Rhodamin B and barium sulfate with the correction package from Shimadzu and multiplied by the EEM spectra (Stedmon et al., 2003). Quinine sulfate standards

were also scanned daily for concentration calibration and for checking the instrument performance. All fluorescence intensities were converted to ppb-QSE units. Data in the two triangular areas corresponding to the Rayleigh and Raman scattering peaks were eliminated in the PARAFAC analysis to acquire better mathematical results (Andersen and Bro, 2003; Christensen et al., 2005).

PARAFAC Modeling

PARAFAC modeling was applied to fluorescence EEM data from all samples except those with the addition of dispersants, using MATLAB (MathWorks R2010b) and DOMFluor Toolbox (Stedmon and Bro, 2008). Sample matrices were calibrated and corrected before running the PARAFAC analysis. No outlier samples were found after a non-negativity outlier test. Thus, no sample was removed as an outlier before split-half analysis and model validation (Harshman and Lundy, 1984; Stedmon and Bro, 2008). The fluorescence intensities of each component extracted from the PARAFAC model were directly related to the component's concentration in the water samples.

Measurements of n-alkanes and PAHs

For hydrocarbon analysis, we mainly focused on *n*-alkanes and PAHs, two major components in oil. While *n*-alkanes represent a group of labile compounds, PAHs are directly related to the fluorescence of oil samples. Hydrocarbons in each sample were serially extracted two times with 20 mL of dichloromethane (DCM) using a separatory funnel. The extracts were combined and passed through 5 g of sodium sulfate, then washed with another 20 mL of DCM through the sodium sulfate column. About 1 mL of the final extract was obtained by

concentrating the extracts with a Rotovap and solvent-exchanged with hexane. An aliquot of the concentrated extract (1 mL) was transferred into silica gel chromatographic columns for sample cleanup and fractionation (Wang et al., 2004). Three grams of activated silica gel topped with 3-5 g of anhydrous granular sodium sulfate (about 1 cm) filled the column. Before transferring the concentrated extracts, 20 mL of hexane was used to condition the column. Just prior to exposure of the sodium sulfate layer to air, the concentrated extracts were transferred into the column. Twelve mL of hexane and 15 ml of 1:1 (v/v) benzene/hexane solutions were used to elute the saturated hydrocarbons and aromatic hydrocarbons, respectively. The hexane fraction of each sample was used for total GC-detectable saturated *n*-alkanes analysis, while the benzene/hexane fraction was for analysis of PAHs. Extracts for each fraction were concentrated by a Rotovap to a final volume of 200 µL for GC-FID and GC-MS analyses.

The distribution of *n*-alkanes (*n*-C_8 through *n*-C_{40}, pristane, and phytane) was measured with a Shimadzu GC-FID 2014 gas chromatography with flame ionization detection, equipped with a JW scientific DB5 column (30 m x 0.25mm, 0.25µm film thickness). The injection volume was 1 µL with a split ratio of 20. The temperature of the column was ramped from 40°C to 280°C at a rate of 8°C min^{-1}, and held at 280°C for 40 min. Calibration of the concentration was performed with an internal standard of hexadecane-d_{34} and external standards of *n*-alkanes, pristane and phytane. Analyses of PAHs were performed with a Shimadzu GC-MS QP2010 plus gas chromatography-mass spectrometry, equipped with a

Restek DB-5 column (20 m x 0.18mm, 0.18m film thickness). The GC-MS analysis was performed in a selective ion mode with a split ratio of 20. The other instrumental parameters were the same as described above.

The relative response factors (RRF) for each compound were calculated relative to the internal standards. Deuterated hexadecane-d_{34} and benzo(*e*)pyrene-d_{12} were used for quantitation. An instrument blank and standard solutions which included authentic *n*-alkanes with pristane and phytane, or authentic target PAHs, were analyzed before each sample batch to monitor accuracy and precision. The recoveries of hexadecane-*d34* and benzo(*e*)pyrene-d_{12} were 77.1±11.0% and 93.2 ±12.1%, respectively.

Results and Discussion

Variations in Organic Carbon Concentrations

Extensive oil degradation was observed under light conditions in both freshwater- and seawater-based treatments. Values of UV absorption coefficient at 254 nm (a_{254}) showed an initial abrupt increase at the beginning of the degradation (~ 3 d) followed by a steady decrease towards the end of the experiment (Figure 1A), indicating considerable oil degradation. The steady drop of $SUVA_{254}$ under light conditions further confirmed the photo-degradation of aromatic components of the crude oil (Figure 1B). However, the concentration of DOC in the light bottles increased during oil degradation, especially during the first 20 days, and remained at a steady concentration or slightly increased afterwards (Figure 1C). We speculated that there was a competition between production of water-soluble components and degradation of optically active oil

components, and that aromatic and hydrophobic components, such as naphthalene and phenanthrene, were preferentially degraded during photodegradation of crude oil. This will result in a reduction in the optically active DOM components, but an increase in less optically active DOM components, such as carboxyl groups, which can be generated during oil degradation (Watson et al., 2002), and which would cause the increase in DOC concentration. Therefore, during oil degradation, the hydrophobic DOM components, and thus the a_{254} and SUVA values decreased while the hydrophilic DOM components, and thus the bulk DOC concentration increased (Figure 1A, B, C).

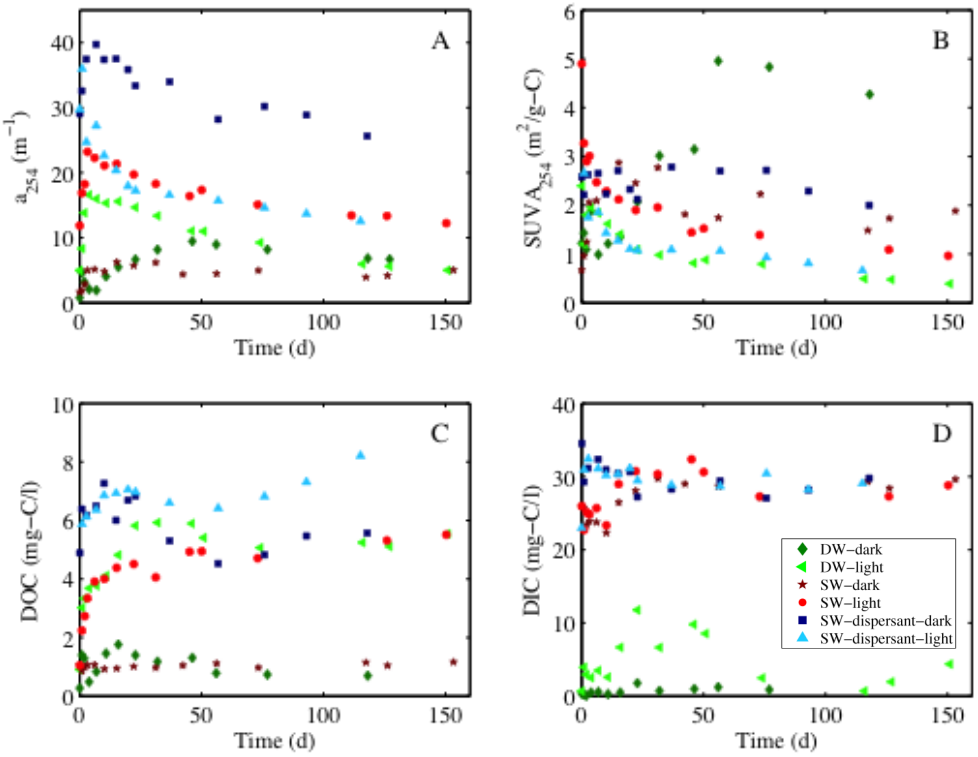

Figure 1. Variations In Absorption Coefficient Value At 254 nm (a254, m-1), Specific UV Absorbance At 254 nm (SUVA254, m2/g-C), And Dissolved Organic Carbon (DOC) And Dissolved Inorganic Carbon (DIC) Concentrations (mg-C/l) During Oil Degradation.

Overall, the dissolution and degradation of crude oil would result in an increased concentration of DOM, as reflected by the increased value in bulk DOC. Among all the hydrocarbons, the more aromatic and optically active components are readily photo-degraded, likely causing the quick drop in absorbance and SUVA values after their initial rise. Concentrations of DIC under light conditions also increased during initial degradation, reflecting the transformation of DOC to DIC. In contrast, although the initial concentration in the dispersant-added treatment was as high as 40 ppm, the DIC concentration remained at the same level (Figure 1D). The spectral slopes slightly increased in treatments with seawater under both light and dark conditions, suggesting preferential decomposition of aromatic DOM in seawater.

Variations in Fluorescence Characteristics during Oil Degradation

Figures 2 and 3 show the fluorescence EEMs of oil samples in the dark and light treatments, respectively, at the initial (left panels) and degraded (right panels) states. Initially, oil in all treatments without dispersant showed the same fluorescence EEMs, with the most prominent peak at Ex/Em 226/240 nm followed by a second peak at Ex/Em 262/315 nm. As shown in Figure 2, degradation under dark conditions gradually lowered the fluorescence intensities at both the 226/240 nm and 262/315 nm peaks, and at the same time gave rise to a third peak at Ex/Em 244/366 nm. On the other hand, degradation under light conditions greatly changed the EEM spectra of oil, resulting in a red shift in fluorescence signatures (Figure 3). Clearly, the fluorescence characteristics of

DOM could be significantly altered during oil degradation regardless of dark or light treatments, reflecting the active transformation of oil components.

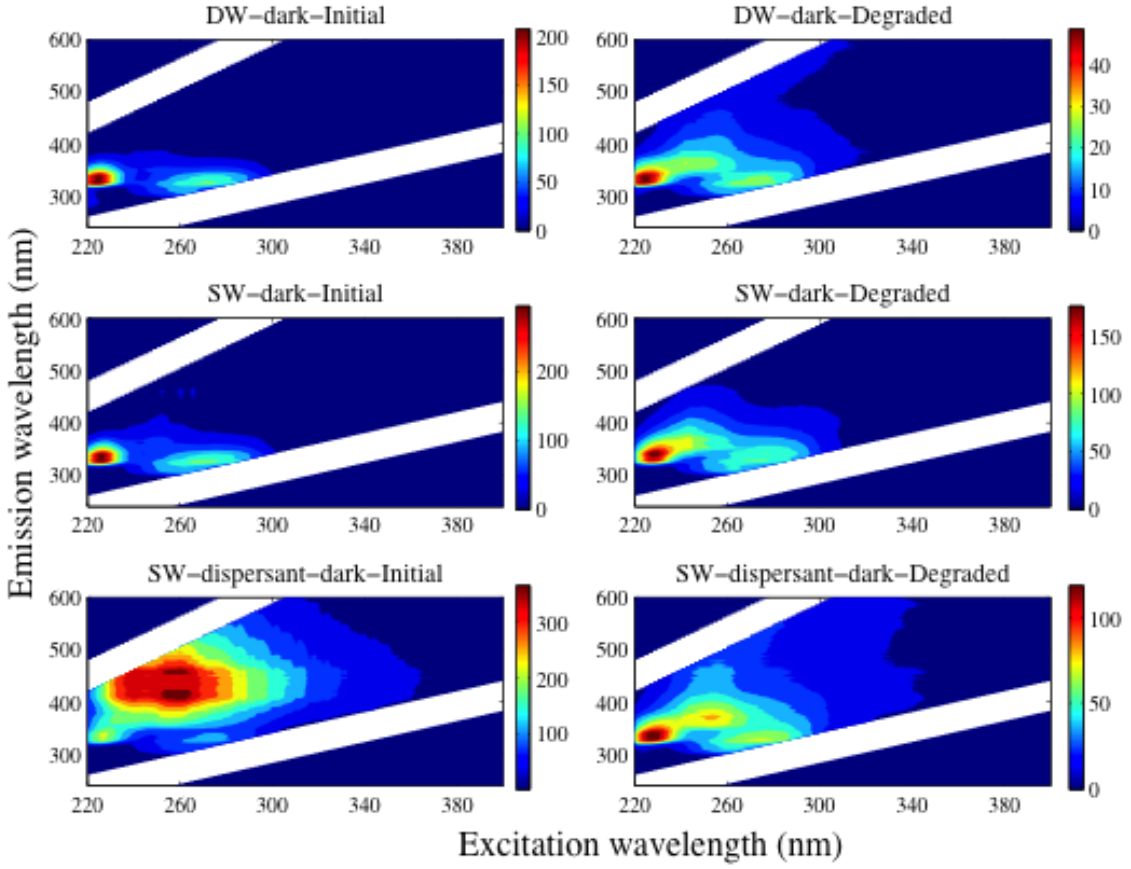

Figure 2. Fluorescence EEM Plots Of Samples Incubated In Dark Bottles In Their Initial (Left Panels) And Degraded (Right Panels) States, Including Oil Dispensed In Milli-Q Water Without Dispersant (Upper Panels), Oil Dispensed in Sea Water Without Dispersant (Middle Panels), And Oil Dispensed In Sea Water With Dispersant (Lower Panels).

The addition of dispersants seemed to enhance fluorescence intensities over a wide range of emission wavelengths between 400-500 nm upon excitation wavelengths from 230 to 280 nm. Similar results were also found by Bugden et al. (2008). Degradation of oil in the presence of dispersants seemed to produce similar degradation products as oil without dispersant under dark and light conditions.

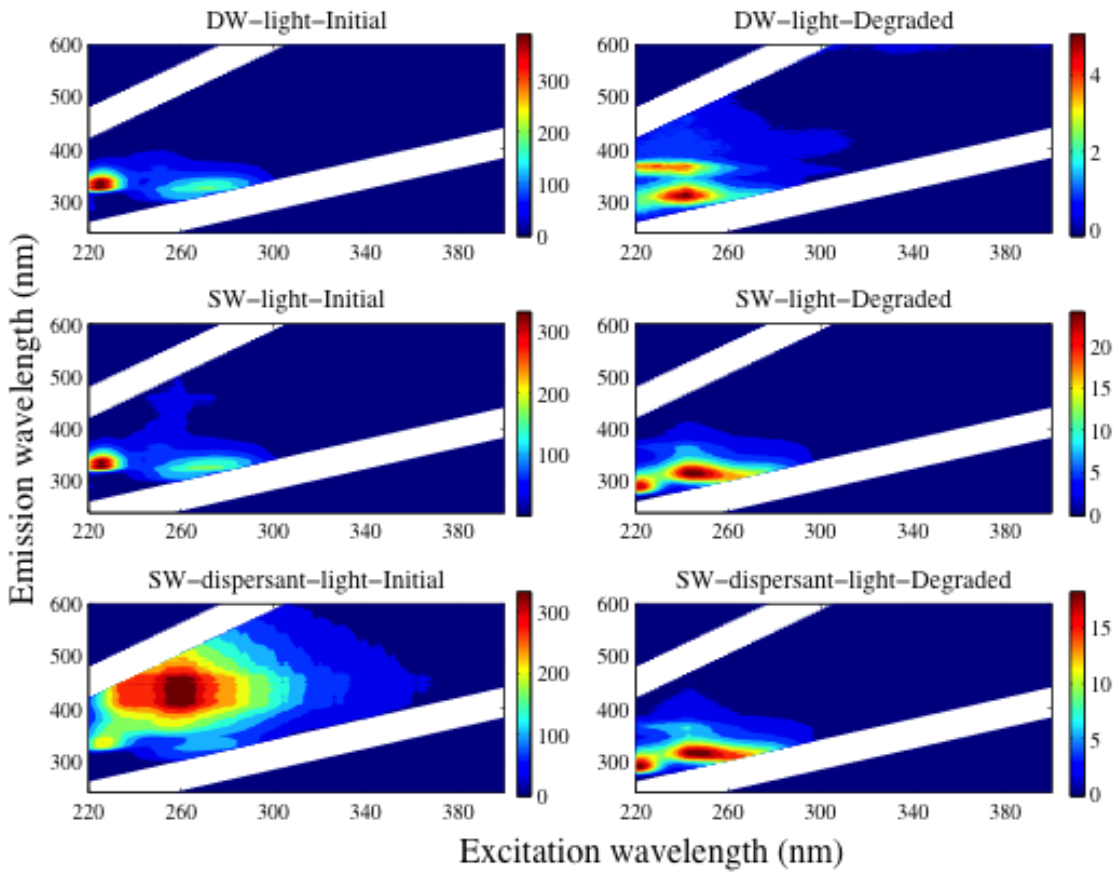

Figure 3. Fluorescence EEM Plots Of Samples Incubated In Light Bottles In Their Initial (Left Panels) And Degraded (Right Panels) States, Including Oil Dispensed In Milli-Q Water Without Dispersant (Upper Panels), Oil Dispensed in Sea Water Without Dispersant (Middle Panels), And Oil Dispensed In Sea Water With Dispersant (Lower Panels).

Four fluorescent DOM components could be identified from PARAFAC modeling using fluorescence EEM data of all the 59 samples from different treatments under light and dark conditions over 150 d (Figure 4). The most dominant oil component, C1, had its maximum fluorescence intensity at Ex/Em 226/328 nm; the second one, C2, showed a peak at Ex/Em 262/315 nm; while the third component, C3, had its characteristic fluorescence signature at Ex/Em 244/366 nm. The first three components were identified as oil-related components (Figure 4; Table 3). The fourth component, C4, having a wide

emission peak over 400-540 nm under excitation of 260 nm, had its maximum fluorescence intensity at Ex/Em 262/507nm, showing UV humic-like DOM characteristics (Figure 4; Table 3).

Table 3

Fluorescent Dissolved Organic Matter (DOM) Components Derived from PARAFAC Modeling

Component	Excitation wavelength (nm)	Emission wavelength (nm)	Description
C1	226	328	Oil-related
C2	262	315	Oil-related
C3	244	366	Oil-related
C4	262	507	Natural DOM

The oil component ratio of C3/C1 under light conditions showed an even more abrupt increase in the beginning of degradation within ~20 d and then steadily decreased (Figure 5B). The relationship between C3 and C1 in light bottles also showed an excess of C3 (Figure 5D). The oil component ratio of C2/C1 under light conditions increased rapidly with time during the first ~30 d, followed by a gradual decrease after ~75 d (Figure 5A). Additionally, the relationship between C2 and C1 showed an excess of C2 compared with C1 during degradation (Figure 5C). These results suggest a preferential degradation of C1 during the early stage of degradation, resulting in the accumulation of C2.

On the other hand, the steadily low C2/C1 ratio (Figure 5A) and the linear relationship between C1 and C2 under dark conditions suggested similar degradation pathways for C2 and C1 in dark treatments (Figure 5C).

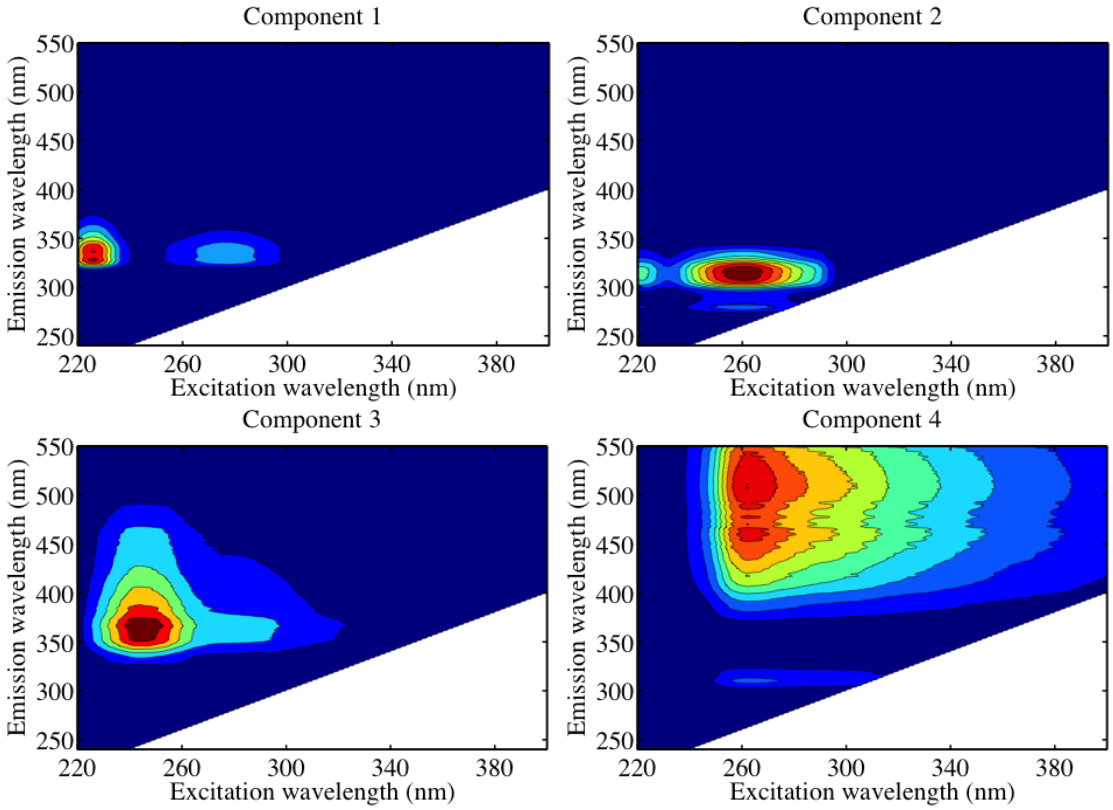

Figure 4. Characteristics Of Four Major DOM Components Derived From PARAFAC Analysis Based On Fluorescence EEMs Of Oil Degradation Samples.

More interestingly, component C3 seemed to decrease with increased C1 when the C1 value was higher than 200 ppb-QSE in dark treatments, suggesting a conversion of organic matter between C1 and C3 under dark conditions. We hypothesized that C3 had part of its origin from C1 through biodegradation. Under light conditions, the decreasing C3/C1 ratios after initial rapid degradation indicated a preferential degradation of C1 and a relatively slower degradation rate of C3 during later stages of degradation (Figure 5B).

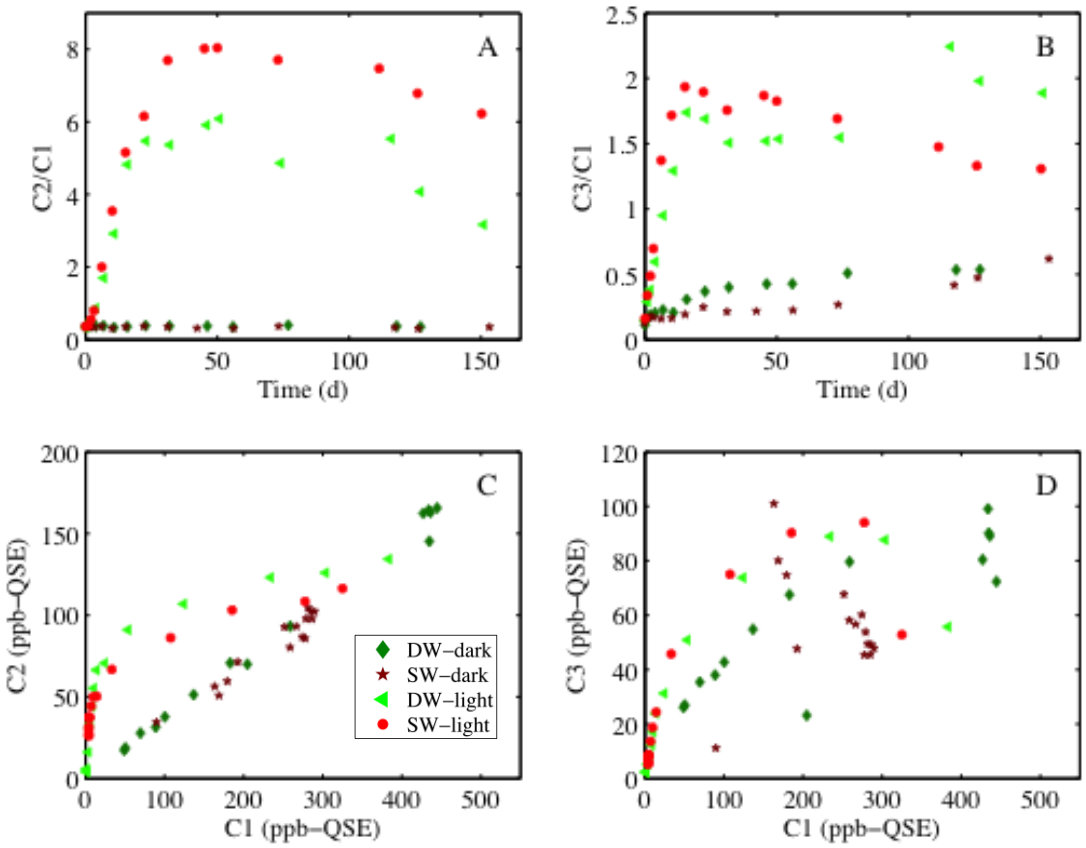

Figure 5. Variations in The Oil Component Ratios C2/C1 (A) and C3/C1 (B) With Time In Light And Dark Conditions And Relationships Between Fluorescent Components C2 And C1 (C), As Well As C3 And C1 (D) During Oil Degradation.

Variations in Hydrocarbon Composition during Degradation

After the first 24 h, *n*-alkanes in the dark bottle were found to be largely depleted in the low molecular weight fractions (C9 - C13) (Figure 6, upper panel), suggesting the preferential degradation of low molecular weight (LMW) fractions. Samples in the light bottle not only showed a large decrease of LMW *n*-alkanes after the onset of degradation, but also exhibited a consistent right shift of the percentage profile (Figure 6, middle panel), with similar preferential loss of LMW *n*-alkanes under light conditions as observed in other studies (Bence et al., 1996; Christensen and Tomasi, 2007; Douglas et al., 2002; Wade et al., 2011). Since

n-alkanes may be less subject to photochemical reactions, it is likely that biodegradation of oil could be enhanced by photochemical processes (Delille et al., 1998).

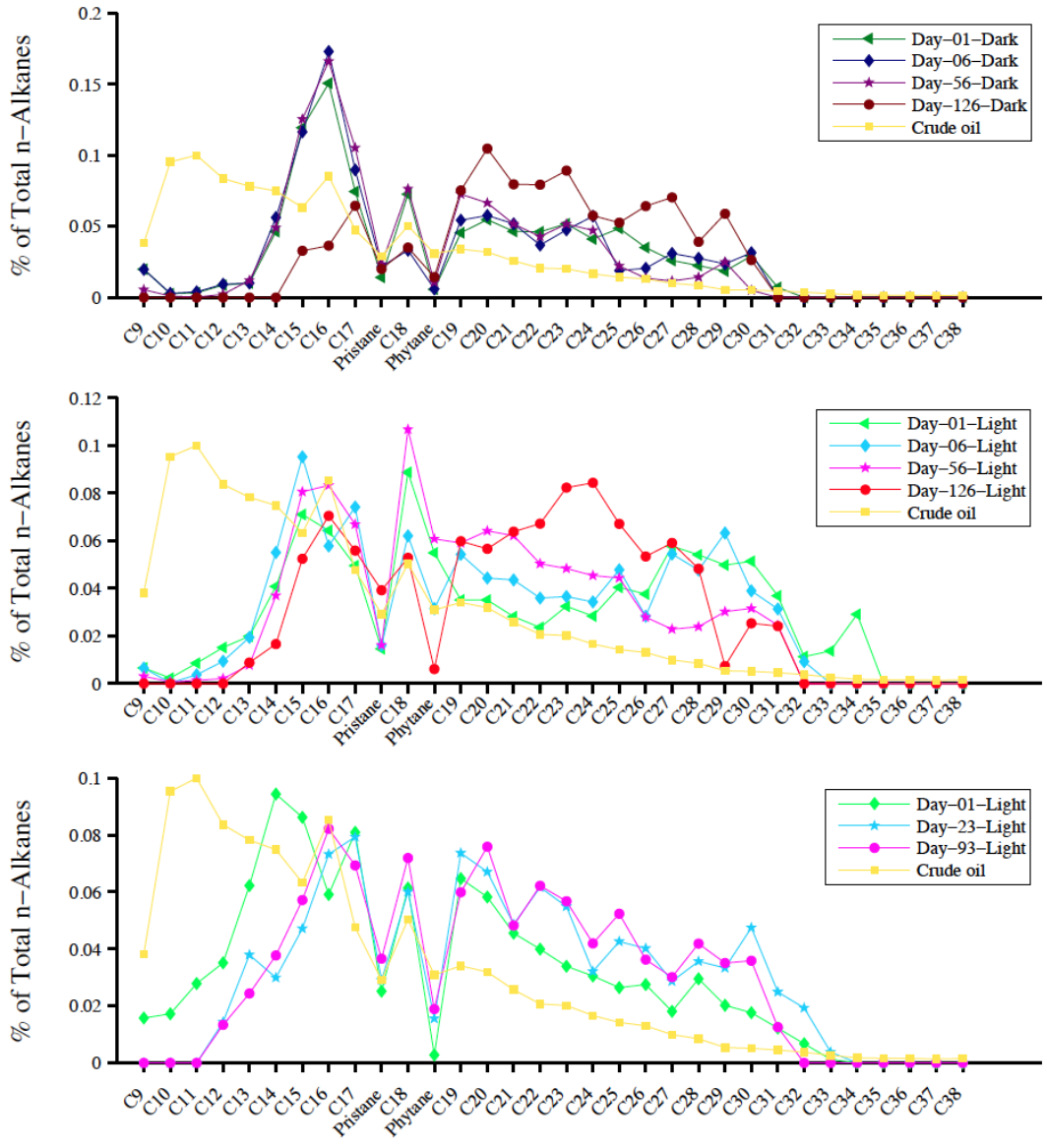

Figure 6. The Variation Of n-alkanes Compositions In Dark Conditions (Upper Panel), Light Conditions (Middle Panel), And With Dispersant Added In Light Conditions (Lower Panel) During Oil Degradation.

In the presence of dispersants, the percentage of LMW hydrocarbons dropped quickly in the beginning of degradation, and remained steady after about ~23 d (Figure 6, bottom panel), suggesting that dispersants enhanced the weathering of oil during the early degradation stage. Compared to the isoprenoids pristane and phytane, the normal alkanes are more readily degraded, resulting in a decrease in the *n*-C_{17}/pristane and n-C_{18}/phytane ratios, which could be used as an index for the extent of crude oil degradation (Bence et al., 1996; Hostettler and Kvenvolden, 1994; Kaplan et al., 1996). Indeed, a general decreasing trend of the *n*-C_{17}/pristane ratio was observed in our time series samples (Figure 7).

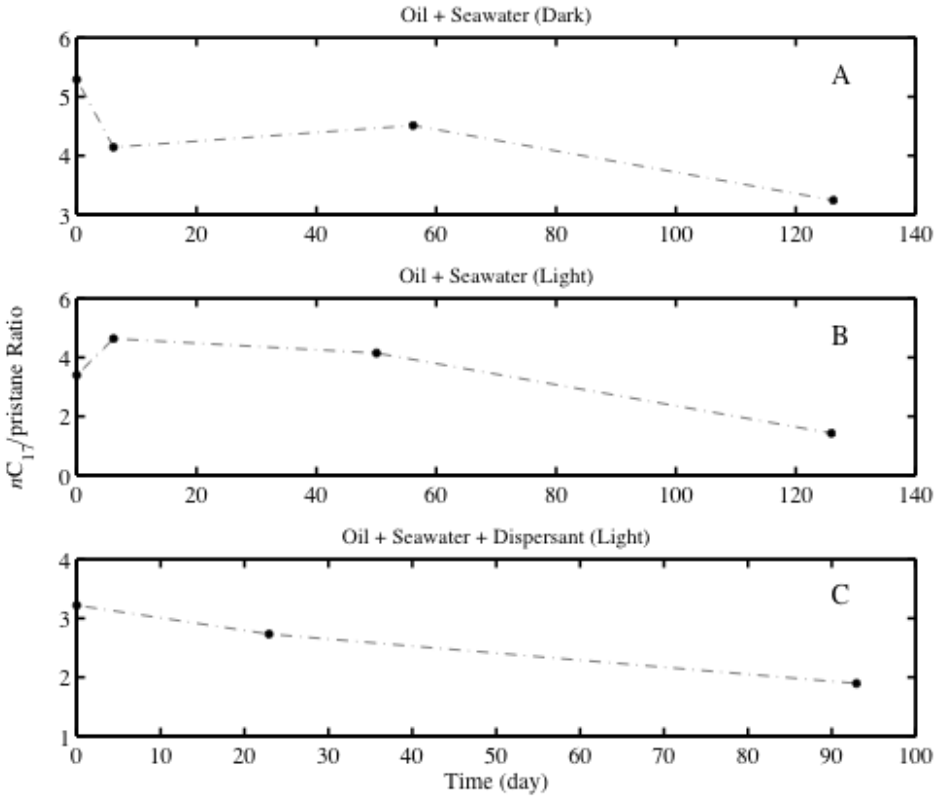

Figure 7. The Variation Of The nC17/Pristane Ratio In Dark Conditions (Upper Panel), Light Conditions (Middle Panel), And With Dispersant Added In Light Conditions (Lower Panel) During Oil Degradation.

Kaplan et al. (1996) also showed a decrease of the *n*-C_{17}/pristane ratio in degraded diesel fuel, bunker C fuel, and others.

The PAHs in oil are mostly the C_1 to C_4 alkylated homologues of their parent PAH components, among which naphthalene, phenanthrene, dibenzothiophene, fluorene and chrysene are the most dominant (Christensen et al., 2005; Wang and Fingas, 2003). This characteristic is also found in the Macondo crude oil (Liu et al., 2012). The degradation rates of different PAHs are linked to their number of rings and degree of alkylation (Bence et al., 1996; Page et al., 1999). As shown in Figure 8, naphthalene, phenanthene, fluoranthene, and chrysene were the most dominant PAHs in the MC252 crude oil. The depletion of naphthalene and phenanthrene is consistent with the change of PAH components during their degradation (Figure 8, middle and bottom panels), suggesting their preferential loss. The addition of dispersants seemed to enhance the degradation of naphthalene and phenanthrene and raised the percentage of fluoranthene and pyrene (Figure 8, bottom panel). Biodegradation also played a role in the weathering of oil, based on the variation of PAH percentages under dark conditions (Figure 8, upper panel).

Linkage between Hydrocarbon Composition and Fluorescence Signatures

The total concentration of PAHs was significantly correlated with the sum of the intensities of fluorescent components ($p < 0.15$) in both dark and light bottles, suggesting that fluorescence intensity could be an alternative for determining the PAH components in a well-defined system. Both the abundance of LMW oil constituents and fluorescence intensities of DOM components

decreased monotonically during the entire degradation process, especially under light conditions (Figures 6, 7, 9).

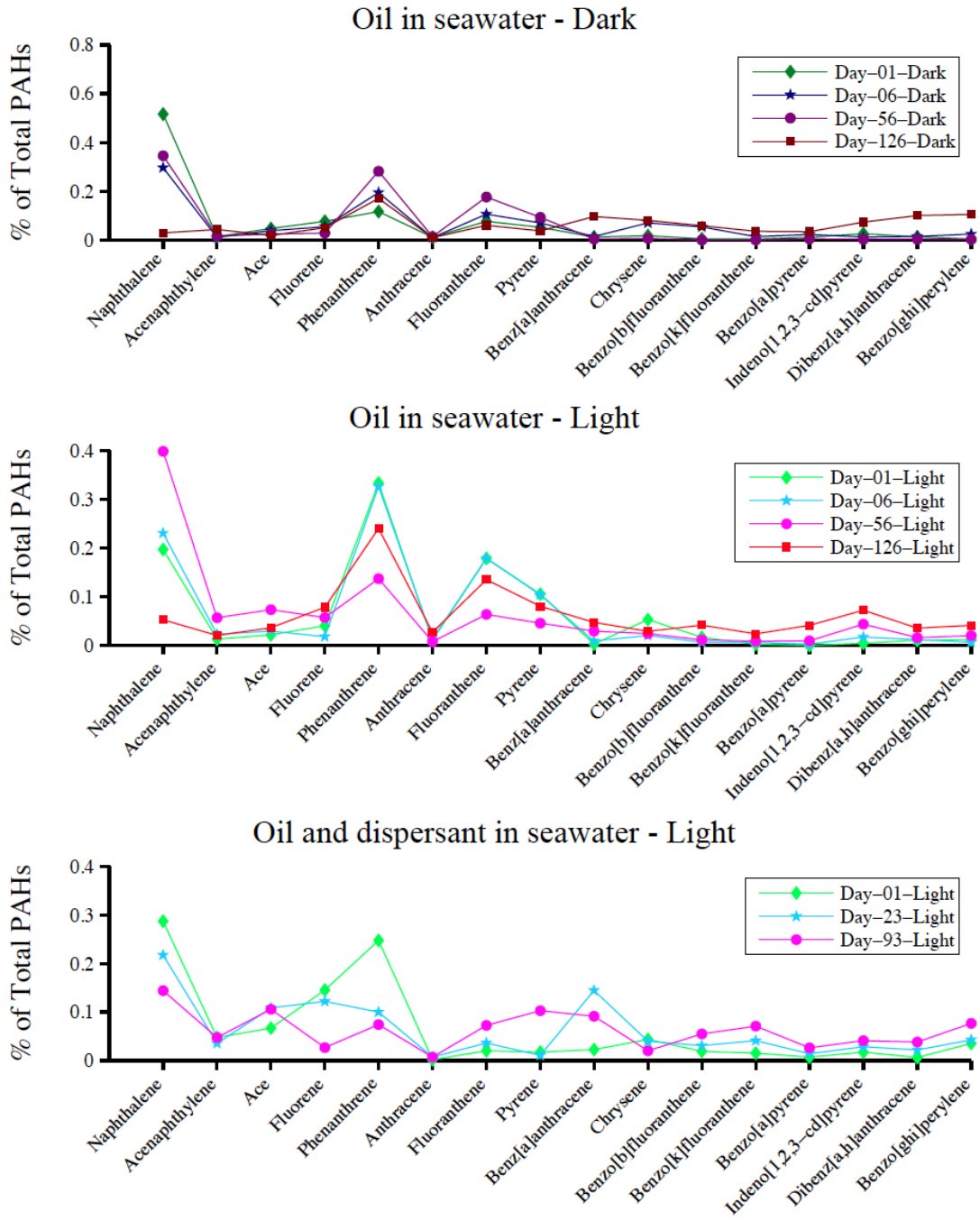

Figure 8. The Variation of PAH Compositions In Dark Conditions (Upper Panel), Light Conditions (Middle Panel), And With Dispersant Added In Light Conditions (Lower Panel) During Oil Degradation.

Thus, both hydrocarbon composition and fluorescence EEM signatures probably reflected the same evolution trend of oil degradation.

Phenanthrene is characterized with a maximum fluorescence intensity at Ex/Em 250/370 nm (Alostaz et al., 2008; Christensen et al., 2005). Component C3 derived from PARAFAC analysis in this study had a peak at Ex/Em 244/366 nm. The correlation between C3 and phenanthrene showed values of $r^2 = 0.95$ and p-value < 0.02 under light conditions, and $r^2 = 0.73$ and p-value <0.14 under dark conditions. It is likely that variations in C3 might be quantitatively linked to the PAH component phenanthrene. More data are needed to establish a more quantitative relationship between fluorescence signatures and hydrocarbon composition.

Degradation Kinetics

Fluorescence intensities of DOM components all decreased with time under light conditions, indicating the loss of fluorescent DOM during oil degradation (Figure 9). To a first approximation, the degradation kinetics of each oil component could be evaluated by fitting their fluorescence intensity (on a logarithmic scale) against time assuming a first-order degradation process. Based on the fitting equations and the slope values from the degradation data of the first 30 d (Table 4), the degradation half-life ($t_{1/2}$) of each fluorescent oil component was estimated to be 2.2, 13.9 and 8.2 d for component C1, C2 and C3, respectively. Interestingly, among the three fluorescent oil components, C1 had the shortest degradation half-life or the fastest degradation rate, followed by component C3, while component C2 had the lowest degradation rate. Thus,

under laboratory degradation conditions, the mean life of these fluorescent oil components was in the order of ~4 - 20 d.

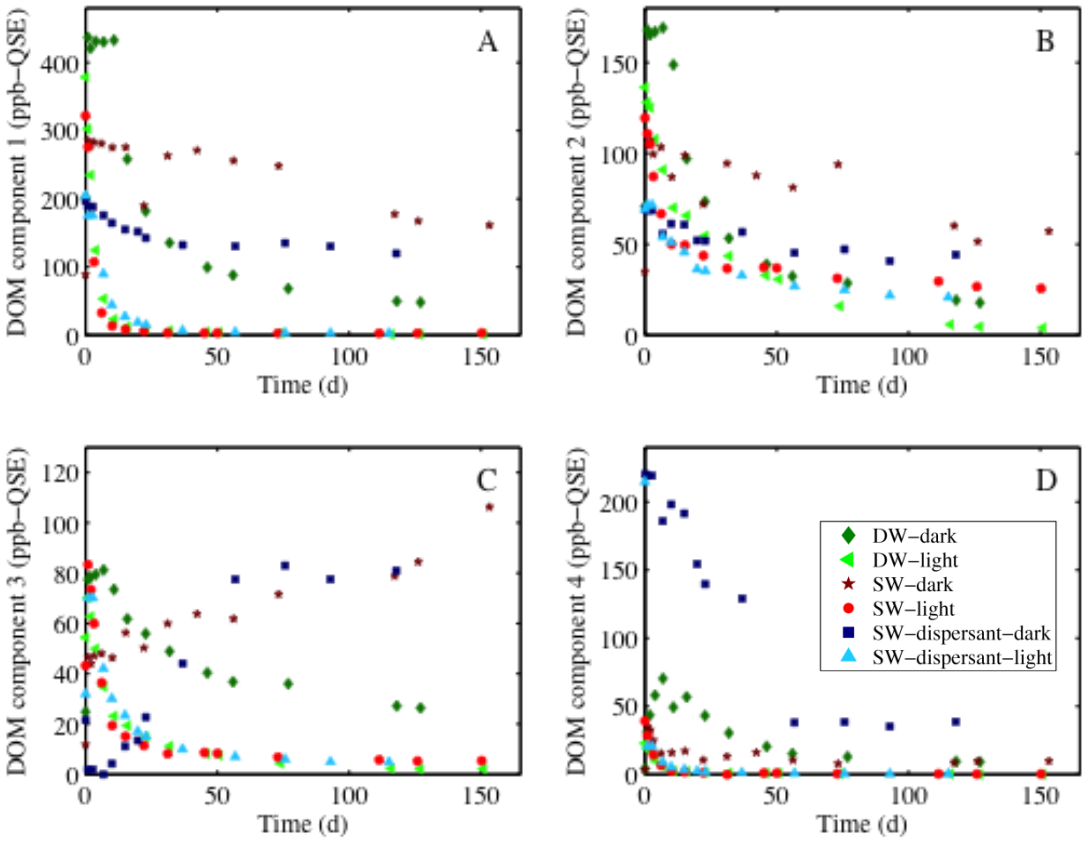

Figure 9. Variations In The Fluorescent DOM Components C1 (A), C2 (B), C3 (C), And C4 (D) During The Degradation Of Macondo Crude Oil.

Our oil degradation time-series sampling was extended to a period of more than five half-lives, allowing the evaluation of the entire degradation process not only for the initial oil components, but also for the degradation derived and transferred components. The distinct degradation rates between different oil components should change the relative importance of fluorescent DOM components during oil degradation and thus their component ratio. For hydrocarbons, the degradation half-lives of total alkanes and total PAHs were

estimated to be 22 and 25 d, respectively, again assuming first-order reactions (Table 5).

Table 4

Intensities of Fluorescent Dissolved Organic Matter (DOM) Components from PARAFAC Modeling

Time (day)	Concentration of fluorescent DOM components (ppb-QSE)		
	Component C1	Component C2	Component C3
0.0	325.0	116.3	52.8
1.0	277.5	108.4	94.0
2.1	185.4	103.2	90.3
3.2	107.6	86.2	75.0
6.1	33.4	66.8	45.8
10.1	14.2	50.4	24.4
15.2	9.7	50.0	18.8
22.2	7.2	44.3	13.6
31.2	4.8	37.2	8.5

These hydrocarbon degradation half-lives corresponded to a mean life of ~34 d, which is slightly longer than that of fluorescent components, likely

resulting from their difference in the sensitivity to photochemical processes between fluorescent organic components and hydrocarbons as a whole. In general, total alkanes and PAHs seemed to have slower degradation kinetics compared to the fluorescent oil components (Table 5).

Table 5

Degradation Half-lives of Hydrocarbon and Fluorescent DOM Components Based on Data from the First 30 Days of Degradation Experiments

Kinetic Parameter	Total Alkanes	Total PAHs	Component C1	Component C2	Component C3
Half–life (d)	22	25	2.2	13.9	8.2
Degradation constant (k, d^{-1})	.031	.028	.32	.05	.08

Effect of Dispersants on Oil Degradation

The addition of dispersants resulted in changes in the fluorescence characteristics of oil in seawater during degradation, with a shift of fluorescence EEM spectra to emission between 400-500 nm when excited from 230-280 nm (Figure 2, bottom left panel). The results of PARAFAC analysis based on all samples, including those with the addition of dispersants, showed an extra fluorescence component with its Ex/Em maximum at 240/446 nm (Figure 10). The fifth fluorescence component, C5, with fluorescence characteristics similar to

those of a natural DOM component found in coastal waters, had a rapid decrease in light bottles, but a gradual decrease in dark bottles (Figure 10). The addition of dispersants seemed to have enhanced the preferential loss of the LMW fraction of oil components, including *n*-alkanes with the number of carbons lower than 17 as well as naphthalene and phenanthrene at their early stage of degradation (Figures 6 and 8).

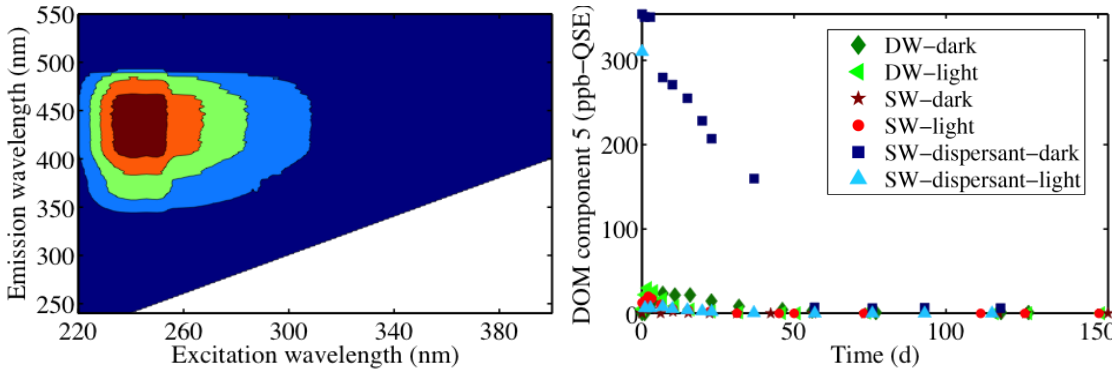

Figure 10. Fluorescent Characteristics Of A DOM Component Extracted From PARAFAC Analysis Applied To Samples Including Dispersant-Treated Experiments (Left Panel) And Its Variation During Oil Degradation (Right Panel).

Applications of Fluorescence Component Ratios to Tracking Oil Degradation

Results from our oil degradation experiments clearly show an increase in the fluorescent oil component ratios C2/C1 and C3/C1 during oil degradation (Figure 5). Based on fluorescence EEM data and PARAFAC modeling of field seawater samples from the Gulf of Mexico, the C2/C1 and C3/C1 ratios also increased consistently in time series field samples taken during and after the Deepwater Horizon oil spill (Zhou and Guo, 2012), which resembled the trends observed in the laboratory degradation experiments (Figure 5). The coincidence between data from our laboratory experiments and results of time series field samples from the Gulf of Mexico indicates that our laboratory experiments using

Macondo oil broadly mimicked oil degradation in the field and supports the use of the oil component ratios as an index for tracking oil degradation and chemical evolution of oil during its degradation in the water column of the Gulf of Mexico.

The increase in both the component ratios, C2/C1 and C3/C1, suggests that components C2 and C3 have lower degradation rates compared with C1, and/or that C2 and C3 are also degradation products of crude oil, consistent with the kinetic results from oil degradation (see previous section). The C2/C1 ratio showed lower values in the deep-water samples and higher values in the surface samples corresponding with a lower and less variable C2/C1 ratio in the dark bottles and higher and an increased C2/C1 ratio in light bottles, suggesting that C2 is less sensitive to photo degradation. In contrast, the C3/C1 ratios had higher values in the deep-water samples compared with surface water samples after the oil spill stopped, suggesting a lower C3 production rate in surface waters compared to its degradation rate.

Values of both component ratios C2/C1 and C3/C1 were smaller in the field samples compared with those found in samples from the laboratory experiments, likely resulting from the efficient degradation of C1 and the nature of the closed system bottle degradation experiments compared to the open environment in the Gulf of Mexico. Overall, the similar trends in fluorescence oil component ratios between laboratory studies and field data support the use of fluorescence signatures to track the fate, transport, and transformation of oil in marine environments.

Conclusions

Water-soluble DOM abundance increased steadily during the oil degradation experiments, while optical activity showed a decreasing trend after a rapid initial increase. Competition between production of water-soluble DOM fractions and photochemical degradation of optically active oil components are likely the cause of this evolving trend. A fraction of DOC was readily transformed into DIC during the degradation process. Photochemical degradation caused a large decline in the aromatic fraction of oil, a preferential loss of low molecular weight alkanes and PAHs, and decreased degradation indexes such as the *n*-C17/pristane ratio.

Three fluorescence oil components, C1, C2, and C3, were identified from samples of the degradation experiments, with their fluorescence intensity maxima at Ex/Em 226/328, 262/315, and 244/366 nm, respectively. The components C2 and C3 had lower degradation rates than C1. Under dark conditions, C2 showed similar degradation rates as C1, while C3 seemed to be produced by oil degradation and was likely derived from C1. We speculated that component C2 mainly was degraded through photodegradation, while C3 was degraded by both microbial and photochemical degradation. The differences in fluorescence component ratios could be used as a proxy for the degradation state of oil in marine environments. The variations in oil components and their ratios resembled those observed in field samples from the Gulf of Mexico, showing a considerable evolution in chemical composition and fluorescence signatures during oil degradation.

Hydrocarbon composition and fluorescence signatures were linked with each other during oil degradation. Similar degradation half-lives were observed for both fluorescence oil components and total alkanes and PAHs, although generally the latter components seemed to have a relatively slower degradation kinetics due to the difference of their sensitivity to photodegradation. Fluorescence oil component C3 was linked to phenanthrene through its chemical characteristics.

The addition of dispersants resulted in a significant change in fluorescence EEM spectra, and enhanced the decomposition of LMW alkanes and PAHs in the early stages of degradation. Photochemical degradation is an effective degradation pathway of oil, resulting in an overall LMW DOM with higher spectral slope values and red-shifted fluorescence maxima. Results from laboratory degradation experiments should facilitate the interpretation of field data and provide new insights on the degradation pathways and mechanisms, and thus the fate and transport of oil components in the Gulf of Mexico.

REFERENCES

Alostaz, M., Biggar, K., Donahue, R. and Hall, G., 2008. Petroleum contamination characterization and quantification using fluorescence emission-excitation matrices (EEMs) and parallel factor analysis (PARAFAC). Journal of Environmental Engineering & Science, 7(3): 183-197, doi: 10.1139/s07-049.

Andersen, C.M. and Bro, R., 2003. Practical aspects of PARAFAC modeling of fluorescence excitation-emission data. Journal of Chemometrics, 17(4): 200-215, doi: 10.1002/cem.790.

Barron, M.G., Carls, M.G., Short, J.W. and Rice, S.D., 2003. Photoenhanced toxicity of aqueous phase and chemically dispersed weathered Alaska North Slope crude oil to Pacific herring eggs and larvae. Environmental Toxicology and Chemistry, 22(3): 650-660, doi: 10.1002/etc.5620220326.

Bence, A.E., Kvenvolden, K.A. and Kennicutt, M.C.I., 1996. Organic geochemistry applied to environmental assessments of Prince William Sound, Alaska, after the Exxon Valdez oil spill-a review. Organic Geochemistry, 24(1): 7-42, doi: 10.1016/0146-6380(96)00010-1.

Boehm, P.D., Feist, D.L., Kaplan, L., Mankiewicz, P. and Lewbel, G.S., 1983. A natural resources damage assessment study: the Ixtoc. In: B. 1983 Oil Spill Conference (Prevention, Control, Cleanup) (Editor). American Petroleum Institute, San Antonio, TX, pp. 507-515.

Booksh, K.S., Muroski, A.R. and Myrick, M.L., 1996. Single-measurement excitation/emission matrix spectrofluorometer for determination of

hydrocarbons in ocean water. 2. calibration and quantitation of naphthalene and styrene. Analytical Chemistry, 68(20): 3539-3544, doi: 10.1021/ac9602534.

Bugden, J.B.C., Yeung, C.W., Kepkay, P.E. and Lee, K., 2008. Application of ultraviolet fluorometry and excitation-emission matrix spectroscopy (EEMS) to fingerprint oil and chemically dispersed oil in seawater. Marine Pollution Bulletin, 56(4): 677-685, doi: 10.1016/j.marpolbul.2007.12.022.

Christensen, J.H., Hansen, A.B., Mortensen, J. and Andersen, O., 2005. Characterization and matching of oil samples using fluorescence spectroscopy and parallel factor analysis. Analytical Chemistry, 77(7): 2210-2217, doi: 10.1021/ac048213k.

Christensen, J.H. and Tomasi, G., 2007. Practical aspects of chemometrics for oil spill fingerprinting. Journal of Chromatography A, 1169(1-2): 1-22, doi: 10.1016/j.chroma.2007.08.077.

Coble, P.G., 1996. Characterization of marine and terrestrial DOM in seawater using excitation-emission matrix spectroscopy. Marine Chemistry, 51(4): 325-346, doi: 10.1016/0304-4203(95)00062-3.

D'Auria, M., Emanuele, L., Racioppi, R. and Velluzzi, V., 2008. Synchronous fluorescence spectroscopy and gas chromatography to determine the effect of UV irradiation on crude oil. Journal of Photochemistry and Photobiology A: Chemistry, 198(2-3): 156-161, doi: 10.1016/j.jphotochem.2008.03.004.

Delille, D., Bassères, A., Dessommes, A. and Rosiers, C., 1998. Influence of daylight on potential biodegradation of diesel and crude oil in Antarctic

seawater. Marine Environmental Research, 45(3): 249-258, doi: 10.1016/s0141-1136(97)00129-3.

Diercks, A.R. et al., 2010. Characterization of subsurface polycyclic aromatic hydrocarbons at the Deepwater Horizon site. Geophysical Research Letters, 37(20): L20602, doi: 10.1029/2010gl045046.

Douglas, G.S., Owens, E.H., Hardenstine, J. and Prince, R.C., 2002. The OSSA II pipeline oil spill: the character and weathering of the spilled oil. Spill Science and Technology Bulletin, 7(3): 135-148, doi: 10.1016/s1353-2561(02)00046-4.

Ferreira, A.M., Micaelo, C. and Vale, C., 2003. Are coastal resources of NW Portugal fingerprinting hydrocarbons released from the Prestige accident? Ciencias Marinas, 29(1): 109-114.

González, J.J. et al., 2006. Spatial and temporal distribution of dissolved/dispersed aromatic hydrocarbons in seawater in the area affected by the Prestige oil spill. Marine Pollution Bulletin, 53(5-7): 250-259, doi: 10.1016/j.marpolbul.2005.09.039.

Green, S.A. and Blough, N.V., 1994. Optical absorption and fluorescence properties of chromophoric dissolved organic matter in natural waters. Limnology and Oceanography, 39(8): 1903-1916.

Guo, L. and Macdonald, R.W., 2006. Source and transport of terrigenous organic matter in the upper Yukon River: Evidence from isotope (δ13C,Δ14C, andδ15N) composition of dissolved, colloidal, and particulate phases. Global Biogeochem. Cycles, 20(2): GB2011, doi: 10.1029/2005gb002593.

Guo, L., Santschi, P.H. and Warnken, K.W., 1995. Dynamics of dissolved organic carbon (DOC) in oceanic environments. Limnology and Oceanography, 40(8): 1392-1403.

Harshman, R.A. and Lundy, M.E., 1984. The PARAFAC model for three-way factor analysis and multidimentional scaling. In: H.G. Law, C.W. Snyder Jr, J.A. Hattie and R.P. E McDonald (Editors), Research methods for multimode data analysis. Praeger, New York, pp. 112-215.

Hazen, T.C. et al., 2010. Deep-sea oil plume enriches indigenous oil-degrading bacteria. Science, 330(6001): 204-208, doi: 10.1126/science.1195979.

Hostettler, F.D. and Kvenvolden, K.A., 1994. Geochemical changes in crude oil spilled from the Exxon Valdez supertanker into Prince William Sound, Alaska. Organic Geochemistry, 21(8-9): 927-936, doi: 10.1016/0146-6380(94)90051-5.

Joye, S.B., MacDonald, I.R., Leifer, I. and Asper, V., 2011. Magnitude and oxidation potential of hydrocarbon gases released from the BP oil well blowout. Nature Geoscience, 4(3): 160-164, doi: org/10.1038/ngeo1067.

Kaplan, I.R., Galperin, Y., Alimi, H., Lee, R.P. and Lu, S.T., 1996. Patterns of chemical changes during environmental alteration of hydrocarbon fuels. Ground Water Monitoring & Remediation, 16(4): 113-124, doi: 10.1111/j.1745-6592.1996.tb01178.x.

Kessler, J.D. et al., 2011. A persistent oxygen anomaly reveals the fate of spilled methane in the deep Gulf of Mexico. Science, 331(6015): 312-315, doi: 10.1126/science.1199697.

Kim, M. et al., 2010. Hebei Spirit oil spill monitored on site by fluorometric detection of residual oil in coastal waters off Taean, Korea. Marine Pollution Bulletin, 60(3): 383-389, doi: 10.1016/j.marpolbul.2009.10.015.

Kujawinski, E.B. et al., 2011. Fate of dispersants associated with the Deepwater Horizon oil spill. Environmental Science and Technology, 45(4): 1298-1306, doi: 10.1021/es103838p.

Liu, Z., Liu, J., Zhu, Q. and Wu, W., 2012. The weathering of oil after the Deepwater Horizon oil spill: Insights from chemical composition of the oil from the sea surface, salt marshes, and sediments. Environmental Research Letters: (in press).

Magi, E., Bianco, R., Ianni, C. and Di Carro, M., 2002. Distribution of polycyclic aromatic hydrocarbons in the sediments of the Adriatic Sea. Environmental Pollution, 119(1): 91-98, doi: 10.1016/s0269-7491(01)00321-9.

Mascarelli, A., 2010. Deepwater Horizon: After the oil. Nature, 467: 22-24, doi: 10.1038/news.2010.378.

Overton, E.B. et al., 1981. Identification of petroleum residue sources after a fire and oil spill, 1981 Off Spill Conference. American Petroleum Institute, Atlanta, GA, pp. 541-546.

Page, D.S. et al., 1999. Pyrogenic polycyclic aromatic hydrocarbons in sediments record past human activity: a case study in Prince William Sound, Alaska. Marine Pollution Bulletin, 38(4): 247-260, doi: 10.1016/s0025-326x(98)00142-8.

Patra, D. and Mishra, A.M., 2002. Total synchronous fluorescence scan spectra of petroleum products. Analytical and Bioanalytical Chemistry, 373(4): 304-309, doi: 10.1007/s00216-002-1330-y.

Ryerson, T.B. et al., 2012. Chemical data quantify Deepwater Horizon hydrocarbon flow rate and environmental distribution. Proceedings of the National Academy of Sciences: doi: 10.1073/pnas.1110564109.

Santos-Echeandía, J., Prego, R. and Cobelo-García, A., 2008. Influence of the heavy fuel spill from the Prestige tanker wreckage in the overlying seawater column levels of copper, nickel and vanadium (NE Atlantic ocean). Journal of Marine Systems, 72(1-4): 350-357, doi: 10.1016/j.jmarsys.2006.12.005.

Schrope, M., 2011. Oil cruise finds deep-sea plume. Nature, 465: 274-275, doi: 10.1038/465274a.

Stedmon, C.A. and Bro, R., 2008. Characterizing dissolved organic matter fluorescence with parallel factor analysis: a tutorial. Limnology and Oceanography - Methods 6: 572-579, doi: 10.4319/lom.2008.6.572.

Stedmon, C.A., Markager, S. and Bro, R., 2003. Tracing dissolved organic matter in aquatic environments using a new approach to fluorescence spectroscopy. Marine Chemistry, 82(3-4): 239-254, doi: 10.1016/s0304-4203(03)00072-0.

Vandermeulen, J.H. et al., 1979. Sediment penetration of Amoco Cadiz oil, potential for future release, and toxicity. Marine Pollution Bulletin, 10(8): 222-227, doi: 10.1016/0025-326x(79)90294-7.

Von Der Dick, H. and Kalkreuth, W., 1986. Synchronous excitation and three-dimensional fluorescence spectroscopy applied to organic geochemistry. Organic Geochemistry, 10(1-3): 633-639, doi: 10.1016/0146-6380(86)90060-4.

Wade, T.L. et al., 2011. Analyses of water samples from the Deepwater Horizon oil spill: documentation of the subsurface plume, Monitoring and Modeling the Deepwater Horizon Oil Spill: A Record-Breaking Enterprise. Geophys. Monogr. Ser. AGU, Washington, DC, pp. 77-82, doi: 10.1029/2011gm001103.

Wakeham, S.G., 1977. Synchronous fluorescence spectroscopy and its application to indigenous and petroleum-derived hydrocarbons in lacustrine sediments. Environmental Science and Technology, 11(3): 272-276, doi: 10.1021/es60126a012.

Wakeham, S.G., 1996. Aliphatic and polycyclic aromatic hydrocarbons in Black Sea sediments. Marine Chemistry, 53(3-4): 187-205, doi: 10.1016/0304-4203(96)00003-5.

Wang, Z. et al., 2004. Characterization and identification of the Detroit River mystery oil spill (2002). Journal of Chromatography A, 1038(1-2): 201-214, doi: 10.1016/j.chroma.2004.03.004.

Wang, Z. and Fingas, M.F., 2003. Development of oil hydrocarbon fingerprinting and identification techniques. Marine Pollution Bulletin, 47(9-12): 423-452, doi: 10.1016/s0025-326x(03)00215-7.

Watson, J.S., Jones, D.M., Swannell, R.P.J. and van Duin, A.C.T., 2002. Formation of carboxylic acids during aerobic biodegradation of crude oil and evidence of microbial oxidation of hopanes. Organic Geochemistry, 33(10): 1153-1169, doi: 10.1016/s0146-6380(02)00086-4.

Yamada, M. et al., 2003. Study on the fate of petroleum-derived polycyclic aromatic hydrocarbons (PAHs) and the effect of chemical dispersant using an enclosed ecosystem, mesocosm. Marine Pollution Bulletin, 47(1-6): 105-113, doi: 10.1016/s0025-326x(03)00102-4.

Yan, B. et al., 2006. Combined application of δ13C and molecular ratios in sediment cores for PAH source apportionment in the New York/New Jersey harbor complex. Organic Geochemistry, 37(6): 674-687, doi: 10.1016/j.orggeochem.2006.01.013.

Zhou, Z. and Guo, L., 2012. Evolution of the optical properties of seawater influenced by the Deepwater Horizon oil spill in the Gulf of Mexico. Environmental Research Letters, 7(2): 025301, doi: 10.1088/1748-9326/7/2/025301.

Ziolli, R.L. and Jardim, W.F., 2003. Photochemical transformations of water-soluble fraction (WSF) of crude oil in marine waters: A comparison between photolysis and accelerated degradation with TiO2 using GC-MS and UVF. Journal of Photochemistry and Photobiology A: Chemistry, 155(1-3): 243-252, doi: 10.1016/s1010-6030(02)00397-0.